Dissertation

Integration of Metabolomics and already established Approaches for Characterization of an Alzheimer´s Disease Model

submitted by

Barbara HINTEREGGER MSc

for the Academic Degree of
Doctor of Philosophy (PhD)

at the
Medical University of Graz

Gottfried Schatz Research Center for Cell Signaling, Metabolism & Aging

Molecular Biology & Biochemistry

under the supervision of

Prof. Dr. Tobias MADL

2020

DECLARATION

I hereby declare that this thesis is my own original work and that I have fully acknowledged by name all of those individuals and organizations that have contributed to the research for this thesis. Due acknowledgement has been made in the text to all other material used. Throughout this thesis and in all related publications I followed the “Standards of Good Scientific Practice and Ombuds Committee at the Medical University of Graz“.

Parts of this thesis have been published in:

Barbara Hinteregger, Tina Loeffler, Stefanie Flunkert, Joerg Neddens, Ruth Birner-Gruenberger, Thomas A. Bayer, Tobias Madl, Birgit Hutter-Paier. *Transgene integration causes RARB downregulation in homozygous Tg4-42 mice.* **Scientific Reports,** doi.org/10.1038/s41598-020-63512-8.

Co-authors that contributed to the data in this thesis:

Tina Loeffler

QPS Austria GmbH, Grambach, Austria

Stefanie Flunkert

QPS Austria GmbH, Grambach, Austria

Joerg Neddens

QPS Austria GmbH, Grambach, Austria

Ruth Birner-Gruenberger

Gottfried Schatz Research Center (for Cell Signaling, Metabolism and Aging) Division of Molecular Biology and Biochemistry, Medical University of Graz, Graz, Austria;
Diagnostic and Research Institute of Pathology & Omics Center Graz, Medical University of Graz, Graz, Austria;
Vienna University of Technology, Institute of Chemical Technologies and Analytics, Vienna, Austria;
BioTechMed-Graz, Graz, Austria

Thomas A. Bayer

Department of Psychiatry and Psychotherapy, Division of Molecular Psychiatry, University Medical Center Göttingen (UMG), Göttingen, Germany

Tobias Madl

Gottfried Schatz Research Center (for Cell Signaling, Metabolism and Aging) Division of Molecular Biology and Biochemistry, Medical University of Graz, Graz, Austria;
BioTechMed-Graz, Graz, Austria

Birgit Hutter-Paier

QPS Austria GmbH, Grambach, Austria

I confirm that all co-authors have agreed to use their data in my thesis (signed confirmations are available). I have included the permission to reprint data from the open access journal Scientific Reports in the appendix.

Date ……

ACKNOWLEDGEMENTS

This work was supported by the Austrian Research Promotion Agency (FFG: 856804) and Barbara Hinteregger was trained within frame of the PhD program Molecular Medicine of the Medical University of Graz.

I would like to thank

Tobias Madl, Michael Khalil and Ruth Birner-Gruenberger for agreeing to serve as members of my thesis committee, and for supervising/discussing my project in our meetings.

Tobias Madl for supervising this PhD project, providing scientific input, major answers and support in applying for grants and writing papers.

Birgit Hutter-Paier for giving me the opportunity to perform my PhD thesis at QPS Austria and for her professional advices and scientific support.

Joerg Neddens for guiding and supporting my PhD study at QPS, interesting discussions, inspiring thoughts and very helpful explanations and extensive support especially in the field of histology.

The whole Madl group for all the support and the great working atmosphere.

All my lab colleagues especially Anita, Martina, Klaus, Johannes, Christa, Julia, Marco and Markus for their helpful advices, assistance and many unforgettable moments in the lab. My PhD would not have been the same in their absence.

The whole team of QPS Austria particularly everyone in the biochemistry, histology department, the animal facility and the tissue sampling team for a successful collaboration and a great time.

A special thank goes to Stefanie Flunkert for her great scientific support!

Finally, I would like to thank my family and friends for their love, support in all ups and downs and encouraging words all over these long academic years. Without you I would have never achieved all my goals. Thank you!

TABLE OF CONTENT

ABBREVIATIONS AND DEFINITIONS

^2H_2O	deuterium oxide
4-HNE	4-hydroxy-2-nonenal
AD	Alzheimer´s disease
AICD	Amyloid precursor protein intracellular domain
ALDH2	Aldehyde dehydrogenase 2
ANOVA	Analysis of variance
AOI	Area of interest
APOE	Apolipoprotein E
APP	Amyloid precursor protein
ATP	Adenosintriphosphate
Aβ	Amyloid beta
Aβ40	Amyloid beta 1-40
Aβ42	Amyloid beta 1-42
BHT	Butylated hydroxytoluene
BSA	Bovine serum albumin
CA1	Cornu ammonis 1
cDNA	complementary desoxyribonucleic acid
CPu	Caudate putamen
CSF	Cerebrospinal fluid
CTF	C-terminal fragment
CTX	Cortex
DAPI	4`,6-Diamidin-2-phenylindole
DCFDA	Dichlorofluorescin diacetate
DEA	Diethylamine
DNA	Desoxyribonucleic acid
EDTA	Ethylenediaminetetraacetic acid
EGTA	Ethylene glycol-bis(β-aminoethyl ether)-N,N,N′,N′-tetraacetic acid
ELISA	Enzyme-linked immunosorbent assay
EOAD	Early-onset Alzheimer´s disease
EPM	Elevated Plus Maze test
ER	Endoplasmatic reticulum
FA	Formic acid
GABA	4-aminobutyrate
GAD67	Glutamate-decarboxylase 67

GAPDH	Glycerinaldehyde-3-phosphate-dehydrogenase
gDNA	Genomic desoxyribonucleic acid
GFAP	Glial fibrillary acidic protein
H_2O_2	Hydrogen peroxide
HC	Hippocampus
HPLC/MS	High-performance liquid chromatography / mass spectrometry
HPRT	Hypoxanthin guanin phosphoribosyl transferase
Iba-1	Ionized calcium binding adaptor molecule 1
IFN-γ	Interferon gamma
IL-2	Interleukin-2
IR	Immunoreactive
IRN	Individual registration number
KC/GRO	Keratinocyte chemoattractant / growth-regulated oncogene
kDa	kilodalton
LOAD	Late-onset Alzheimer´s disease
MDA	Malondialdehyde
MeOH	Methanol
MGSCv37	Mouse genome assembly version mm9
min	minute
mRNA	Messenger ribonucleic acid
MS	Mass spectrometry
MSD	Mesoscale discovery
MWM	Morris Water Maze test
N-CTRL	Negative control
NE	Northeast
NeuN	Neuronal nuclei
NF-L	Neurofilament light chain
NFTs	Neurofibrillary tangles
NMR	Nuclear magnetic resonance
NTG	Non-transgenic
NW	Northwest
OF	Open Field test
O-PLS-DA	Orthogonal-partial-least-square-discriminant analysis
PBS	Phosphate-buffered saline
PCA	Principal component analysis

ppm	parts per million
PSEN 1	Presenilin 1
PSEN 2	Presenilin 2
PT	Probe trial
PTMs	Posttranslational modifications
qPCR	Quantitatife polymerase chain reaction
Rarb	Retinoic acid receptor beta
ROS	Reactive oxygen species
RT	Room temperature
sAPPα	Soluble amyloid precursor protein alpha
SDS	Sodium dodecyl sulfate
SE	Southeast
sec	second
SEM	Standard error of the mean
SOD	Superoxide dismutase
SP-CTRL	Specificity control
TBARS	Thiobarbituric acid reactive substances
TDP-43	Transactive response DNA binding protein 43
TG	Transgenic
Thy1	Thymus cell antigen 1
TLA	Target locus amplification
TNF-α	Tumor necrosis factor alpha
TRH	Thyrotropin-releasing hormone
TSP	Sodium trimethylsilyl [2,2,3,3-2H4] propionate
WT	Wild type

ZUSAMMENFASSUNG

Die Alzheimer Krankheit ist die häufigste Form der Demenz und wurde bereits bei Millionen von Menschen diagnostiziert. Durch den signifikanten Anstieg einer schnell alternden Bevölkerung in Entwicklungs- und Industrieländern ist die Alzheimer Demenz ein weltweit wachsendes Problem. Die Alzheimer Erkrankung ist eine unheilbare Störung und bisher gibt es zur Behandlung dieser Krankheit nur symptomatische Therapien. Alle klinischen Studien mit neuartigen Therapien waren bislang leider nur von begrenztem Erfolg.

Aus diesem Grund sind die Erforschung von zugrundeliegenden Mechanismen, beteiligten Stoffwechselwegen und neuen Biomarkern der Alzheimer Erkrankung von sehr großer Wichtigkeit. Darüber hinaus können in Folge neue Medikamente erprobt werden, um vielversprechende Behandlungsoptionen gegen die Alzheimer Krankheit zu finden.

Tiermodelle menschlicher Krankheiten, welche die Krankheitspathologie genau nachahmen sind entscheidend, um zugrundeliegende molekulare Mechanismen zu verstehen und präklinische Studien voranzutreiben. Zur Untersuchung der Alzheimer bezogenen Pathophysiologie wurden in den letzten Jahren viele verschiedene transgene Mausmodelle entwickelt. Obwohl keines der transgenen Alzheimer-Mausmodelle die menschliche Krankheit vollständig abbilden kann, wurden durch die Untersuchung von pathologischen Prozessen in lebenden Tieren neue Einblicke in die Pathogenese der Krankheit erlangt.

Das erste Ziel dieser Arbeit war die umfassende Charakterisierung des neuartigen Tg4-42 Mausmodells unter Einbeziehung der metabolischen Phänotypisierung sowie von bereits etablierten Methoden wie Verhaltenstests, Histologie und Biochemie. Dies sollte zu einem besseren Verständnis der zugrundeliegenden Krankheitsmechanismen in diesem Alzheimer-Tiermodell beitragen.

Dazu wurden verschiedene Verhaltenstests, Immunhistologie und biochemische Analysen, sowie eine NMR-basierte metabolische Phänotypisierung von Wildtyp und Tg4-42 +/+ Mäusen unterschiedlichen Alters durchgeführt. Tg4-42 +/+ Mäuse nahmen im Laufe der Zeit nicht an Körpergewicht zu und zeigten im Morris Water Maze ein verändertes Lernverhalten sowie Gedächtnisstörungen. Darüber hinaus waren Glutamin- und 4-Aminobutyrat Konzentrationen in verschiedenen Hirnregionen der Tg4-42 +/+ Mäuse im Vergleich zu nicht transgenen Mäusen signifikant verringert. Um diese Ergebnisse zu verifizieren, wurden in diesem Stoffwechselweg involvierte Enzyme histologisch analysiert, was signifikant erhöhte Glutaminase- und GAD67-Niveaus in Tg4-42 +/+ Mäusen zeigte. Basierend auf diesen Ergebnissen wurden dann auch zugrundeliegende Effekte wie erhöhte Aβ42-Konzentrationen, erhöhte Neuroinflammation, ein massiver Verlust von Neuronen sowie ein fehlender Retinsäure-Rezeptor Beta festgestellt. Dieses Ergebnis wirft jedoch die Frage auf, ob der

Phänotyp dieser Mäuse ausschließlich von der Aß4-42-Überexpression abhängt oder auch durch das Fehlen des Retinsäure-Rezeptors Beta beeinflusst wird. Aus diesem Grund wurde der zweite Teil der Arbeit mit einem anderen Tiermodell, nämlich APP_{SL} Mäusen, durchgeführt. Es wird angenommen, dass die oftmals beschriebenen pathologischen Prozesse und Veränderungen in den Gehirnen von an Alzheimer erkrankten Personen, wie zum Beispiel die Entstehung toxischer Aβ-Peptide und die Bildung von Amyloid Plaques, von neurofibrilläre Bündel, Neuronenverlust oder Neuroinflammation ein oxidatives Ungleichgewicht verursachen und dadurch oxidativer Stress eine wichtige Rolle bei der Entstehung der Alzheimer Krankheit spielt. All diese pathologischen Ereignisse führen zur Bildung toxischer Aldehyde, was in weiterer Folge zu einer Akkumulation von hochreaktiven Zwischenprodukten im Gehirn und im Blut führt. Daher ist ein Mechanismus zur schnellen und effektiven Beseitigung dieser schädlichen Zwischenprodukte entscheidend, um Zellen und Gewebe vor Schäden zu schützen. Insbesondere die schnelle Entgiftung durch Enzyme spielt dabei eine Schlüsselrolle. Das Enzym Aldehyddehydrogenase 2 (ALDH2) ist für die Umwandlung von endogenen toxischen zu unschädlichen Verbindungen verantwortlich. Aus diesem Grund wurde eine Vielzahl von niedermolekularen Substanzen entwickelt, welche die katalytische Aktivität von ALDH2 erhöhen, was in weiterer Folge zu einer verstärkten Entgiftung in Zellen führt. Somit könnte die Erhöhung der katalytischen Aktivität des ALDH2 Enzyms auch einen vielversprechenden, molekularen Angriffspunkt für die Behandlung der Alzheimer Krankheit darstellen.

Basierend auf dieser Idee wurden im zweiten Teil, die Auswirkungen eines ALDH2-Agonisten auf das Fortschreiten der Alzheimer Krankheit typischen Pathologien bei APP_{SL}-Mäusen genauer untersucht.

Dazu erhielten männliche transgene APP_{SL} Mäuse und deren nicht-transgene Geschwistertiere für die Dauer von 2 oder 4 Monaten entweder einen ALDH2-Aktivator (AD-9308) oder Vehikel über das Trinkwasser verabreicht. Im Anschluss daran wurden Verhaltenstests, Immunhistochemie sowie eine NMR-basierte metabolische Phänotypisierung aller Mäuse durchgeführt. In vivo Ergebnisse zeigten eine hoch signifikante Verbesserung des räumlichen Lernens bei APP_{SL} + AD-9308 im Vergleich zu APP_{SL}-Tieren. Darüber hinaus zeigte eine nicht zielgerichtete metabolische Phänotypisierung erhöhte Serumacetatspiegel in APP_{SL} + AD-9308 im Vergleich zu APP_{SL} Mäusen. Zusätzlich wurden weitere Messungen durchgeführt, um die Behandlungseffekte des ALDH2-Aktivators in APP_{SL} Mäusen noch näher zu analysieren. Dabei wurden in AD-9308 behandelten APP_{SL} im Vergleich zu Kontroll-Mäusen verringerte humane Aβ1-40 Werte sowie eine erniedrigte Malondialdehyd Konzentration gemessen. Aufgrund der aktuellen Ergebnisse ist es leider noch nicht möglich anzugeben,

welche Pfade vom ALDH2-Aktivator beeinflusst werden. Aus diesem Grund sind weitere Analysen erforderlich, um die Wirkung dieses Arzneimittels besser verstehen zu können. Die Ergebnisse dieser Studie zeigen jedoch, dass die Erhöhung der Entgiftungsaktivität von ALDH2 ein vielversprechender Ansatz zur Bekämpfung der Alzheimerkrankheit zu sein scheint.

ABSTRACT

Alzheimer's disease (AD) is the most common cause of dementia. Millions of people have already been diagnosed with AD and with the significant increase of a rapidly aging population in developing and developed countries, AD is a growing problem around the world. Until now only symptomatic pharmacological therapies for AD exist, no clinical trials with novel therapies have demonstrated efficacy so far, the benefits are often marginal, non-permanent and therefore unfortunately only of limited success.

For that reason, research on the primary mechanisms of AD pathophysiology, the involved pathways to find new biomarkers as well as the testing of new drugs are mandatory to find promising targets and treatment options against AD.

Animal models of human diseases which accurately mimic a specific pathology are crucial to understand molecular mechanisms and to advance preclinical studies. To investigate the AD-related pathophysiology, several transgenic mouse models have been established in the recent years. Although none of these transgenic mouse models fully replicates the human disease, the ability to study similar pathological processes in living animals has provided new insights into the pathogenesis of the disease.

Thus, the first aim of this thesis was to perform a comprehensive characterization of the novel Tg4-42 mouse model by integrating metabolomic phenotyping and already established approaches such as behavioral tests, histology and biochemistry for in-depth characterization and to better understand the underlying disease mechanisms.

To reach this first aim, different behavioral tests, immunohistochemistry, biochemical analyses as well as untargeted NMR-based metabolic phenotyping of wild type and Tg4-42 +/+ mice of different ages were performed. Tg4-42 +/+ mice did not increase their body weight over time and showed impaired learning behavior and memory deficits in the Morris water maze test. Furthermore, untargeted NMR-based metabolic profiling showed significantly decreased glutamine and 4-aminobutyrate levels in different brain areas compared to control mice. To verify these results, enzymes within this pathway were analyzed histologically resulting in significantly increased glutaminase as well as GAD67 levels in Tg4-42 +/+ mice. Based on these results, downstream effects were analyzed showing increased Aβ42 levels, increased neuroinflammation, loss of neurons as well as a knockdown of the retinoic acid receptor beta in Tg4-42 +/+ transgenic mice, the latter questioning the cause of the evaluated phenotype of these mice to be solely dependent on Aß4-42 expression. This was the reason, why for the second part of this thesis a different AD animal model, the APP_{SL}, had been used.

The described pathological processes and alternations in AD brains like toxic Aβ peptides and amyloid plaques, neurofibrillary tangles, neuron loss or neuroinflammation are thought to

cause oxidative imbalance suggesting that oxidative stress plays a major role in AD progression. All these pathological events lead to the generation of toxic aldehydes, resulting in an accumulation of such highly reactive intermediates in the brain and blood. Therefore, a mechanism for rapid clearance of these highly diffusible and harmful aldehydes is crucial to protect cells and tissues from damage. In particular, the detoxification by enzymes such as aldehyde dehydrogenase 2 (ALDH2) plays a key role in oxidizing endogenous aldehydic products. For that reason, a variety of small molecule modulators of ALDH2 has been discovered which are able to enhance the catalytic activity of ALDH2 leading to an increased detoxification in cells. Thus, activation of the ALDH2 pathway could be a molecular target for AD.

Therefore, the second aim of this thesis was to evaluate the effects of an ALDH2 agonist on AD disease progression in APP_{SL} mice.

To reach this aim male transgenic APP_{SL} mice and their non-transgenic littermates received either an ALDH2 activator or vehicle via the drinking water for the duration of 2 or 4 months. Behavioral tests, immunohistochemistry as well as untargeted NMR-based metabolic phenotyping of all mice were performed. *In vivo* results revealed a highly significant improvement in spatial learning in APP_{SL} + AD-9308 compared to APP_{SL} animals. Moreover, untargeted metabolic phenotyping showed increased serum acetate levels in AD-9308 treated APP_{SL} mice. Additionally, further measurements were performed to analyze treatment effects of the ALDH2 activator in APP_{SL} mice which revealed decreased Aβ-40 and MDA levels due to the treatment. However, based on current results it is not yet possible to specify which pathways are influenced by the ALDH2 activator and further analyses are necessary to better understand the effects of this drug. Nevertheless, the results of this study demonstrate that increasing the detoxification activity of ALDH2 seems to be a promising approach to target Alzheimer´s disease pathology.

1 INTRODUCTION

Alzheimer´s disease (AD) is the most common cause of dementia, as well as a major cause of death and was first identified more than 100 years ago by Dr. Alois Alzheimer (1, 2). He described the histopathological features now commonly associated with AD like intracellular tangles and extracellular plaques in an AD case report on a 56-year-old woman. (3-5). AD is described as an irreversible and progressive neurodegenerative disease that slowly destroys cognitive functions, memory and thinking skills by damaging or even destroying neurons (6). Millions of people have already been diagnosed with AD and with the significant increase of a rapidly aging population in developing and developed countries, AD is a growing problem around the world (7-9). Until now no curative treatment exists and clinical trials with novel therapies have not been successful yet. For that reason, research on the primary mechanisms of AD pathophysiology, the involved pathways to find new biomarkers as well as the testing of new drugs are mandatory to find promising targets and treatment options against AD (3, 10, 11).

1.1 Epidemiology and different forms of AD

In 2019, it was estimated that over 50 million people were living with dementia worldwide and this number is expected to double by 2030 and more than triple by 2050 to 115 million (12). In Austria around 100.000 people suffer from dementia and AD is responsible for 60-80 % of these cases (13). Nowadays it is thought that AD is a multifactorial disease and that ~70 % of AD risk is attributable to genetic factors and ~30 % to environmental factors. AD is mostly sporadic, but also rare familial AD forms appear in very few cases (<1 %). In these familial forms mutations in three different genes like amyloid precursor protein (APP), presenilin 1 (PSEN 1) and presenilin 2 (PSEN 2) are described. These genetic types usually develop earlier symptoms than sporadic AD, typically between the age of 30 and 65 years and are also known as early-onset AD (EOAD). The pathology of sporadic or late-onset AD (LOAD) appears at a higher age (>65 years) and progresses more slowly. Genetically, the ε4 allele of the apolipoprotein E (APOE), which is a major cholesterol carrier that supports lipid transport and injury repair in the brain, is the largest risk factor for LOAD (14-16). Although many different environmental as well as genetic risk factors are well described to be involved in the pathogenesis of AD, overall impairments in amyloid-β (Aβ) clearance are probably a major cause of disease development and play therefore a central role in the onset and progression of AD (17).

1.2 Neuropathology of AD

Major neuropathologic hallmarks of AD are neurofibrillary tangles (NFTs) and amyloid plaques that contain Aβ peptides (18, 19). Neurofibrillary pathology consists of aberrant, partly insoluble hyperphosphorylated tau aggregates. Amyloid plaques are extracellular, roughly spherical structures composed of abnormally folded Aβ with 40 or 42 amino acids (Aβ40 and Aβ42) which are products of proteolytic APP processing. Within plaques, Aβ42 is more abundant than Aβ40 because of its higher rate of insolubility and fibrillization (20). Downstream consequences of these pathologies can include amyloid angiopathy, age-related brain atrophy, synaptic changes, neuron loss and neuroinflammation which may contribute to cognitive impairments but are not considered as pathognomonic features of AD (16, 21, 22).

Neurofibrillary tangles (NFTs) seem to be not specific for AD because they are described in many different types of brain diseases and are also found in healthy aging subjects. For example, NFTs were found in the hippocampus of control and demented subjects and a study of tau biomarkers reported that NFTs are universally present in subjects older than 70 years, even in persons with intact cognition (21, 23).

Like NFTs, amyloid plaques are not universal since they are found in a high proportion of elderly persons (24, 25). There are different known subtypes for example “neuritic plaques” which are described to be more likely associated with cognitive impairment than “diffuse plaques” (26, 27). Neuritic plaques are surrounded by degenerating axons and dendrites that often contain hyperphosphorylated tau aggregates (21).

Although NFTs and amyloid plaques are the major hallmarks of AD, they do not develop according to the same temporal and anatomic pattern in AD brains (28, 29). Studies have shown that most LOAD diagnosed patients do not have “pure AD” which consists of plaques and tangles. Instead, these cases have varying combinations of additional α -synculein and TDP-43 deposits with further hippocampal sclerosis and microvascular changes which makes symptomatology of LOAD variable and unspecific (30-32).

While the relationship between tangle formation, amyloid production and neuronal death is still unknown, it seems clear that both pathologies dramatically target and disrupt the fundamental units of neuronal function which leads to the loss of synapses, misshaped dendrites, dysmorphic axons and white matter lesions (33).

1.3 Amyloid Precursor Protein (APP) and Amyloid-β (Aβ)

One of the main players in AD are amyloid-β peptides, which are a cleavage products of the amyloid precursor protein (APP), a transmembrane protein which is expressed at high levels in the brain. In humans the APP gene is located on chromosome 21 and due to alternative splicing different isoforms with varying amino acid length exist. Some of the currently known isoforms are APP 751 and 770 which are expressed in glial cells as well as APP 695 which is the predominate form expressed in neurons (34).

The cellular localization of APP is dynamic and it is proteolytically processed at several different subcellular sites (35). After the release from the endoplasmatic reticulum (ER) and subsequent post-translational modification APP can move to the plasma membrane. But only a small fraction of nascent APP molecules of around 10 % reach the cell surface, whereas the majority of APP is trafficked to the Golgi apparatus and trans-Golgi network. APP which reached the plasma membrane is either cleaved by secretase enzymes or re-internalized which requires the “YENPTY” domain. In case of endocytosis, APP is delivered to endosomes and is recycled to the cell surface or undergoes degradation in lysosomes (36-40).

Two main pathways are described in connection with APP processing, the non-amyloidogenic and the amyloidogenic pathway. In the non-amyloidogenic pathway APP is cleaved by α-secretase into soluble APP α (sAPPα) which is released into the extracellular space while the shorter C-terminal fragment remains embedded in the plasma membrane. A further cleavage of this C-terminal fragment by γ-secretase releases a small p3 peptide into the extracellular space and the APP intracellular domain (AICD) into the cytoplasm. In contrast, in the amyloidogenic pathway APP is first cleaved by β-secretase into soluble APP β (sAPPβ) which is released into the extracellular space and an APP C-terminal fragment which remains embedded in the plasma membrane. A further cleavage by γ-secretase results in Aβ and the AICD that are released into the extracellular space and the cytoplasm, respectively (Figure 1; (36, 39, 41, 42). Due to an imprecise cleavage by γ-secretase the cleavage within the transmembrane domain of APP can take place at multiple sites, resulting in C-terminally truncated peptides with different length (43-45). The main final Aβ forms are mostly ending at position 38, 40 or 42. In the cerebrospinal fluid of healthy controls, about 50 % of the Aβ ends at amino acid 40, 16 % ends at amino acid 38 and approximately 10 % with the alanine at position 42. The rest consist of many other minor cleavage sites at position 34, 37, 39, 43 or even shorter γ-secretase dependent isoforms named Aβ 1-17/18/19/20 have been detected (43, 46). Aβ1-42 is described to have a stronger tendency to aggregate and is the driving factor for the formation of Aβ plaques and neurotoxic effects (47).

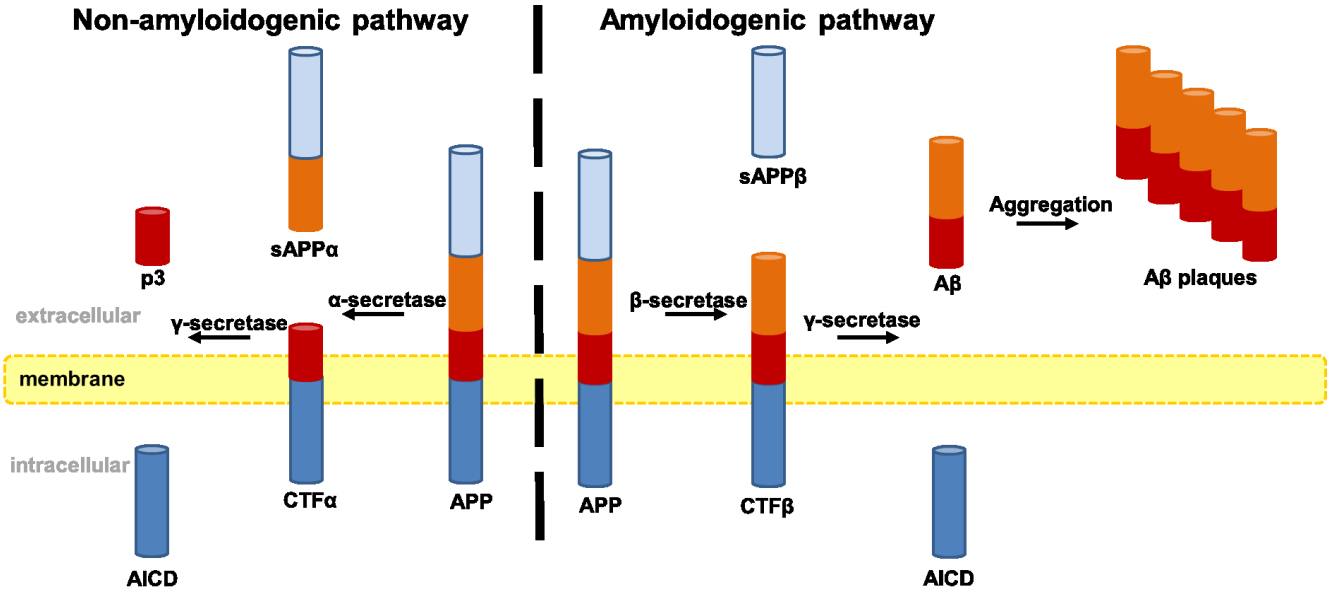

Figure 1: APP processing - the non-amyloidogenic pathway and the amyloidogenic pathway. APP intracellular domain (AICD), CTF (C-terminal fragment), soluble APP α (sAPPα), soluble APP β (sAPPβ).

Although the proteolytic processing of APP can lead to the pathological production of Aβ, generally the cleavage of transmembrane proteins is a physiological process (48). It is assumed that the primary pathological process is driven through an imbalance between Aβ production and clearance (16). It is still unknown how these pathways are regulated; however, many different factors like hormones or mutations seem to play an important role.

1.4 Modified and N-terminally truncated Aβ peptides

The aggregative and toxic potential of Aβ peptides may be driven by factors other than changes in the production of certain Aβ peptides and is thought to depend on the primary amino acid sequence as well as on posttranslational modifications (PTMs); (46). Many different PTMs such as oxidation, pyroglutamylation, phosphorylation, isomerization have been discovered which increase the aggregation rate of Aβ.

Moreover, N-terminal truncations of Aβ which also increase the propensity of Aβ to form aggregates are described in the literature (49). So far, a variety of different N-truncated peptides starting with amino residue alanine-2, pyroglutamylated glutamate-3, phenylalanine-4, arginine-5, histidine-6, aspartate-7, serine-8, glycine-9, tyrosine-10 and pyroglutamylated glutamate-11 have been identified. All these different forms cannot be explained by the cleavage of the above-mentioned secretases but have been observed in AD brains (50).

Although the precise enzymatic activities which lead to the generation of these N-truncated Aβ peptides are not known in detail, in most of the cases several different proteases (aminopeptidase A, meprin-β, neprilysin, angiotensin-converting enzyme, plasmin) and possibly involved cleavage sites have been reported (51).

One of the first reported truncated versions which is highly abundant in AD brains was the N-terminal truncated 4-x species (43, 52, 53). It is described that Aβ4-42 peptides are not produced under non-disease conditions, that they aggregate quickly and irreversible into soluble toxic oligomers, that they are more toxic compared to full-length Aβ1-42 *in vitro* and *in vivo* suggesting that these N-truncated Aβ4-42 peptides represent an ideal therapeutic target to be investigated in AD. These N-terminally truncated Aβ peptides have not only been described in human AD samples but have also been investigated in a variety of transgenic AD mouse models in recent years. Some of these transgenic APP mouse models produce N-truncated Aβ peptides, but in relatively small amounts, which do not reflect the situation in the AD brain. Others for example the Tg4-42 transgenic mouse model which overexpress Aβ4-42 with no mutation in the Aβ sequence is described to develop hippocampus-related reference memory deficits and consistently neuron loss but no plaque pathology was observed in these mice (51, 54).

1.5 Transgenic mouse models

Animal models of human diseases which accurately mimic disease pathology are crucial to understand molecular mechanisms and to advance preclinical studies. In recent years, many transgenic mouse models have been established to investigate the AD-related pathophysiology (55, 56). Although none of the AD transgenic mouse models fully replicates the human disease, the ability to study similar pathological processes in living animals has provided new insights into the pathogenesis of the disease (57). Several AD mouse models have been developed which represent relevant features of AD (58). Numerous groups developed first-generation transgenic mouse models which overexpress proteins linked to familial AD for example APP with or without mutations using various promotors (59). Some mice carry more than one mutation in the transgene and one of the most used mutations is the Swedish mutation which leads to an overproduction of total Aβ (60). Although these APP overexpressing mice exhibit the key features of amyloid pathology, several limitations are described. For example, Aβ species may appear that are different from those found in clinical AD brains, overproduced non-Aβ APP fragments interact unphysiologically with cellular proteins or due to the overexpression additional phenotypes that are unrelated to AD can appear. Due to these limitations second-generation mouse models were generated to

overproduce pathogenic Aβ such as Aβ42 without overexpressing APP (59). To achieve this, single APP knock-in mouse models were generated, in which the murine Aβ sequence was humanized by changing the three amino acids that differ between mice and humans and further introduce familial AD mutations into the endogenous mouse APP gene (61). These developed second-generation mice show Aβ accumulation without phenotype-related overexpression but they are not yet a clinical recapitulation of human AD (59, 62).

Within this thesis two different APP mouse models, namely the Tg4-42 mouse model (second-generation) as well as the APP_{SL} mouse model (first-generation) were investigated in detail.

The Tg4-42 mouse model was established in 2013 by Bouter et al. (53) and overexpresses human Aβ4-42 which leads to an intracellular Aβ accumulation in the brain of these mice. Subsequently, the secreted Aβ4-42 forms soluble, neurotoxic aggregates albeit without plaque formation. It is currently the only model which expresses N-truncated human Aβ4-42 without any other mutations. The Aβ4-42 peptide, which begins with a phenylalanine at position 4, is a particularly abundant form of N-truncated Aβ in the human brain. The inserted construct was fused to the murine thyrotropin-releasing hormone (TRH) signal peptide under the control of the Thy1 promotor, which leads to Aβ secretion in a neuron-specific manner. This mouse model does not express human APP which means that the effects of Aβ4-42 could not be influenced by APP or other cleavage products. Furthermore, these mice develop age-dependent severe synaptic impairments and neuronal loss as well as neuroinflammation indicated by micro- and astrogliosis (53, 63-65).

APP transgenic mice (APP_{SL}), over-express human APP751SL under control of the murine Thy-1 promoter. In this mouse model the human APP with London (717) and Swedish (670/671) mutations is expressed at high levels, resulting in an age-dependent increase of Aβ40 and Aβ42, the pathologically relevant forms of amyloid protein. Mice develop plaques consisting of amyloid depositions in early age, starting at 3 – 6 months in the frontal cortex. Severity of the brain pathology correlates with increasing age and behavioral deficits. Transgenic human APP_{SL} mice are a well-established mouse model which is suitable and frequently used to study the influence of drugs on amyloid production, sequestration and deposition as well as on memory (66-68).

1.6 Biomarkers in AD research

Biomarkers are widely used in basic and clinical research. Various definitions and also different classifications of biomarkers are described in the literature. A very common definition describes a biomarker as “a characteristic that is objectively measured and evaluated as an indicator of healthy biological processes, pathogenic processes or responses to an exposure

or therapeutic intervention" (69, 70). Moreover, biomarkers are defined as "any substance, structure, or process that can be measured in the body or its products and influence or predict the incidence or outcome of disease" (70, 71). The classification of biomarkers is based on different parameters such as imaging biomarkers (computed tomography, positron emission tomography, magnetic resonance imaging) or molecular biomarkers, including gene mutations, peptides, proteins, lipids, metabolites or other small molecules, which can be measured in biological samples. Biomarkers can also be classified based on their application as pharmacodynamic biomarkers which are markers of a certain pharmacological response or as disease prognosis biomarkers which are very common in cancer research (72). A large number of clinical studies reflect key elements of AD pathophysiology and measure CSF biomarkers like Aβ42, total tau and phosphorylated tau (73). However, the heterogeneity as well as complexity of LOAD calls for further biomarkers and investigations, understanding how perturbations in metabolism are related to AD neuropathology. For that reason *-omics* technologies may be a promising tool to investigate relationships between different pathways in AD and different pathologies.

1.7 NMR-based metabolomic phenotyping

Novel *-omics* technologies and platforms are establishing possibilities to measure biomarkers and range from the identification of genes (genomics), messenger RNA (mRNA, transcriptomics), epigenetic factors (epigenomics), to proteins (proteomics), lipids (lipidomics) and metabolites (metabolomics; 74, 75).

Metabolites are small molecules (<1,500 Da) involved in biological functions. The human metabolome is estimated to contain approximately 150,000 or more metabolites nevertheless, a large fraction of human metabolites is still undefined. Because of the diversity of sample composition and the complex nature of the human metabolome several analytical platforms and techniques have been developed for the quantification and characterization of these metabolites (76).

In last years, the two most commonly used analytical techniques in quantitative metabolomics are mass spectrometry (MS), often combined with chromatographic separation and nuclear magnetic resonance (NMR) spectroscopy (77-79). These approaches provide relatively high-throughput analyses and each method brings its own advantages and limitations. For instance, NMR spectroscopy is quantitative, reproducible and does not require extra steps such as separation or derivatization prior to measurement. But although the sensitivity has increased enormously it is still less sensitive compared to MS (77).

The analysis of metabolomics can be separated into the categories of untargeted or targeted analysis. Untargeted metabolic phenotyping is a powerful tool for mapping global biochemical changes in disease and treatment. In contrast to targeted biochemical approaches alone which focus on single metabolites, both approaches can simultaneously identify hundreds to thousands of metabolites. Disturbances in the metabolic network can help to better understand biochemical pathways, underlying disease progression and possibly provide complementary markers for the evaluation of mouse models for pre-clinical research (80-83).

1.8 Mitochondria as potential targets in AD treatment

To date only symptomatic pharmacological therapies for AD exist and the benefits are often marginal, nonpermanent and unfortunately only of limited success (84-86).

Many publications describe mitochondrial dysfunction as a key feature and hallmark of AD (87, 88). The described pathological processes and alternations in AD brains like Aβ peptides and plaques, NFTs, neuron loss or neuroinflammation are thought to cause oxidative imbalance suggesting that oxidative stress plays a major role in AD progression (89). Oxidative stress is defined as the redox state of a cell resulting in an imbalance between the generation and detoxification of reactive oxygen species (ROS; 90). ROS are broadly defined as oxygen-containing chemicals with reactive properties (91). They are unavoidable physiological byproducts in biological systems and can act as signaling molecules in controlled conditions (90). ROS can be produced enzymatically for example in macrophages to kill invaders or non-enzymatically, as a side reaction for example in the respiratory chain (92). Under healthy conditions ROS levels are kept relatively low and the rate of production and clearance is always in a balance (93).

Nevertheless, under pathological conditions like in AD, the brain is highly susceptible to oxidative imbalance. This is caused by its high energy demand and oxygen consumption, the rich abundance of easily polyunsaturating fatty acids, the high level of potent ROS catalyst iron, the relative deficit of antioxidants and related enzymes. In that condition ROS can lead to damage by oxidizing major biomolecules including nucleic acids like DNA / RNA, as well as proteins or lipids when presented in excess amounts (94). So it is no surprise that oxidative imbalance and as a consequence oxidative stress mediated damage to biomolecules is often reported in AD (93).

Furthermore, an enhancement in lipid peroxidation has been reported in AD. Lipid peroxidation is defined as a process where lipids are attacked by ROS through a free radical chain reaction mechanism to generate lipid peroxidation products. The most common lipid peroxidation

products which were found to be significantly increased in AD patients are reactive aldehydes like 4-hydroxynonenal (4-HNE), malondialdehyde (MDA) and acrolein (2-propenal; 93).
Mitochondrial dysfunction is a further pathological event which occurs in AD. The intact structure of mitochondria is essential to keep the proper electrochemical gradient. It is reported that mitochondria are the major source of endogenous ROS and that dysfunctional mitochondria are less efficient producers of ATP but more efficient producers of ROS (93, 95, 96).
All these described pathological events lead to the generation of toxic aldehydes, resulting in an accumulation of such highly reactive intermediates in the brain and blood.
Therefore, a mechanism for rapid clearance of highly diffusible and harmful aldehydes is crucial to protect cells and tissues from damage (93).
In particular, the detoxification by enzymes such as aldehyde dehydrogenase 2 (ALDH2) plays a key role in oxidizing endogenous aldehydic products. ALDH2, a mitochondrial enzyme is mainly responsible for detoxification of acetaldehyde or other reactive aldehydes derived from alcohol, food, drugs or endogenous metabolism to nontoxic products like acetate. Moreover, ALDH2 dysfunction is clinically associated with a variety of human diseases including neurodegenerative diseases, stroke or cancer.
For that reason, a variety of small molecule modulators of ALDH2 has been discovered with the effect to enhance the catalytic activity of ALDH2 which leads to an increased detoxification in cells (84). The here used compound is named AD-9308 which is a prodrug of a potent selective activator (AD-5591) of ALDH2. The parent compound and active metabolite, AD-5591 was found to promote ALDH2 activity. Thus, activation of the ALDH2 pathway could be a molecular target for AD (Figure 2).

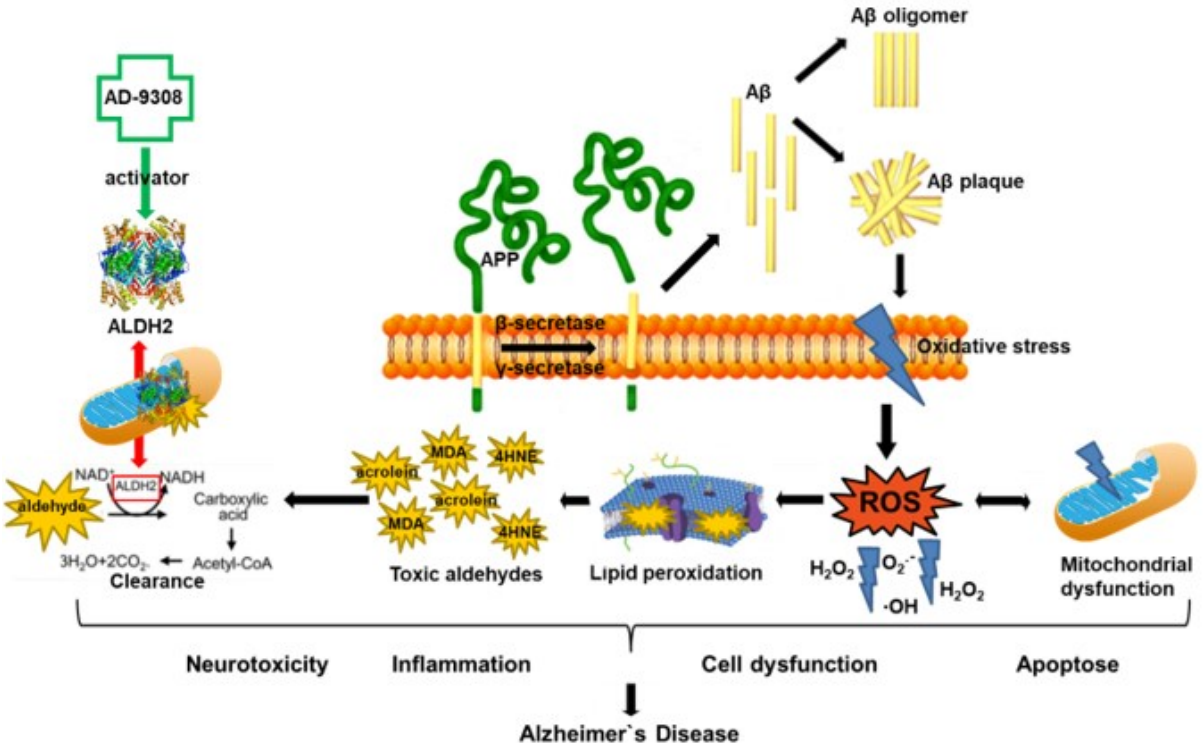

Figure 2: Graphic overview of pathological conditions described in AD and a proposed model of ALDH2 activation with AD-9308 as a molecular target for AD.

2 AIMS AND MOTIVATION

Several transgenic mouse models have been established in recent years to investigate Alzheimer-related pathophysiology. Although none of the AD transgenic mouse models fully replicates the human disease, the ability to study similar pathological processes in living animals provides new insights into the effects and underlying pathways of the disease and opportunities to test new therapeutic approaches. Despite general applicability of transgenic mouse models in basic and applied research, quantitative tools to monitor AD pathology as well as associated rewiring of metabolic pathways on a systemic level are still lacking. So, there is a critical need for a simple and accurate method to detect complementary markers for the evaluation of mouse models for preclinical studies and drug discovery in addition to the already established approaches.

This PhD project consists of two different parts. In both parts, NMR-based metabolic phenotyping was combined with already established approaches such as immunohistology, behavioral studies and biochemistry. The central aim of this thesis was to use NMR-based untargeted metabolic phenotyping for preclinical AD research in order to reveal changes in biomarkers and to draw conclusions about the human situation. Furthermore, this novel integrative approach was planned to be used to test the impact of a pharmaceutical compound on AD disease progression, to check whether therapeutic intervention causes changes in metabolites that can be detected by NMR.

In the first part of this thesis, a comprehensive characterization of the novel Tg4-42 mouse model using this integrative approach was performed to better understand the underlying disease mechanisms in this animal model of AD.

To reach this aim of the first part, 3, 6 and 9 months old Tg4-42 +/+ and NTG mice were analyzed in different behavioral tests like the Elevated Plus Maze, Open Field, Irwin and Morris Water Maze test to characterize the phenotype of this mouse model. As a next step untargeted metabolic phenotyping was carried out to evaluate involved metabolites and pathways and to monitor perturbations in a large pool of metabolites. Based on significantly altered biomarkers, further histological investigations were performed to validate NMR results.

To further analyze this mouse model downstream effects like neuroinflammation, Aβ42 levels as well as neurodegeneration were determined. As a next step sequencing analyses provided detailed information about the integration site of the Aβ4-42 transgene and additionally showed retinoic acid receptor beta (Rarb) knockdown, which questions the cause of the previously described phenotype of homozygous Tg4-42 mice to be solely dependent on Aß4-42 expression.

As it was not clear at this point whether this Rarb knockdown also has an impact on the phenotype of hemizygous Tg4-42 animals, it was decided to switch to a well-established APP overexpressing mouse model, the APP_{SL} mouse, for the second part of the project namely the drug evaluation study.

It is known that progressive loss of mitochondrial function or defects in mitochondrial metabolism in AD can lead to the generation of reactive oxygen species resulting in oxidation of membrane lipids and accumulation of toxic aldehydes such as 4-hydroxy-2-nonenal (4-HNE) in the brain and blood. Additionally, 4-HNE accumulates in the hippocampal region of patients with mild cognitive impairment and patients with early AD. The progressive accumulation of amyloid plaques correlates with neurodegeneration and subsequent atrophy of the affected brain regions (95, 96). Therefore, a mechanism for rapid clearance of these highly diffusible and harmful aldehydes is crucial to protect cells and tissues from damage. In particular, ALDH2 plays a key role in oxidizing endogenous aldehydic products that arise from lipid peroxidation under oxidative stress. It is therefore hypothesized that diminishing toxic aldehydes during the early stages of AD may reduce or prevent the disease progression.

Thus, the second aim of this thesis was to evaluate the effects of an ALDH2 agonist on AD disease progression in APP_{SL} mice by performing a drug evaluation study.

To reach this aim 7-month-old, male, hemizygous APP_{SL} mice and non-transgenic littermates received either an ALDH2 activator or vehicle via the drinking water for the duration of 2 or 4 months. The test substance was AD-9308, an ALDH2 activator that is supposed to increase the catalytic activity of ALDH2. This would result in reduced oxidative stress-induced cell and organ dysfunction. Also, in this part of the study different behavioral tests like the Elevated Plus Maze, Open Field, Y-maze, Irwin and Morris Water Maze test were performed after 2 and 4 months of treatment to evaluate compound effects on general health conditions, anxiety levels, spontaneous alternation as well as spatial learning behavior. Furthermore, metabolic phenotyping, biochemical assays as well as histological evaluations were performed to analyze treatment effects of the ALDH2 activator in APP_{SL} mice.

3 MATERIALS AND METHODS

Detailed formulations of used buffers and reagents are listed in the appendix section 8.1 reagents and chemicals.

3.1 Animals & schedule of *in vivo* phase

In the first study, the Tg4-42 mouse model which over-expresses Aβ4-42 under control of the neuron-specific Thy-1 promoter on a C57Bl/6J background was used. This mouse model was established by Bouter et al. in 2013 (53) and overexpresses human Aβ4-42.
Male homozygous (Tg4-42 +/+) and non-transgenic wild type (NTG) control mice used in the first part of the study are shown in Table 1.

Table 1: Overview of Tg4-42 +/+ and NTG mice

Age	**homozygous Tg4-42**	**NTG C57Bl/6J**
3 months	15 animals	15 animals
6 months	15 animals	15 animals
9 months	15 animals	15 animals

Only animals in apparently good health condition were included in the study. Randomization of group allocation were done per cage. Because the number of animals in a starting group (cohort) is limited to ensure the same age and uniform handling, the animals were assigned to three different cohorts each comprising animals of each group. Cohorts were started approximately 1 month apart. The *in vivo* phase of all three cohorts was assigned as shown in Table 2.

Table 2: In vivo behavioral test schedule of Tg4-42 +/+ and NTG mice

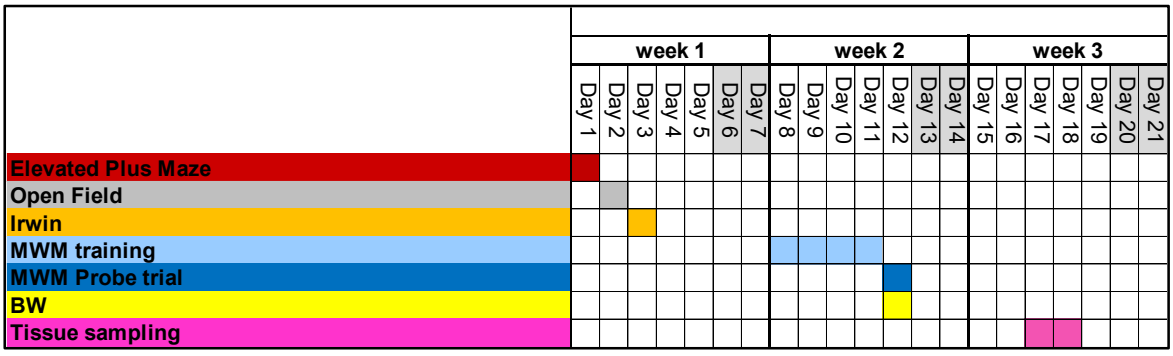

In the second part of this study APP transgenic mice (APP_{SL}), which over-express human $APP751_{SL}$ under the control of the murine Thy-1 promoter were used. In this mouse model the human APP with London (717) and Swedish (670/671) mutations are expressed in high levels. For this part of the study 51 male APP_{SL} transgenic mice and 29 non-transgenic (NTG) littermates were bred at QPS Austria and used starting at the age of 7 months.

Before the start of the study, the compound sponsor provided any relevant information regarding the stability of the test item/adjuvant under storage and test conditions as well as any known risk involved.

At study start all animals were single housed. Test item or vehicle was administered orally in drinking water for 2 or 4 months. All bottles were changed once a week. Body weights of all animals and the bottle weights were recorded once a week. Thus a minimal loss of test item and a smallest possible error of water consumption were ensured. The consumption of each animal was calculated as follows: *bottle weight at start – bottle weight after 7 days) / number of days.* Detailed treatment information is listed in Table 3.

Table 3: Treatment information

Name of the Test item.:	AD-9308 (Foresee-Pharma)
Vehicle:	Water
Treatment dosages:	50 mg/kg/day
Administration:	Oral via drinking water
Remarks:	Estimated drinking volume 5 to 7.5 ml per animal per day

Before study start an initial health check was performed with all animals to ensure that all mice are in an apparently good health condition. After that 7 transgenic APP_{SL} mice and 7 non-transgenic littermates were allocated to the baseline group and sampled at study start. Further 7 animals of each of the three different treatment groups (A-C) were treated for 2 months tested in a series of behavioral tests and sacrificed. Animals of group D - F were treated for 4 months and tested in the same behavior tests after 2 months of treatment and tested again in other behavior tests after 4 months. Animals were also sacrificed and tissue of all groups was collected for biochemical and histological analyses. Detailed information about group allocation is shown in Table 4.

Table 4: Group allocation

Group	Genotype	N	Treatment	Duration of treatment
Baseline TG	APP_{SL} TG	7	-	-
Baseline NTG	APP_{SL} NTG	7	-	-
A	APP_{SL} TG	7	AD-9308 50 mg/kg/day	2 months
B	APP_{SL} TG	7	Placebo	2 months
C	APP_{SL} NTG	7	Placebo	2 months
D	APP_{SL} TG	15	AD-9308 50 mg/kg/day	4 months
E	APP_{SL} TG	15	Placebo	4 months
F	APP_{SL} NTG	15	Placebo	4 months

Randomization of group allocation were performed for the behavioral testing. Because the number of animals in each cohort was limited to ensure the same age and uniform handling animals were staggered in two cohorts comprising animals of each group. Cohorts were started approximately 1 month apart. The *in vivo* phase of both cohorts was assigned as shown in Table 5.

Table 5: Overview of in vivo phase of the treatment study

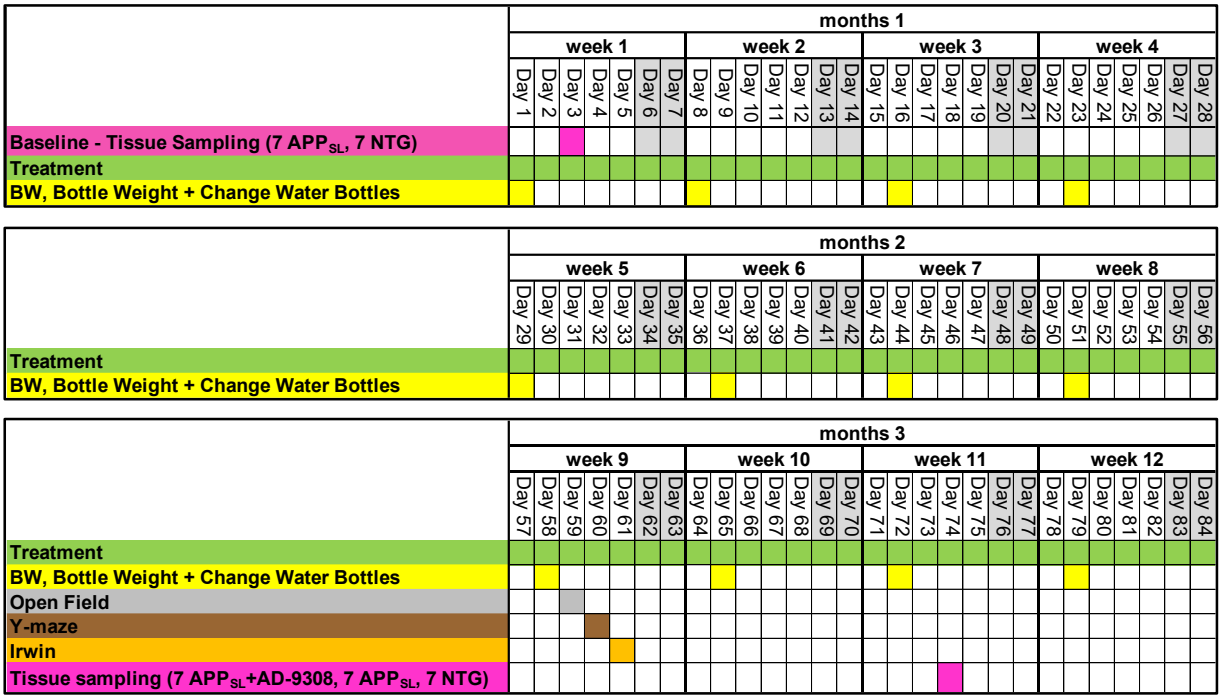

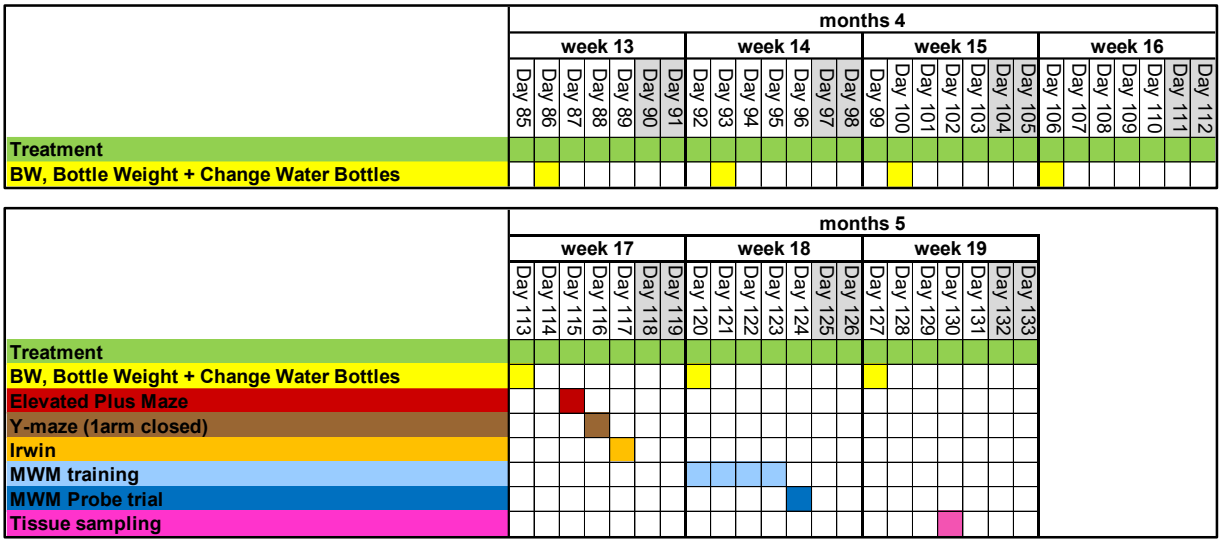

3.2 Animal housing and identification

Animals were housed in individually ventilated cages on standardized rodent bedding supplied by Rettenmaier, Germany. Each cage contained a maximum of five mice of the same sex. In both studies only male mice were used. The room temperature was maintained at approximately 21 °C and the relative humidity was maintained between 40 to 70 %. Animals were housed under a constant light/dark-cycle (lights on at 6:00 a.m. and lights off at 6 p.m. Central European Summer Time). Dried, pelleted standard rodent chow (Altromin, Germany) as well as normal tap water was available to the animals ad libitum. Animals were numbered consecutively by classical ear punching. Each cage was identified by a colored card indicating the study number, sex, the individual registration numbers (IRN) of the animals, date of birth, as well as the genotyping date and the group allocation. The genotype (transgenic or non-transgenic) of each animal was determined by polymerase chain reaction specific for the transgenic construct. Each mouse was genotyped twice using DNA isolated from ear punch tissue and tail tips prior to study start.

Only animals in apparently good health condition were included in the study. All animals were randomly assigned to starting groups (cohort).

All experiments including animal tissue were performed in accordance with the Austrian guidelines for the care and use of laboratory animals (Tierversuchsgesetz 2012-TVG 2012, BGBl. I Nr. 114/2012). Animal housing and euthanasia were approved by the Styrian government (Amt der Steiermärkischen Landesregierung, Abteilung 13 – Umwelt und Raumordnung Austria; ABT13-78Jo115/2013-2016; ABT13-78Jo-118/2013-13).

3.3 Behavioral analysis

All behavioral tests were performed during the early phase of the light cycle and animals were habituated to the experimental room for at least one hour prior to testing.

3.3.1 Evaluation of the health status and motor abilities with the Irwin test

An Irwin test was performed prior to any behavioral investigation, to test and survey general health conditions of each mouse (200). Using this test battery, physical characteristics and conspicuities, sensorimotor reflexes and motor abilities were evaluated. The collected physical characteristics were body weight, constitution of the fur and the eyes, existence of whiskers as well as individual remarks (e.g. bites or other lesions). Furthermore, whiskers-orienting, righting, ear twitch, eye blink and pupillary reflexes were evaluated. The wire suspension time was calculated and the vertical pole test was carried out. Piloerection, exophthalmos, and palpebral closure were measured and the presence of bald patches was assessed. The righting reflex was evaluated by turning the mouse onto its back. Normal mice immediately turned themselves over to right themselves onto all four feet. Other basic neurological reflexes measured were the eye blink, ear twitch and whisker-orienting responses to an approaching cotton swab or light brush, respectively. The pupillary reflex is a simple measurement to evaluate visual abilities via the response to light. The beam of a small flashlight was directed to the eye. Pupil contraction occurs immediately, followed by pupil dilation when the light is removed. With the calculated wire suspension time, it is possible to detect neuromuscular abnormalities as measure of motor strength. For this test, a wire cage lid was used where duct tape was placed around the perimeter to prevent the mouse from walking off the edge and the animal was placed on the top of the cage lid. The lid was lightly shaken three times to force the mouse to grip the wires and then the lid was turned upside down. The lid was held at a height of approximately 20-30 cm above a soft underlay, high enough to prevent the mouse from jumping down, but not high enough to cause harm in the event of a fall. The latency to fall off was quantified but a 300-second cut-off time was used in this test, although a normal mouse can hang upside down for several minutes. The vertical pole test was a further measurement of motor coordination and balance. For that test, a wooden pole (2 cm diameter) was wrapped with cohesive tape for improved traction. The mouse was placed in the center of the pole, which was held in horizontal position. The pole was lifted to a vertical position. The latency to fall off the pole was the dependent variable. Healthy mice stay on the pole and may walk up or down the length of the pole. Deficits in motor coordination and balance are detected by falling off before reaching a 45°angle.

3.3.2 Open Field test (OF)

This test is widely used to analyze locomotion, anxiety, as well as stereotypical behaviors such as grooming and rearing in rodents (97). For the present investigation, a Plexiglas Open Field (48x48 cm; TSE-System®) was used. The infrared photo beams were placed in a 1.4 cm distance around the box. To detect rearing (standing on the hind paws) another row of photo beams were mounted 4 cm above the first one. Each test session lasted for 20 minutes to check the mouse' behavior in the new surroundings. Parameters like activity, hyperactivity, distance, thigmotaxis and rearing duration were evaluated. Thereafter the number of fecal boli was counted as a measure of emotionality. The Open Field was cleaned with 70 % ethanol after each mouse to remove odor traces. Testing was performed under standard room lighting conditions during the light phase of the circadian cycle.

3.3.3 Elevated Plus Maze test (EPM)

The elevated plus maze (EPM) is at present one of the most widely used tests to study anxiety in small rodents (98). This test is based on the aversion of rodents to open spaces and height. The equipment is a four arm maze with two opposing open arms and two opposing closed arms (sheltered arms, with walls), raised 50 cm above the surface. The test took place under red light illumination. The mouse was placed in the center area facing the open arm. The behavior during the test session was recorded for five minutes and behavioral parameters were calculated such as time spent in the open and in the closed arms, number of visits in the open and closed arms as well as the latency to enter the open arm. Data were generated by using Noldus Ethovision XT software.

3.3.4 Modified Y-Maze test

The modified Y-maze test was performed to measure spontaneous alternation behavior. Alternation reflects the motivation of the animal to explore its environment. Animals do not need to be deprived of such resources to show alternating behavior. In this case, it is called 'spontaneous alternation' which is superb at detecting hippocampal dysfunction.

The Y-maze apparatus consists of three identical white arms (length x width x height = 38 x 6.5 x 13 cm). The testing was performed under standard room light conditions. To avoid odor traces the maze was cleaned with 70 % isopropanol between animals. The process was video recorded and analyzed using Videomot 2 provided by TSE systems, Bad Homburg, Germany. The sequence of arm entries as well as number of total arm visits were recorded automatically. In the discrete trial procedure, there are two phases in each trial: a sample phase, this is the information gathering phase where the animal runs to one goal arm of the maze and a memory

trace of this event is formed. A choice phase, the animal's choice between the sampled and unsampled arms may or may not be guided by the memory of recently visiting the former arm. The animals have a free choice of goal arm on both the sample and choice trials. The advantage of a free choice procedure is that hippocampal-lesioned animals often develop a side preference and can therefore score below 50 % (the minimum achievable on a balanced left/right forced schedule) and so the control-hippocampal difference could be larger.

The mouse was placed in the start area, allowing to choose a goal arm and was confined in the chosen arm by quietly sliding the door down. After 30 sec, the animal was removed as gently as possible and the guillotine door of the sample arm was raised. After that the animal was replaced in the start area facing away from the goal arm. Mice were then allowed to choose between the two open goal arms. These two trials were performed 5 times with each animal.

An alternation was defined as entering each of the two arms of choice consecutively and the percentage or proportion of correct alternations per animal was calculated.

3.3.5 Morris Water Maze test (MWM)

Spatial learning capacities and memory of all animals were tested in the Morris Water Maze (MWM). Animals were randomly placed at three different starting positions in a circular pool with a diameter of 100 cm filled with water (22 ± 1 °C). Mice had to find an invisible platform which was always placed on the same position of the pool. Visual cues displayed on the wall helped the mice to orientate. Light conditions were kept constant at 60 ± 5 Lux.

The MWM was performed using the following protocol: Four trials on each of four consecutive days were performed. In all trials, the platform was located in the northeast (NE) quadrant of the pool. Mice started from predefined positions (southeast (SE), southwest (SW), northwest (NW), see Table 6). A single trial lasted for a maximum of 60 seconds. In case the mouse did not find the hidden, diaphanous platform within this time, the experimenter guided the mouse to the target. Mice were allowed to rest on the platform for 10-15 sec to orientate in the surroundings.

On day five mice were tested in the probe trial (PT). During the PT, the platform was removed from the pool and the number of crossings over the former target position as well as the abidance in the target quadrant was recorded. For the quantification of escape latency (the time [sec] to find the hidden platform), of distance travelled (the length of the trajectory [meter] to reach the target), of target zone crossings and of the abidance in the target quadrant in the PT, a computerized video tracking system (Biobserve Viewer III) was used.

Table 6: Starting positions of the different days and trials

	Trial 1	**Trial 2**	**Trial 3**	**Trial 4**	**PT**	**Plat-form**
Day 1	SW	SE	NW	SW	-	NE
Day 2	NW	SE	SW	NW	-	NE
Day 3	SW	NW	SE	SW	-	NE
Day 4	SE	SW	NW	SE	-	NE
Day 5	-	-	-	-	SW	NE

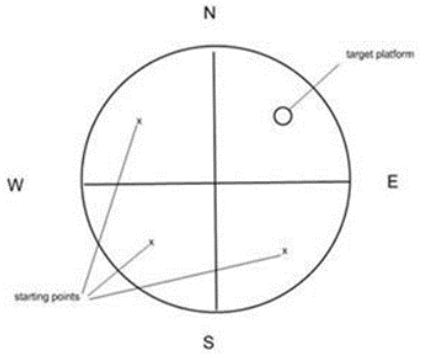

3.4 Tissue sampling and sample preparation for biochemical and histological analyses

All animals were euthanized either at baseline or after the behavioral tests by pentobarbital injection (600 mg/kg). Blood, CSF, brain and in study part two also organs like spleen, liver, kidneys, heart and lungs were collected.

CSF collection was obtained by blunt dissection and exposure of the foramen magnum. Upon exposure, a Pasteur pipette was inserted to the approximate depth of 0.3 - 1 mm into the foramen magnum. CSF was collected by suction and capillary action until flow fully ceased. Samples were immediately frozen on dry ice and stored at -80 °C until further analysis.

For blood collection the thorax was opened and blood was collected by heart puncture with a 23-gauge needle. The blood was transferred to a serum sample tube (Serum Z-Gel 1.1 ml, brown, 485.41.1378.005, Biomats, Norway) and inverted thoroughly.

To collect brains and organs, all mice were transcardially perfused with 0.9 % saline. For this purpose a 23 G needle connected to a bottle containing 0.9 % saline was inserted into the left ventricle of the heart. The right ventricle of the heart was opened with scissors. A constant pressure of 100 to 120 mm Hg was maintained on the perfusion solution by connecting the solution bottle to a manometer-controlled air compressor. Perfusion was continued until all tissues (e.g. liver) completely turned pale and no visible blood passed out of the right heart ventricle. Thereafter, brains were removed and hemisected.

Left brain hemispheres from all animals were dissected in cortex, hippocampus, cerebellum, striatum and rest brain, weighed and immediately frozen and stored at -80 °C for biochemical analyses.

Some of the right brain hemispheres were fixed by immersion in freshly prepared 4 % paraformaldehyde in PB (pH 7.4) for two hours at room temperature (RT). Thereafter, right hemispheres were transferred to a 15 % sucrose PBS solution until sunk to ensure cryo-

protection. On the next day, fixed hemispheres were frozen, embedded in OCT media within cryo-molds in dry-ice cooled liquid isopentane and stored at -80 °C until used for histological analysis.

All organs (heart, liver, kidneys, spleen, lung) were transferred to pre-labeled tubes, immediately frozen and stored at -80 °C.

3.5 Biochemical methods

3.5.1 Targeted Locus Amplification and sequence alignment

Targeted Locus Amplification (TLA) of Tg4-42 mice was performed by Cergentis (Utrecht, Netherlands) as previously described (99). During the analysis by Cergentis, PCR products were purified and library-prepped using the Illumina NexteraXT protocol and sequenced on an Illumina Miseq sequencer. Reads were mapped using BWA-SW, which is a Smith-Waterman alignment tool. This allows partial mapping which is optimally suited for identifying break spanning reads. For mapping the mouse genome, mouse genome assembly version mm9 (MGSCv37) was used by this company (100). The complete gene sequencing report can be found in the appendix.

3.5.2 mRNA analyses (RNA extraction, cDNA synthesis and quantitative PCR)

Total striatal RNA was extracted using peqGOLD TriFast Kit according to the manufacturers protocol (VWR Life Science, Erlangen, Germany). 1 µg of total RNA was reverse transcribed into single stranded cDNA using iScript gDNA Clear cDNA Synthesis Kit according to the manufacturers protocol (Bio-Rad Laboratories, Hercules, USA). Quantitative RT-PCR (qPCR) was performed with Bio-Rad CFX Connect thermo cycler using Takyon No Rox SYBR MasterMix dTTP Blue according to the manufacturers protocol (Eurogentec, Seraing, Belgium) with the primers (Microsynth, Balgach, Switzerland) listed in *Table 7*. The ΔΔCq method was applied to calculate the relative fold-change in gene expression after normalization to HPRT (Hypoxanthin-Guanin-Phosphoribosyl-Transferase).

All PCR amplifications were performed in a total volume of 20 µl, containing 2 µl of cDNA, 10 µl of 2x Takyon SYBR mix, 1 µl of each primer and 6 µl of aqua bidest. The amplification protocol consisted of an initial denaturation at 95 °C for 3 min, followed by 39 cycles of denaturation at 95 °C for 10 sec, annealing at 60 °C for 30 sec and extension at 72 °C for 30 sec (100).

Table 7: List of PCR primers

Gene	Primer Sequence
RARB primer pair 1	F: GCCTCTGGGACAAATTCAGT R: GTCAGTCAGAGGACCGAAGC
RARB primer pair 2	F: CTGCTTCGTTTGCCAGGACA R: GGAAAAAGCCCTTGCACCC
RARB primer pair 3	F: CGAAAGGTGCCGAACGTGTA R: TGAACTTGGGGTCAAGGGTT
HPRT	QuantiTect Primer Assay HPRT_1 (Quiagen, Germany)

RARB: Retinoic acid receptor beta; F: Forward primer sequence; R: Reverse primer sequence; HPRT: Hypoxanthin-Guanin-Phosphoribosyl-Transferase (100).

3.5.3 Protein sample preparation

Mouse striatal samples were weighted and lysed in 15 volumes RIPA buffer and sonicated with the Ultra-Turrax for 30 sec. Afterwards tissue homogenates were centrifuged at 20,000 x g at 4 °C for 10 min to remove insoluble material. The protein concentration of the supernatant was determined using Pierce BCA protein assay kit according to the manufacturers protocol (Thermo Scientific, USA). For capillary simple Western blotting homogenates were diluted to 0.65 mg protein/ml sample, using sample buffer (100).

3.5.4 Simple Western blot system

Samples were prepared and analyzed according to the manufacturer`s instructions (Protein Simple, San Jose, USA). Briefly, four volumes of sample were mixed with one volume of fluorescent 5x Master Mix (Protein Simple) and denatured at 95 °C for 5 min. Primary antibodies against retinoic acid receptor beta 2 (sc-514585; Santa Cruz Biotechnology, Heidelberg, Germany) and Glycerinaldehyde-3-phosphate-dehydrogenase (GAPDH; G9545; Sigma-Aldrich, St. Louis, USA) were diluted 1:10 (RARB) and 1:100 (GAPDH) in antibody diluent 2. The samples, biotinylated ladder, primary antibodies, secondary antibodies, chemiluminescent substrate, Stacking Matrix 2 and the Separation Matrix 2 (12-230 kDa; supplied by the manufacturer) were dispensed into the assay plate. After adding Simple Western assay buffer subsequent separation, immunodetection and analysis steps were performed automatically and digitally by the Wes System.

"Compass for SW" software (Protein Simple version 4.0.0), the data analysis application for Simple Western instruments, was used to visualize Simple Western lanes digitally, automatically analyze signal peaks and calculate the area under the curve of the peak of interest (100).

3.5.5 Measurement of inflammation markers

Homogenized tissue samples were diluted 1:2 and analyzed for various cytokines (IFN-γ, IL-1β, IL-2, IL-4, IL-5, IL-6, KC/GRO, IL-10, IL-12p70, TNF-α) with a commercially available immunosorbent assay kit (V-plex Proinflammatory Panel 1 (mouse) K15048D, Mesoscale Discovery) according to the instructions of the manufacturer. Briefly the plate was washed 3 times with 150 µl/well of wash buffer. Then 50 µl of prepared samples, calibrators and controls were added per well. The plate was sealed and incubated at RT with shaking for 2 h. After that the plate was washed 3 times (150 µl/well of wash buffer) and 25 µl detection antibody solution was added to each well. The plate was sealed and incubated with shaking further 2 h at RT. Plate was washed again 3 times (150 µl/well of wash buffer), 150 µl 2x Read Buffer T was

added to each well and then the plate was read on an MSD instrument. Data were evaluated in comparison to standards provided in the kit and were expressed as pg/ml.

3.5.6 Aβ1-38, Aβ1-40 and Aβ1-42 measurements

Left cortex samples were homogenized in tissue homogenization buffer, aliquoted and stored at -80 °C until further use.

For extraction of non-plaque associated proteins, THB homogenate was mixed with 1 part diethylamine (DEA) solution (0.4 % DEA, 100 mM NaCl). The mixture was centrifuged for 120 min at 20,000 x g at 4 °C. The supernatant was neutralized with 1/10 of the volume 0.5 M Tris-HCl, pH 6.8, vortexed briefly and stored at -20 °C.

For extraction of deposited proteins, THB homogenate was mixed with 2.2 parts cold formic acid (FA), sonicated for 30 sec on ice and centrifuged for 120 min at 20,000 x g at 4 °C. The supernatant was mixed with 19 parts FA Neutralization Solution, vortexed briefly and stored at -20 °C.

Aβ1-38, Aβ1-40 and Aβ1-42 were measured in the DEA and FA fractions from cortex samples using an immunosorbent assay (Aβ Peptide Panel 1 (6E10); K15200E-2; Meso Scale Discovery) according to the instructions of the manufacturer. In brief 150 µl of diluent 35 were added to each well. The plate was sealed and incubated at RT with shaking for 1 h. Then the plate was washed 3 times with 150 µl/well wash buffer. After that 25 µl of detection solution and 25 µl of prepared samples, calibrators or controls were added to each well. The plate was sealed and incubated at RT with shaking for 2 h. The plate was washed again 3 times (150 µl/well of wash buffer), 150 µl 2x Read Buffer T was added to each well and then the plate was read on an MSD instrument. Aβ levels were evaluated in comparison to standards provided in the kit and are expressed as pg per mg brain wet weight.

3.5.7 Detection of murine Neurofilament light chain (NF-L)

The NF-light® (Neurofilament-light) ELISA 10-7001 CE from UmanDiagnostics was used for analysis of Neurofilament-light chain levels in serum samples.

Samples were diluted 1:15 in sample diluent and analyzed according to the manufacturers protocol. In brief, after dilution 50 µl of the sample was added to the pre-coated well and incubated for 1 h at RT with gentle agitation on a vibratory plate (800 rpm). Wells were washed three times with assay wash buffer and 100 µl of the tracer antibody was added. After 45 min incubation (RT, 800 rpm) wells were again washed three times. Thereafter 100 µl of conjugate were added and incubated for 30 min (RT, 800 rpm). After 3x washing, 100 µl of TMB substrate were added to each well and incubated for 15 min at RT. 50 µl stop reagent was added and

after short gentle agitation, the plate was read at 450 nm (reference wavelength 620-650 nm) on the µQuant reader (Biotek, Vermont, USA).
Data were evaluated in comparison to standards provided in the kit and were expressed as pg/ml medium.

3.5.8 TBARS assay

For lipid peroxidation measurements, a standard calibration curve was prepared by a serial dilution of 1,1,3,3-Tetramethoxypropane (TMP) in 0.9 % NaCl. Subsequently, 1 µl butylated hydroxytoluene (BHT) stock solution (0.5 M) was added to 100 µl brain homogenate or standard sample. Then, 50 µl TBA working solution (1.33 % thiobarbituric acid) and 100 µl 20 % acetic acid pH 3.5 were added before vortexing and incubating the samples for 1 h at 95 °C. After cooling the samples to RT, 250 µl butanol/pyridine (15:1 v/v) were added per sample before vigorous vortexing. After centrifugation at RT for 4 min at 10,000 x g, 200 µl of the upper organic phase containing the red dye were transferred to a black 96 well plate and fluorescence was determined using a fluorometer (485 nm excitation, 535 nm emission).

3.5.9 Measurement of complex 1 activity

For the measurement of complex I activity, a colorimetric assay from abcam (ab109721) was used. The left hippocampus was used for complex I analysis.
Tissue homogenates were prepared as described in the complex I assay manual (abcam ab109721) by homogenization of the tissue with the tissue ruptor in PBS with the addition of 1x protease inhibitor cocktail (Millipore/539131-10VL). Thereafter protein concentrations were adjusted (1.1 mg/ml) and samples treated with detergent as described within the manual. After centrifugation for 20 min at 4 °C at 15,000 x g, the supernatant was collected and stored at -80 °C until measurement.
For the measurement, samples were loaded onto the plate in duplicates (40 µg total protein/well) and after initial incubation for 3 h and three washing steps with wash buffer, the working reagent was added and kinetics were recorded at 450 nm for 30 min in 3 min intervals.

3.5.10 Reactive Oxygen Species (ROS) assay

For ROS measurement, the hippocampal homogenates generated for the complex I activity assay were used. Samples were loaded in duplicates onto a dark plate (20 µg total protein/well) and DCFDA (D6883, Sigma-Aldrich, St. Louis, USA) was added to the wells. After incubation for 30 min at 37 °C the plates were read with the Spectra Fluor microplate reader (Tecan, Austria) with 485 nm excitation and 538 nm emission filters.

3.5.11 4-Hydroxy-2-nonenal (4-HNE) assay

For measurement of 4-HNE, an assay kit from abcam (ab238538) was used. The right hippocampus, right cortex and serum were used for 4-HNE analysis.

Tissue homogenates were prepared by homogenization of the tissue with UPHO tissue homogenizer (Geneye, Sheung Wan, Hong Kong) in 10 volumes of PBS. Thereafter samples were diluted with PBS/0.1 % BSA and the assay was performed as described in the manual. In brief, after dilution 50 µl of the sample was added to the pre-coated wells and incubated for 10 min at RT with gentle agitation (700 rpm). Then 50 µl of the diluted anti-4-HNE antibody was added to each well and incubated for 1 h at RT with gentle agitation (700 rpm). Wells were washed three times with assay wash buffer and 100 µl of the tracer antibody were added. After 1 h incubation (RT, 700 rpm) wells were again washed three times. Thereafter 100 µl of substrate solution were added and incubated for 2-20 min (RT, 700 rpm). After color changing, 100 µl stop solution were added and after short gentle agitation, the plate was read at 450 nm (reference wavelength 620-650 nm) on the µQuant reader (Biotek, Vermont, USA). Data were evaluated in comparison to standards provided in the kit and are expressed as µg/ml.

3.6 Histological analyses

3.6.1 Cryo-sectioning

Eight cryosections per level (5 levels in total) were sagittally cut at 10 µm thickness on a Leica CM3050S cryotome. The next 52 sections per level were discarded. Sectioning levels were chosen according to the brain atlas of Paxinos and Franklin “The Mouse Brain in Stereotaxic Coordinates” (199). Collection of sections started at ~0.5 mm lateral from midline and extended through the hemisphere in order to ensure systematic random sampling through the target regions (Figure 3). Sections were stored at -20 °C.

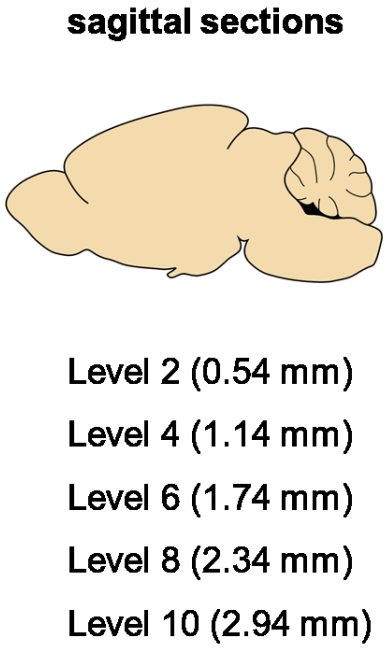

Figure 3: Used levels for immunofluorescent labelling of medio-sagittal sections obtained following the sectioning protocol.

3.6.2 Immunofluorescent labelling

Cryosections were air-dried for 45 min, washed in PBS for 10 min, treated with a freshly prepared 1 mg/ml sodium borohydride/PBS solution for 4 min, washed in PBS again and subsequently blocked with M.O.M. blocking reagent (BMK-2202, Vector Laboratories, Burlingame, California, USA) in 0.1 % TritonX-100/PBS for 60 min in a humid chamber. After that, sections were washed 3 times for 5 min in PBS and incubated with primary antibodies (see Table 8) in M.O.M. diluent (Vector Laboratories) over night at 4 °C in a humid chamber. Binding of the primary antibody was visualized using highly cross-absorbed labeled secondary

antibodies (see Table 9) for 60 min in a humid and light-protected chamber at RT. After further 3 washing steps in PBS, slides were incubated with 4`,6-Diamidin-2-phenylindole (DAPI, A1001.0025, AppliChem GmbH, Darmstadt, Germany) for 15 min to label cell nuclei and afterwards covered with Mowiol (81381, Sigma-Aldrich, St. Louis, USA) and cover slips using a Leica CV5030 coverslipper.

Table 10: List of antibodies used for immunofluorescent labelling

Antibody/ Fluorophore	**Primary/ Secondary**	**Manufacturer**	**Item number**	**Host**	**Dilution**	**Incubation**
GAD67	primary	Synaptic Systems	198006	chicken	1:800	1
Glutaminase	primary	Abcam	Ab93434	rabbit	1:1000	1
NeuN	primary	Synaptic Systems	266004	guinea pig	1:2000	1, 3
GFAP	primary	Merck Millipore	MAB360	mouse	1:2000	2
Iba-1	primary	Synaptic Systems	234004	guinea pig	1:2000	2
Aβ1-42	primary	Invitrogen	700254	rabbit	1:1000	2
GFAP	primary	Abcam	ab53554	goat	1:300	3
Iba-1	primary	Synaptic Systems	234013	rabbit	1:5000	3
Aβ (6E10)	primary	Bio Legend	SIG-39320	mouse	1:1000	3
anti-rabbit Alexa Fluor 555	secondary	Abcam	ab150066	donkey	1:500	1
anti-chicken Alexa Fluor647	secondary	Jackson ImmunoResearch	703-605-155	donkey	1:500	1
anti-guinea pig Alexa Fluor 488	secondary	Jackson ImmunoResearch	706-545-148	donkey	1:500	1, 3
anti-mouse DyLight 488	secondary	Abcam	ab98794	donkey	1:500	2
anti-guinea pig Alexa Fluor 647	secondary	Jackson ImmunoResearch	706-605-148	donkey	1:500	2
anti-rabbit Alexa Fluor 555	secondary	Abcam	ab150066	donkey	1:500	2
anti-goat DyLight 550	secondary	Abcam	ab96936	donkey	1:500	3
anti-mouse DyLight 755	secondary	Thermo Scientific	SA5-10171	donkey	1:500	3
anti-rabbit DyLight 650	secondary	Abcam	ab96922	donkey	1:500	3

Incubation 1 & 2 were performed on Tg4-42 and incubation 3 on APP_{SL} tissue slides.
Mosaic images of the labelled sections were recorded on a Zeiss automatic microscope AxioScan Z1 with high aperture lenses, equipped with a Zeiss Axiocam 506 mono and a Hitachi 3CCD HV-F202SCL camera and Zeiss ZEN 2.3 software.

3.6.3 Quantitative evaluations

Image analysis was performed with Image Pro 6 (Media Cybernetics). Target areas (cortex, hippocampus and striatum) were identified by drawing an area of interest (AOI). If necessary, a second AOI excluded wrinkles, air bubbles, or any other artifacts interfering with the measurement and defined the area for quantitative image analysis.

Afterwards, parameters for the detection of the targeted objects were defined in a test run. The determined parameters were then used for quantitative image analysis of all images. Edge Plus filtering was used to correct for background signal and to facilitate detection of immunoreactive objects. Detection of immunoreactive objects was carried out by applying adequate thresholding and morphological filtering (size and shape factors). The image analysis was macro-based and ran automatically so that the results are operator-independent and fully reproducible

Raw data were organized and sorted in Excel, and then transferred to GraphPad Prism for statistical analysis and preparation of graphs.

3.7 NMR-based metabolic phenotyping

3.7.1 Sample preparation for NMR-based metabolomic phenotyping

Tissues of different brain regions or organs were weighted in tubes with Precellys ceramic beads for soft homogenization. Normalized to the weight, approximately 1 ml 4 °C cold methanol / MiliQ H_2O (2:1) was added to precipitate proteins. Then the tissue was homogenized with the Precellys instrument (2 x 20 sec), followed by a centrifugation step for 60 min at 4 °C at 13,000 rpm. After that the supernatant was pipetted in a new tube, freeze-dried, diluted in 500 µl NMR-based metabolomics buffer with an internal standard and transferred into NMR tubes for measurement.

For biofluids, like serum, double volume of 4 °C cold methanol was added for precipitation of proteins (400 µl MeOH + 200 µl serum), followed by a centrifugation step for 30 min at 4 °C at 13,000 rpm. All further steps were similar to the tissue sample preparation as described above.

3.7.2 NMR measurement

To receive a biochemical profile of animal samples, one-dimensional ^1H NMR measurements were recorded at 310 K on an Avance Neo Bruker Ultrashield 600 MHz spectrometer equipped with a TXI probe head with Bruker Topspin version 4.0.2. For one-dimensional experiments the cpmgpr 1 d pulse sequence (Bruker, size of fid 73728, 11904.76 Hz spectral width, 128 scans, d 1 = 4 s and L4 of 128) was used. Chemical shifts were reported in parts per million (ppm). For chemical shift referencing (set to 0 ppm) TSP (Sodium trimethylsilyl [2,2,3,3-$^2H_4$] propionate) was used as internal standard.

3.7.3 Analysis of NMR measurements with statistical tools

NMR raw data were processed and a phase and baseline correction was performed. For the statistical analysis of these complex data, Matlab software was used to perform Principal Component Analysis (PCA) as well as Orthogonal-Partial Least Square-Discriminant Analysis (O-PLS-DA). Therefore, NMR raw data were imported into Matlab, water (δ 4.45-5.15), MeOH (δ -3.39 – 3.41) and TSP (δ -0.2 – 0.2) signals were excluded and data points were aligned using the setup for NMR-based metabolomics phenotyping. Normalization reduced effects of dilution or different concentrations. PCA was performed to analyze similarities and also outliers in spectra. Orthogonal projections on partial least square discriminant analysis were used to characterize differences in transgenic animals and non-transgenic littermates. R^2 values (>0.4) showed significantly altered metabolites. Furthermore, a back-scaling transformation and projection was used for biomarker visualization. Increased or decreased signals indicated

positive or negative covariance with NTG controls, respectively. A color code of spectrum enabled identification of biomarker-rich regions based on the correlation matrix.
For further statistical analysis of these complex data, MetaboAnalyst 4.0 was used to perform additional multivariate statistical analysis.
For the identification of metabolites Chenomx NMR Suite Professional 8.2 (Chenomx Inc.) was used. Within this software chemical shifts and splitting patterns of the own sample spectrum are matched with the compound signatures from the software to identify specific compounds. Quantification of metabolites was applied by using the integral area of the metabolite of interest of the normalized NMR spectra.

3.8 Statistical analysis

Basic statistical analysis was performed using Graph Pad Prism 8.3.1 software (GraphPad Software Inc., California, USA). All graphs are displayed with group means and the standard error of the mean (SEM). Raw data were tested for normality by using the Kolmogorov-Smirnov-Test. If normal distribution was confirmed, group differences were analyzed with one-way or two-way analysis of variance (ANOVA) followed by Tukey`s multiple comparisons or Bonferroni`s *post hoc* test. For comparing two groups the Unpaired t-test was used for normal distributed data and the Mann Whitney U test was performed as a non-parametric test. For not normally distributed data with more than two groups differences were analyzed with the Kruskal-Wallis test and Dunn's *post hoc* test. Outliers for all analyses were identified by Grubbs `outlier test. All data were presented as mean ± SEM. Exact statistical tests and sample numbers are mentioned in the figure legends. Significance was set as * $p < 0.05$, ** $p < 0.01$ and *** $p < 0.001$.

4 RESULTS

This study consists of two parts. The first section of this PhD thesis contains a basic characterization of the Tg4-42 mouse model with behavioral, biochemical and histological analyses. The Tg4-42 mouse model was firstly described in 2013 by Bouter *et al.* (53). Homozygous animals are named Tg4-42 +/+, heterozygous are named Tg4-42 +/- and as a control, non-transgenic mice (NTG) of the same age were used.
Some of the results of the first part have already been published in Scientific Reports (100).
The second part of this thesis dealt with the *in vivo* drug evaluation of the ALDH2 agonist AD-9308 specified in 4.2.

4.1 Tg4-42 characterization

To evaluate the general health, activity and anxiety as well as cognitive deficits
animals were tested at the age of 3, 6 and 9 months using the Irwin test, Open Field test, Elevated Plus Maze and Morris Water Maze test. Furthermore, untargeted metabolic phenotyping was performed. Based on significantly altered biomarkers further histological investigations were carried out to validate NMR results. To additionally analyze this mouse model in detail and to examine downstream effects neuroinflammation, Aβ42 levels as well as neurodegeneration was determined. Finally, sequencing analyses provided detailed information about the integration site of the Aβ4-42 transgene.

4.1.1 Analysis of general health status (Irwin test)

The body weight was highly significant decreased in Tg4-42 +/+ animals already at 3 months of age. Furthermore, Tg4-42 +/+ animals did not increase their body weight over all age groups compared to NTG animals (Figure 4). Body temperature and the wire suspension time of all tested groups did not significantly change (data not shown).

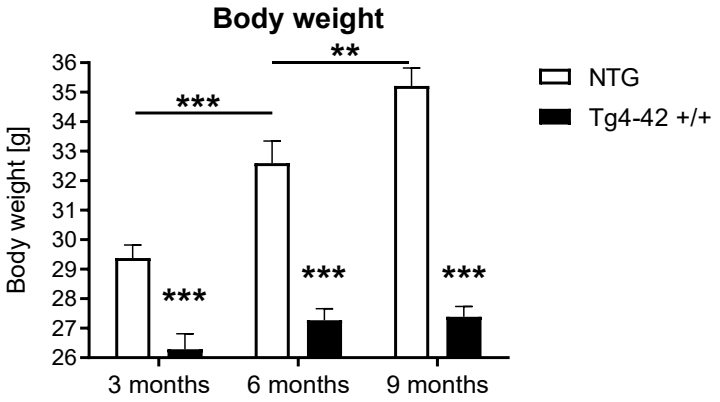

*Figure 4: Body weight over age. Body weight was measured at the age of 3, 6 and 9 months in Tg4-42 +/+ and NTG mice. Statistics: Two-way ANOVA followed by Bonferroni`s post hoc test. n = 15 per group. Data are represented as mean ± SEM. **p<0.01, ***p<0.001.*

4.1.2 Analysis of general activity levels (Open Field test)

This test was performed to analyze the emotional and anxiety behavior of the animals as well as the general activity levels. After 20 minutes of testing there were no significant differences between the genotypes in all measured parameters activity, hyperactivity, total distance, total rearing duration and numbers, thigmotaxis and defecation (data not shown). When analyzing data over age the total activity, total hyperactivity, total rearing duration and numbers progressively decreased in Tg4-42 +/+ mice. Total activity of NTG animals did not change over age (Figure 5 A-E).

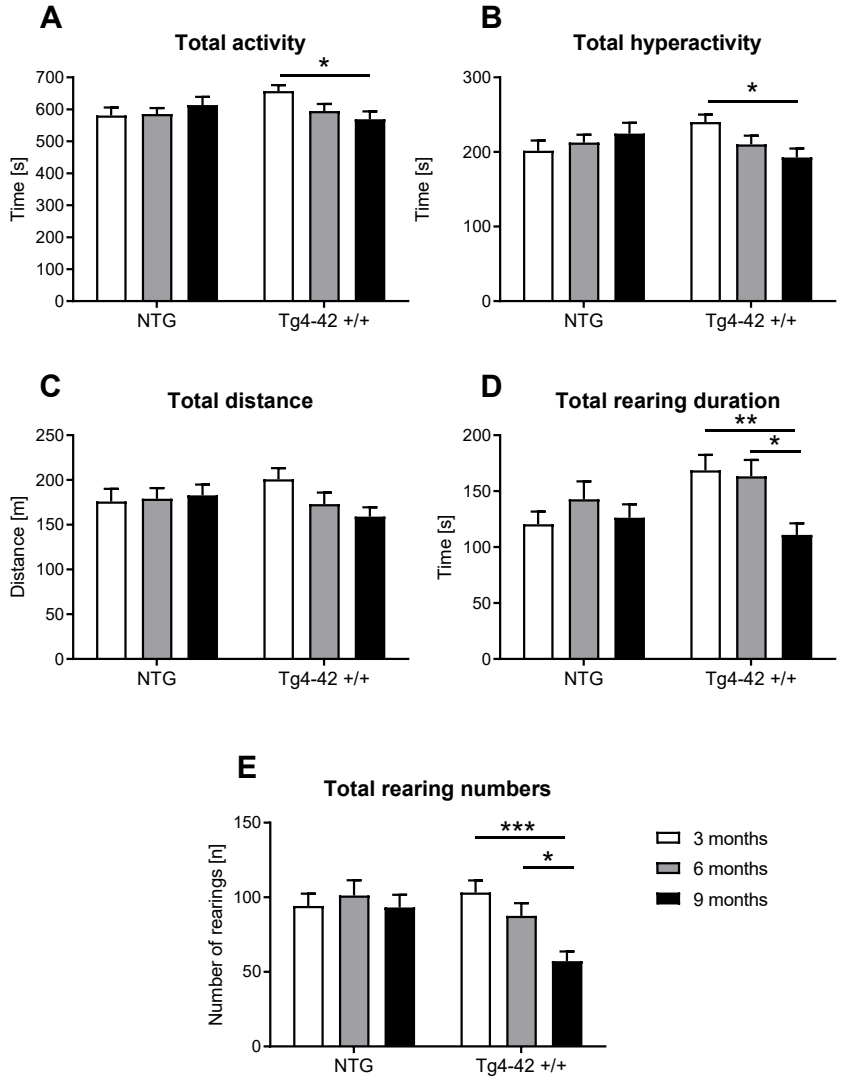

*Figure 5: Open Field test analyses over age. Total activity (A), total hyperactivity (B), total distance (C), total rearing duration (D) and total rearing numbers (E) were measured in 3, 6 and 9 months old Tg4-42 +/+ and NTG mice. Statistics: Two-way ANOVA followed by Bonferroni`s post hoc test. n = 15 per group. Data are represented as mean ± SEM. *p <0.05, **p<0.01, ***p<0.001.*

4.1.3 Analysis of anxious behavior (Elevated Plus Maze test)

In this behavioral test emotion and anxiety of the animals were analyzed. Anxious behavior is expressed by the animal spending more time in the closed arms of the test apparatus. The duration in the closed arms was significantly increased in 3 and 6 month old Tg4-42 +/+ mice while the duration in the neutral zone was significantly decreased in 3 and 6 month old Tg4-42 +/+ animals (Figure 6 A, B). Furthermore, the number of entries in the open arms and in the closed arms was significantly decreased in Tg4-42 +/+ animals at 9 month of age (Figure 6 C, D). Moreover, also the distance and speed were reduced in 9-month-old Tg4-42 +/+ animals (see Figure 6 E, F).

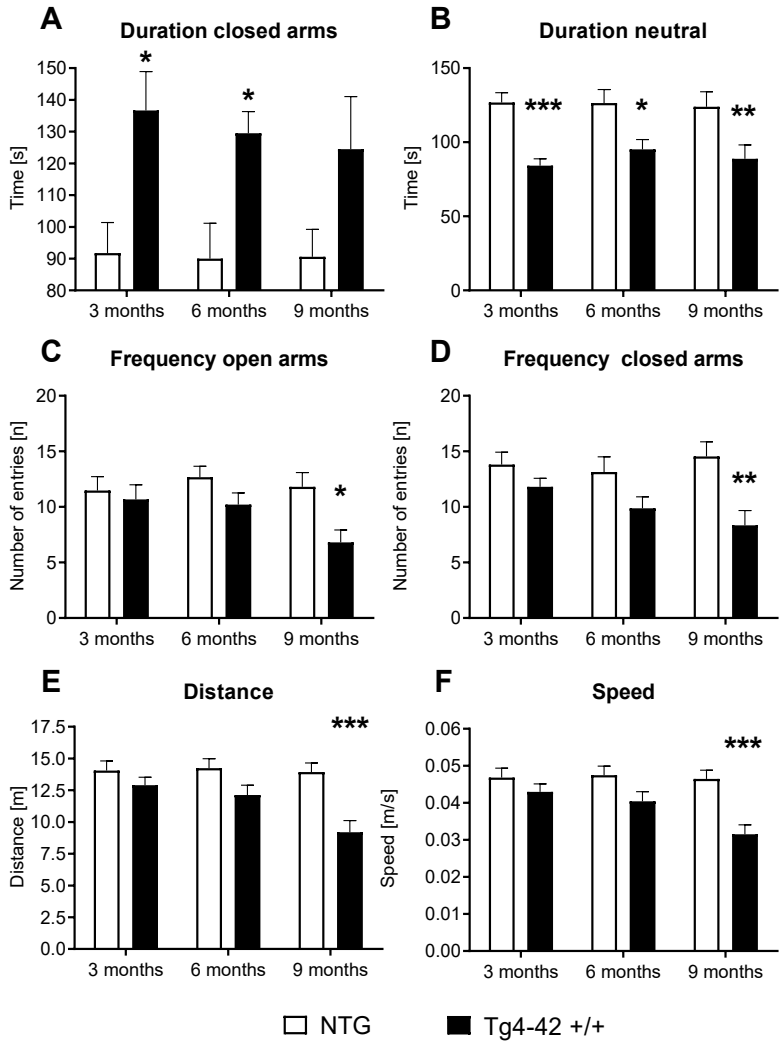

*Figure 6: Anxious behavior measured by Elevated Plus Maze test. Duration in closed arms (A), duration in the neutral zone (B), frequency in open (C) and closed arms (D), distance (E) and speed (F) were evaluated in 3, 6 and 9 months old Tg4-42 +/+ and NTG mice. Statistics: Two-way ANOVA followed by Bonferroni`s post hoc test. n = 15 per group. Data are represented as mean ± SEM. *p <0.05, **p<0.01, ***p<0.001.*

4.1.4 Investigation of spatial learning and memory (Morris Water Maze test)

To investigate spatial learning the Morris Water Maze test was performed. Tg4-42 +/+ mice exhibited learning deficits reflected by a progressive reduction of time to discover the hidden platform at 3, 6 and 9 months of age (Figure 7 A). The length of the swim path was only significantly increased in 3 and 6-month-old Tg4-42 +/+ mice compared to NTG controls (Figure 8 B). However, floating behavior was significantly higher in Tg4-42 +/+ mice at all ages compared to NTG mice (Figure 9 C).

The speed was significantly decreased and thigmotaxis was significantly increased inTg4-42 +/+ mice compared to NTG animals at all ages. (Figure 10 D, E).

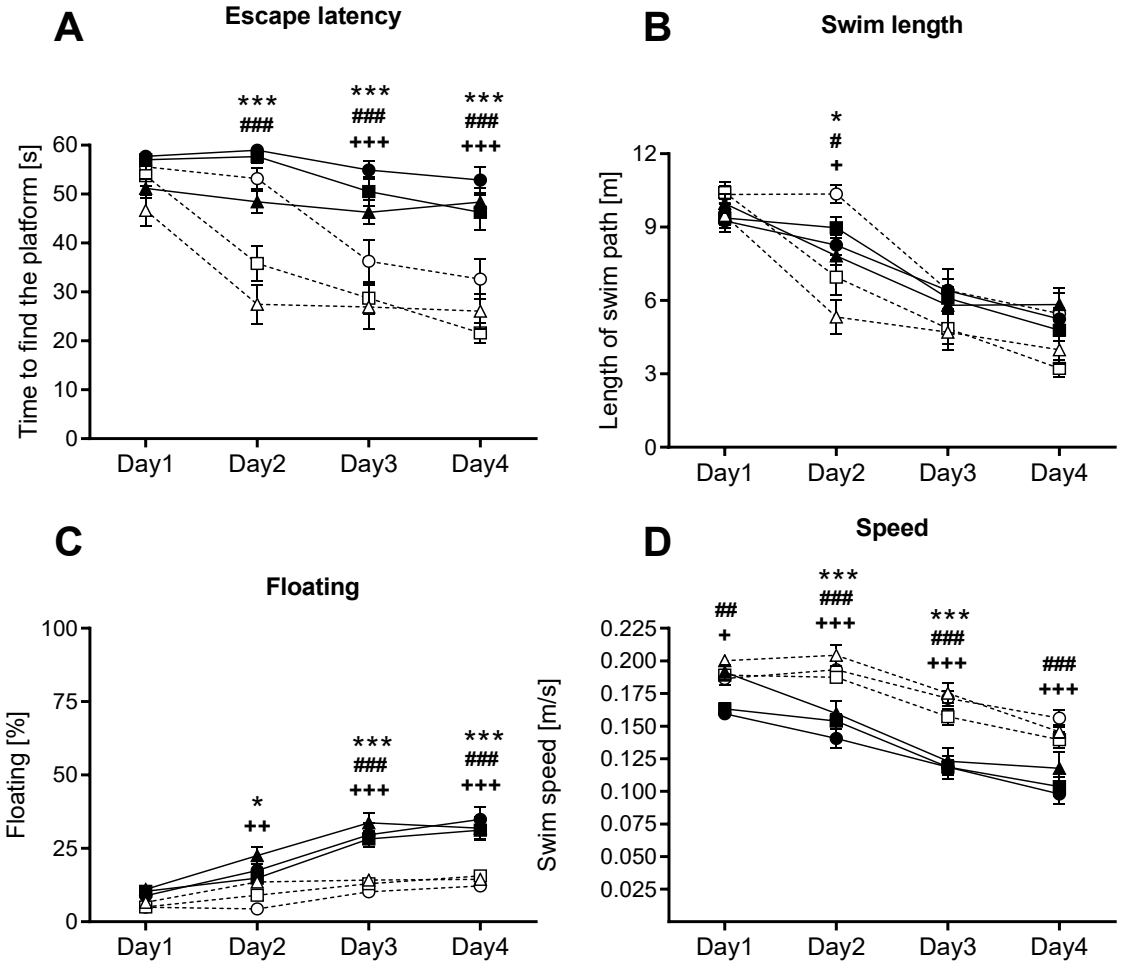

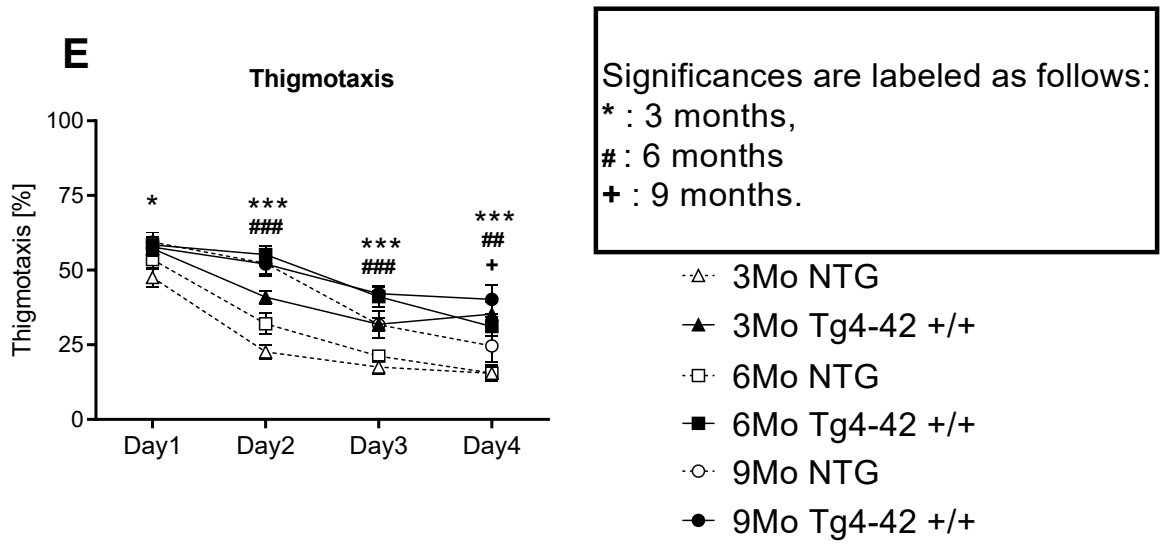

*Figure 10: Spatial learning behavior measured by Morris Water Maze test. Escape latency (A), swim length (B), floating (C), speed (D) and thigmotaxis (E) were measured in 3, 6 and 9 months old Tg4-42 +/+ and NTG mice in the MWM. Statistics: Two-way repeated measure ANOVA followed by Bonferroni`s post hoc test. n = 15 per group. Data are represented as mean ± SEM. * p <0.05, ** p <0.01, *** p <0.001. To distinguish between the different ages instead of * asterisks, #, and + was used.*

Twenty-four hours after the last training trial the platform in the MWM was removed and animals were tested for their ability to locate the previous platform position. This experiment is called probe trial. The time, animals spent in the quadrant where the platform was the last four days (NE quadrant; Figure 11 A), was significantly lower in Tg4-42 +/+ mice at 6 and 9 months. Tg4-42 +/+ mice spent significantly more time in the quadrant were they were entered on the probe trial day (SW quadrant, Figure 11 B) at all ages. Furthermore, also the target zone crossings (Figure 11 C) were significantly lower in Tg4-42 +/+ mice at 9 months. The time animals needed to first visit the target zone was significantly increased in Tg4-42 +/+ mice at all ages. In addition, also the speed (Figure 11 E) and the swim length (Figure 11 F) was significantly reduced in Tg4-42 +/+ animals at all tested ages.

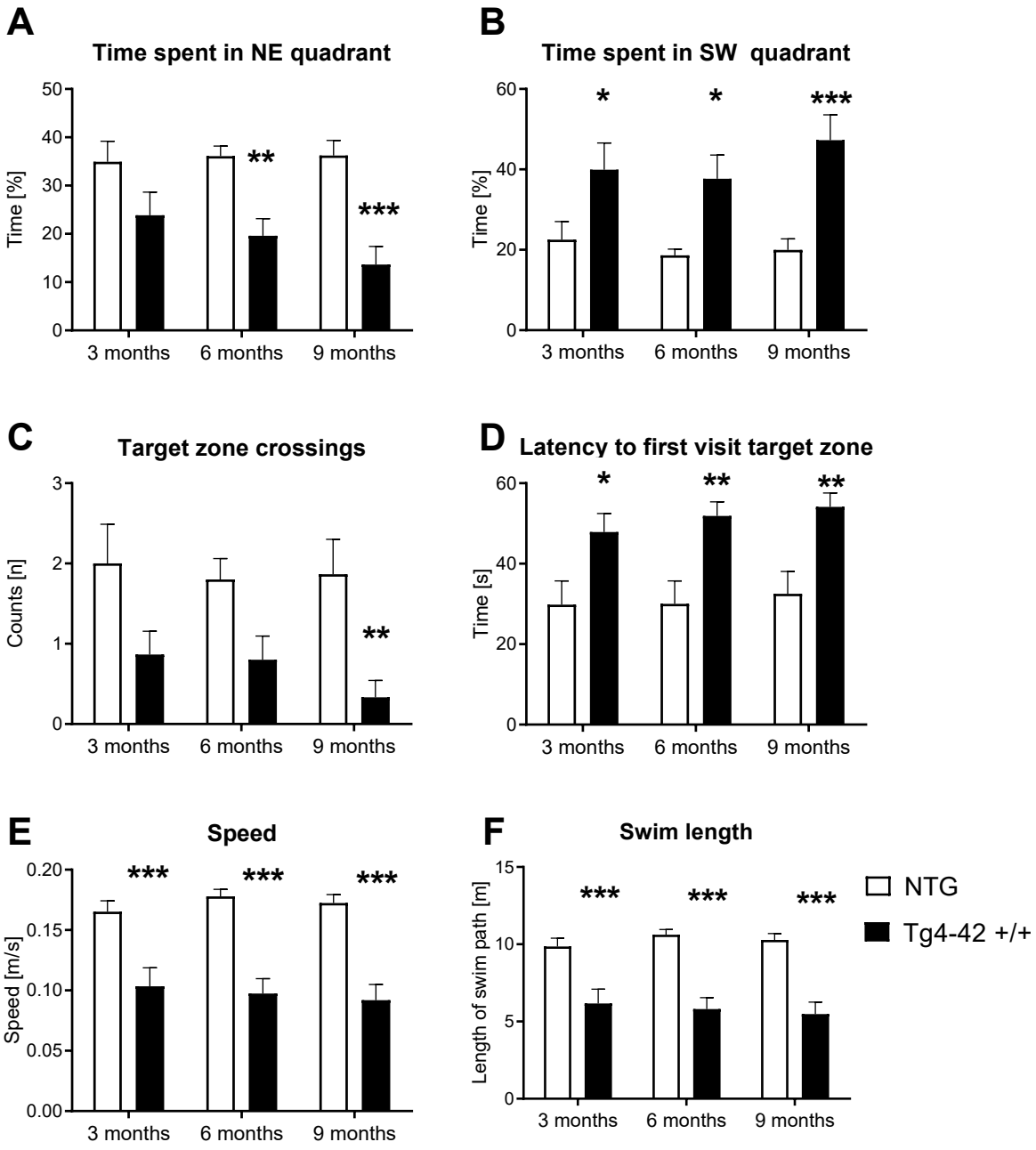

*Figure 11: Assessment of memory deficits in the probe trial of the Morris Water Maze. After 4 days of training, the time spent in NE quadrant (A), time spent in SW quadrant (B), number of target zone crossings (C), latency to first visit target zone (D), speed (E) and swim length (F) were evaluated during the probe trial in 3, 6 and 9 months old Tg4-42 +/+ and NTG mice. Statistics: Two-way ANOVA followed by Bonferroni`s post hoc test. n = 15 per group. Data are represented as mean ± SEM. * p <0.05, ** p <0.01, *** p <0.001.*

4.1.5 Identification and quantification of altered metabolites in Tg4-42 +/+ brain samples

In order to assess metabolic differences in 9-month-old Tg4-42 +/+ and NTG mice, nuclear magnetic resonance (NMR) metabolic profiling was performed in cortex and caudate putamen brain samples. Comparing metabolic fingerprints between both groups revealed clustering in the Principal Component Analysis (PCA; Figure 12 A & Figure 13 A) and a strong clustering in Orthogonal Partial Least Squares – Discriminant Analysis (O-PLS-DA) of both brain regions with correlation coefficients R^2 of up to 0.6 and a Q^2 of 0.3 (Figure 12 B & Figure 13 B). Reduced NMR spectra showed altered metabolite levels in normalized cortex and caudate putamen brain samples (Figure 12 C & Figure 13 C) and indicated that the levels of glutamine as well as 4-aminobutyrate (GABA) were lower in cortex and caudate putamen brain samples of Tg4-42 +/+ mice.

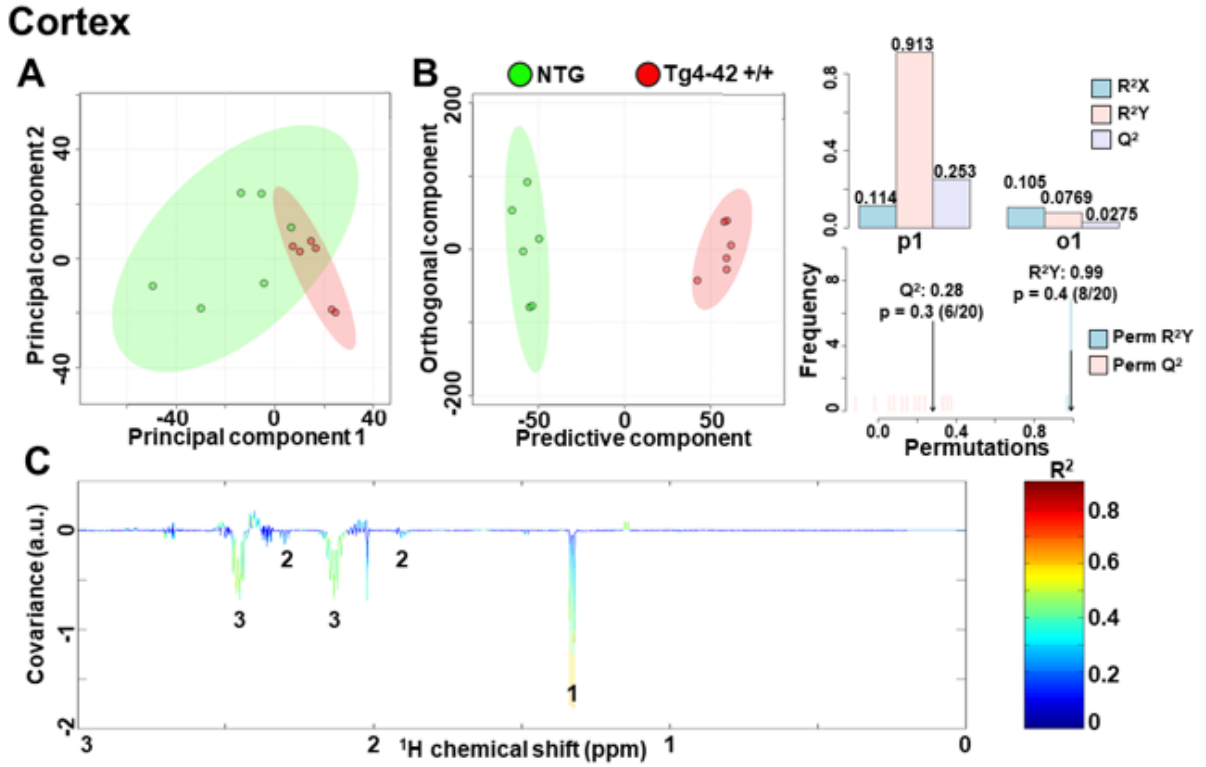

Figure 12: NMR metabolic profiling. (A) PCA and (B) O-PLS-DA plot of cortex samples. (C) Reduced NMR spectra reveal altered metabolites in normalized cortex samples.1: lactate, 2: 4-aminobutyrate, 3: glutamine. Positive covariance corresponds to increased metabolite levels, whereas negative covariance corresponds to decreased metabolite levels in 9-month-old homozygote animals (Tg4-42 +/+) compared to non-transgenic controls (NTG). Predictivity is represented by R^2 and Q^2.

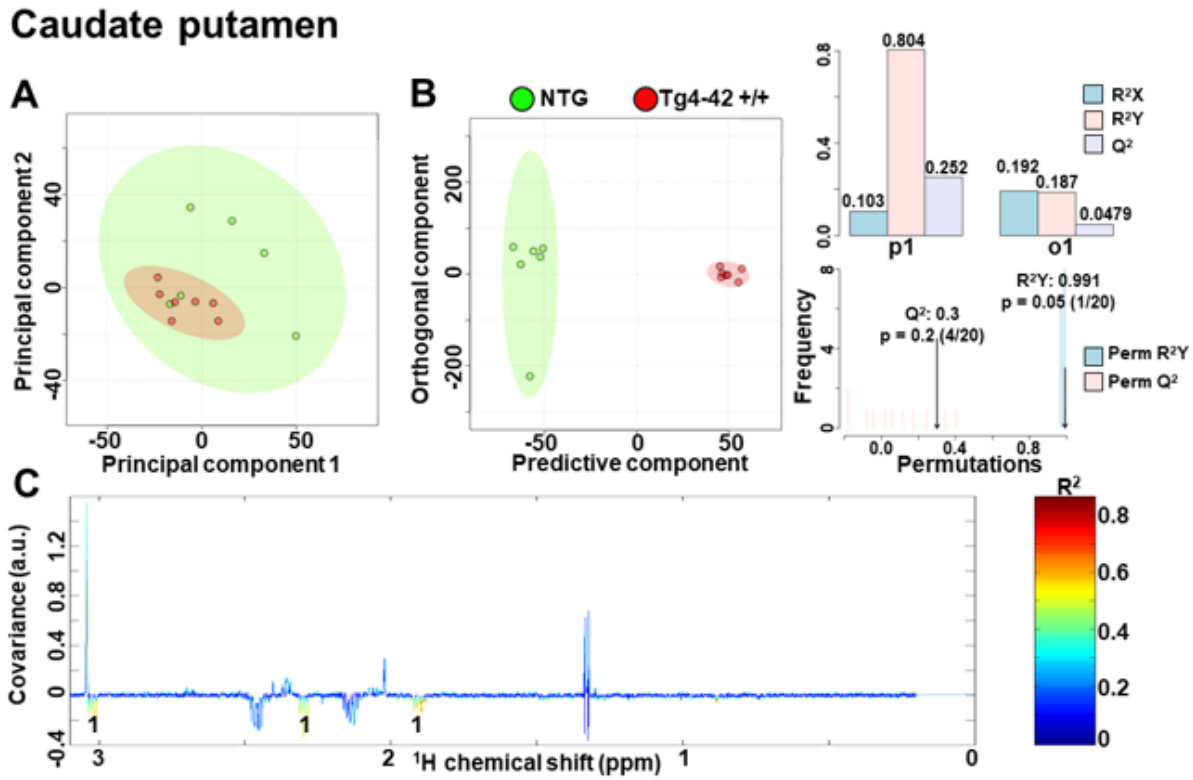

Figure 13: NMR metabolic profiling. (A) PCA and (B) OPLS-DA plot of caudate putamen (CPu) samples. (C) Reduced NMR spectra reveal altered metabolites in normalized caudate putamen samples.1: 4-aminobutyrate. Positive covariance corresponds to increased metabolite levels, whereas negative covariance corresponds to decreased metabolite levels in 9-month-old homozygote animals (Tg4-42 +/+) compared to non-transgenic controls (NTG). Predictivity is represented by R^2 and Q^2.

Subsequently the amount of glutamine, lactate and 4-aminobutyrate was analyzed using the integrated signals in the normalized spectra. In line with the multivariate statistical analysis, all three metabolites were significantly decreased in Tg4-42 +/+ animals compared to NTG mice (Figure 14 A, B, C). Because of time limiting factors and the reported changes in glutamate, GABA and glutamine levels in AD patients, it was decided to focus on the glutamate pathway. For that reason, lactate was not further investigated in this study.

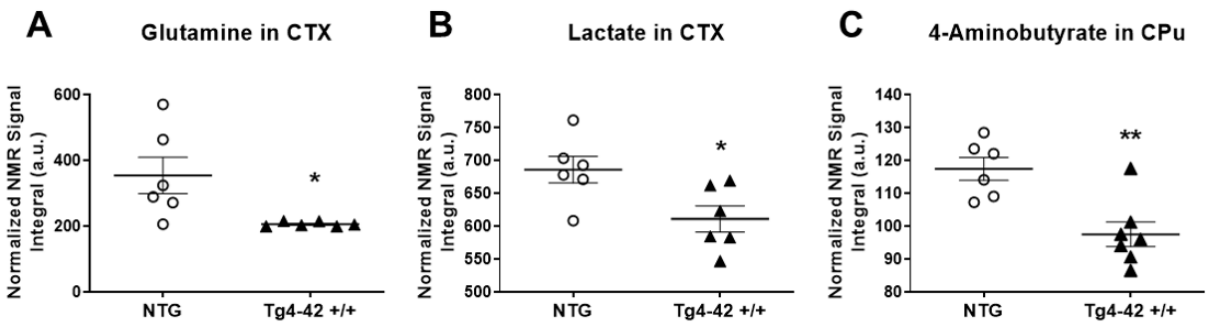

*Figure 14: Quantification of significantly decreased metabolites in Tg4-42 +/+ mice compared to NTG controls. (A) Quantification of glutamine in cortex (CTX) samples (n = 6). (B) Quantification of lactate in cortex (CTX) samples. (C) Quantification of 4-Aminobutyrate in caudate putamen (CPu) samples (n = 7). One NTG sample was removed from the calculations because of contamination. Statistics: Unpaired t-test. Data are represented as mean ± SEM. *p< 0.05, **p< 0.01.*

4.1.6 Evaluation of Glutamate-Decarboxylase (GAD67) and Glutaminase levels in Tg4-42 +/+ mice

To further examine the effects of altered metabolites on changes in metabolic pathways, histological analysis of GAD67 and glutaminase were performed. For this reason, the immunoreactive area of GAD67 and glutaminase was quantified. At 9 month of age, Tg4-42 +/+ mice showed significantly increased GAD67 (Figure 15 A, B) and glutaminase levels (Figure 15 C, D) in the cortex and caudate putamen. These results are also shown in representative images of NTG and Tg4-42 +/+ brain sections (Figure 15).

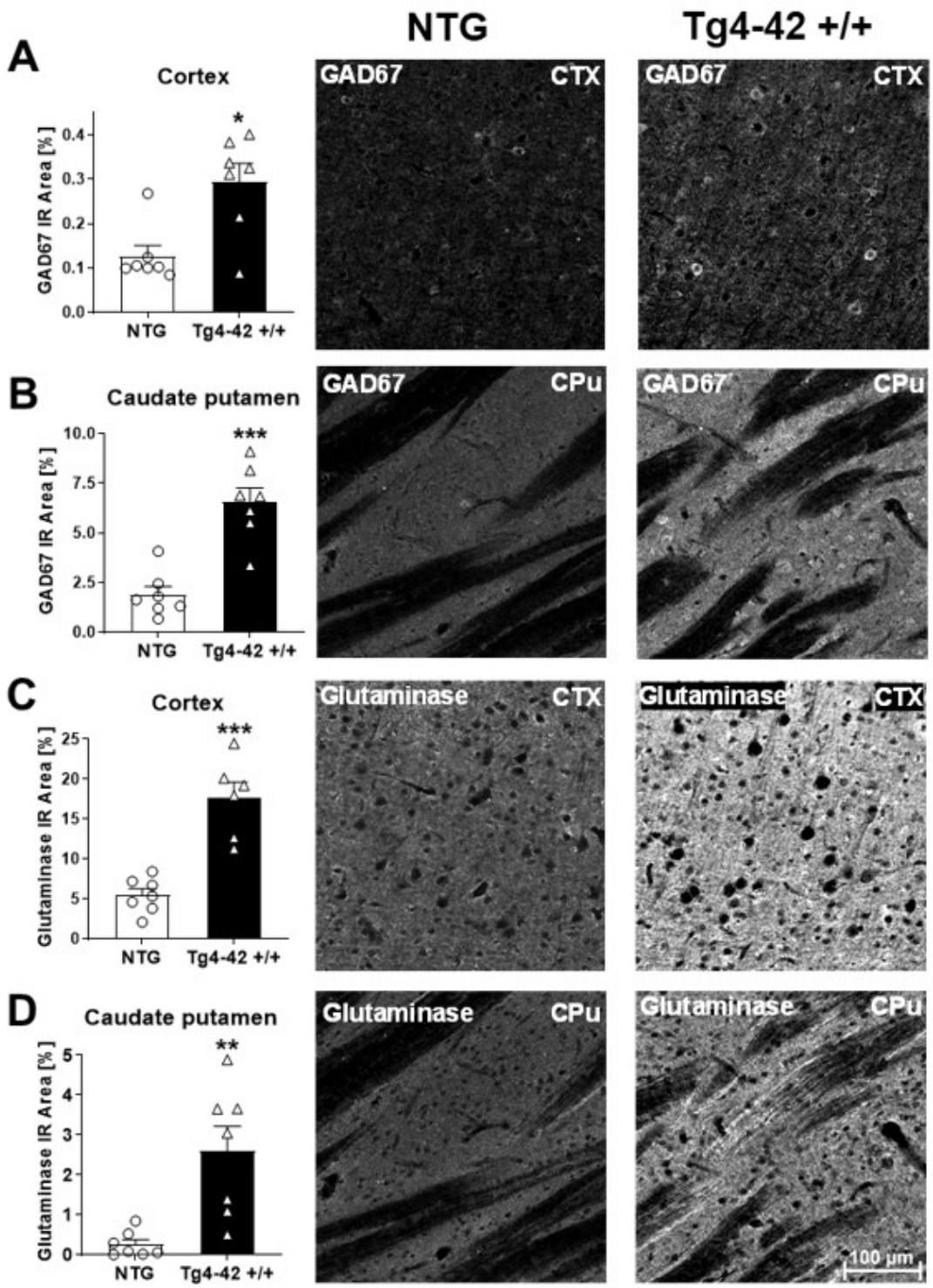

*Figure 15: Expression of GAD67 and glutaminase in 9-month-old Tg4-42 +/+ mice. Quantitative GAD67 expression in cortex (CTX; A) and caudate putamen (CPu; B) and glutaminase expression in cortex (C) and caudate putamen (D) shown as immunoreactive area in percent. Representative images of NTG and Tg4-42 +/+ brain sections. Scale bar 100 µm for all images. (A-D) Statistics: Unpaired t-test. n = 7 per group. Data are represented as mean ± SEM. *p<0.05, **p<0.01, ***p<0.001.*

4.1.7 Amyloid-β 42 levels in the central nervous system of Tg4-42 +/+ mice

Total amyloid-β 42 levels were analyzed by quantification of the immunoreactive area in different brain regions of Tg4-42 +/+ mice. Significantly increased total Aβ42 levels (endogenous mouse Aβ1-42 and human Aβ4-42) in Tg4-42 +/+ mice compared to NTG animals could be found in the cortex (Figure 16 A), caudate putamen (Figure 16 B) and hippocampus (Figure 16 C) at the age of 9 months. These increased total Aβ42 levels in Tg4-42 +/+ mice can also be observed in the representative images in Figure 16 D where the highest Aβ42 levels were found in the CA1 region of the hippocampus. In order to evaluate total and soluble human Aβ4-42 concentrations, corresponding cortex samples were further analyzed using the Meso Scale Discovery assay. As expected, these results were in line with histological evaluations, showing a significant increase of total and also soluble human Aβ4-42 levels in Tg4-42 +/+ cortex samples (Figure 16 E, F).

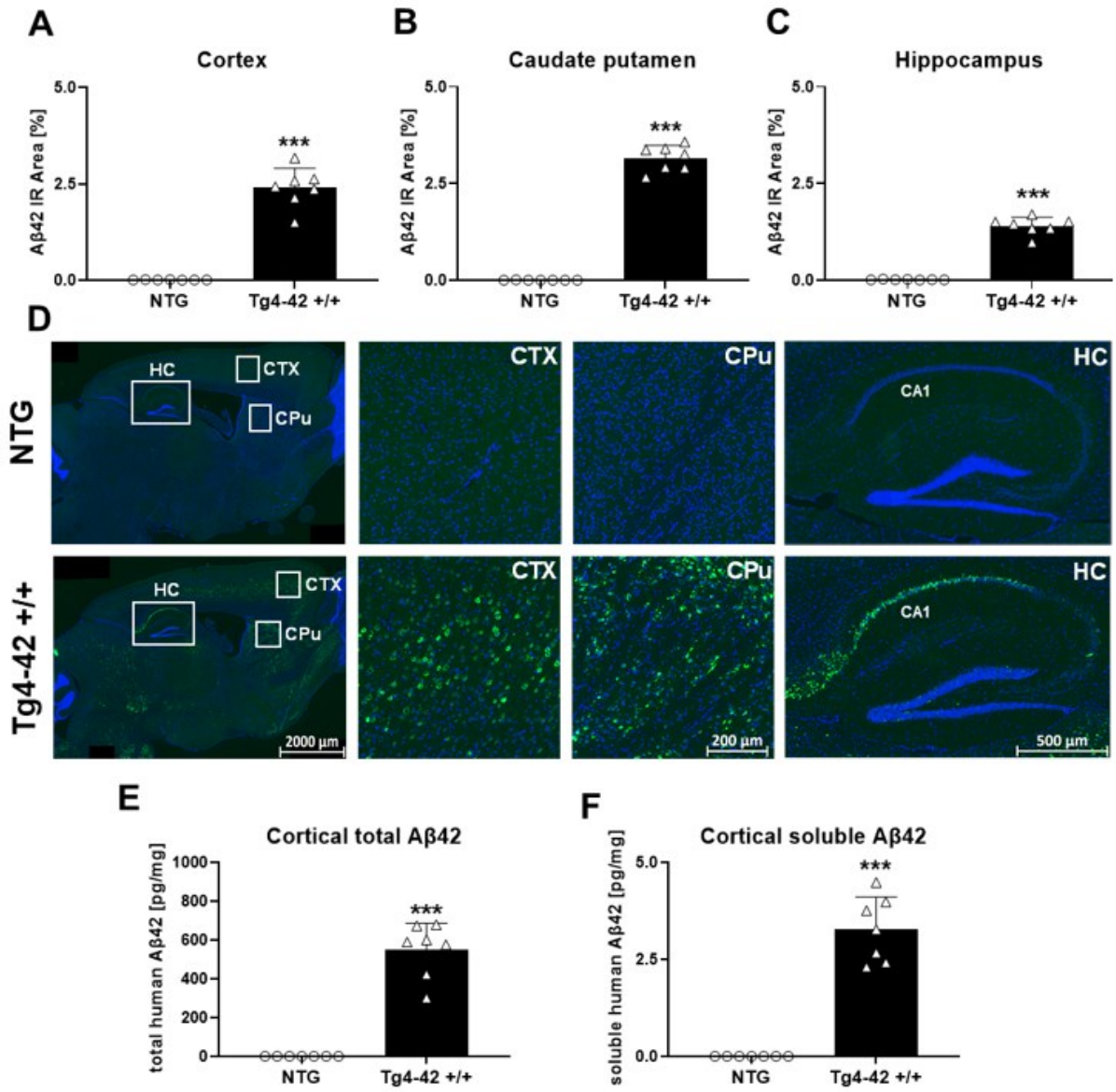

*Figure 16: Quantification of Amyloid-β 42 (Aβ42) expression in the central nervous system of Tg4-42 +/+ mice. Histological quantification of Aβ42 expression (endogenous mouse Aβ1-42 and human Aβ4-42) in (A) cortex (CTX), (B) caudate putamen (CPu) and (C) hippocampus (HC) in 9-month-old Tg4-42 +/+ mice. (D) Representative images of Aβ42 (green) and DAPI (blue) labeling in 9-month-old Tg4-42 +/+ and non-transgenic mice. (E) Biochemical quantification of cortical total human Aβ4-42 levels in pg/mg and (F) soluble human Aβ4-42 levels in pg/mg. (A-F) Statistics: Unpaired t-test. n = 7 per group. Data are represented as mean ± SEM. ***p<0.001.*

4.1.8 Neuroinflammation in Tg4-42 +/+ mice

Quantification of the immunofluorescence signal was used to measure neuroinflammation, as it was described to play a significant role in neurodegenerative diseases like Alzheimer´s disease (7, 101).

To analyze inflammation in the brain of Tg4-42 +/+ animals, an inflammation assay was performed. Therefore 10 different inflammation markers (IFNγ, IL-10, IL-12, IL-13, IL-1b, IL-2, IL-4, IL-6, KC and TNFα) were measured in 5 different brain regions (cortex, hippocampus, striatum, cerebellum und remaining brain) of Tg4-42 +/+ and NTG animals at the ages of 3, 6, 9 months. Most of these inflammation markers were under the limit of detection in both groups. Only interleukin 4 (IL-4), neutrophil chemokines (KC) and TNF-α could be measured quantitatively in most of the tissues but were not significantly altered in Tg4-42 +/+ animals (data not shown).

Furthermore, the immunoreactive area of glial fibrillary acidic protein (GFAP) as a marker for reactive astrocytes and ionized calcium binding adaptor molecule 1 (Iba-1) as a marker for activated microglia, was quantified over age. Significantly increased levels of GFAP in Tg4-42 +/+ mice compared to NTG animals were found at 9 month of age in the cortex (Figure 17 A) and hippocampus (Figure 17 C). In the caudate putamen an age-dependent increase of astrocytosis by GFAP labeling could be observed in Tg4-42 +/+ mice (Figure 17 B) starting already at 3 month of age. Analysis of Iba-1 immunoreactive area in the cortex and hippocampus revealed no significant difference between genotypes (Figure 17 D, F). In the caudate putamen, Iba-1 levels were significantly increased in Tg4-42 +/+ mice at 6 and 9 month of age compared to NTG animals (Figure 17 E). Representative images of GFAP and Iba-1 labeling in the caudate putamen region are shown in Figure 17 G.

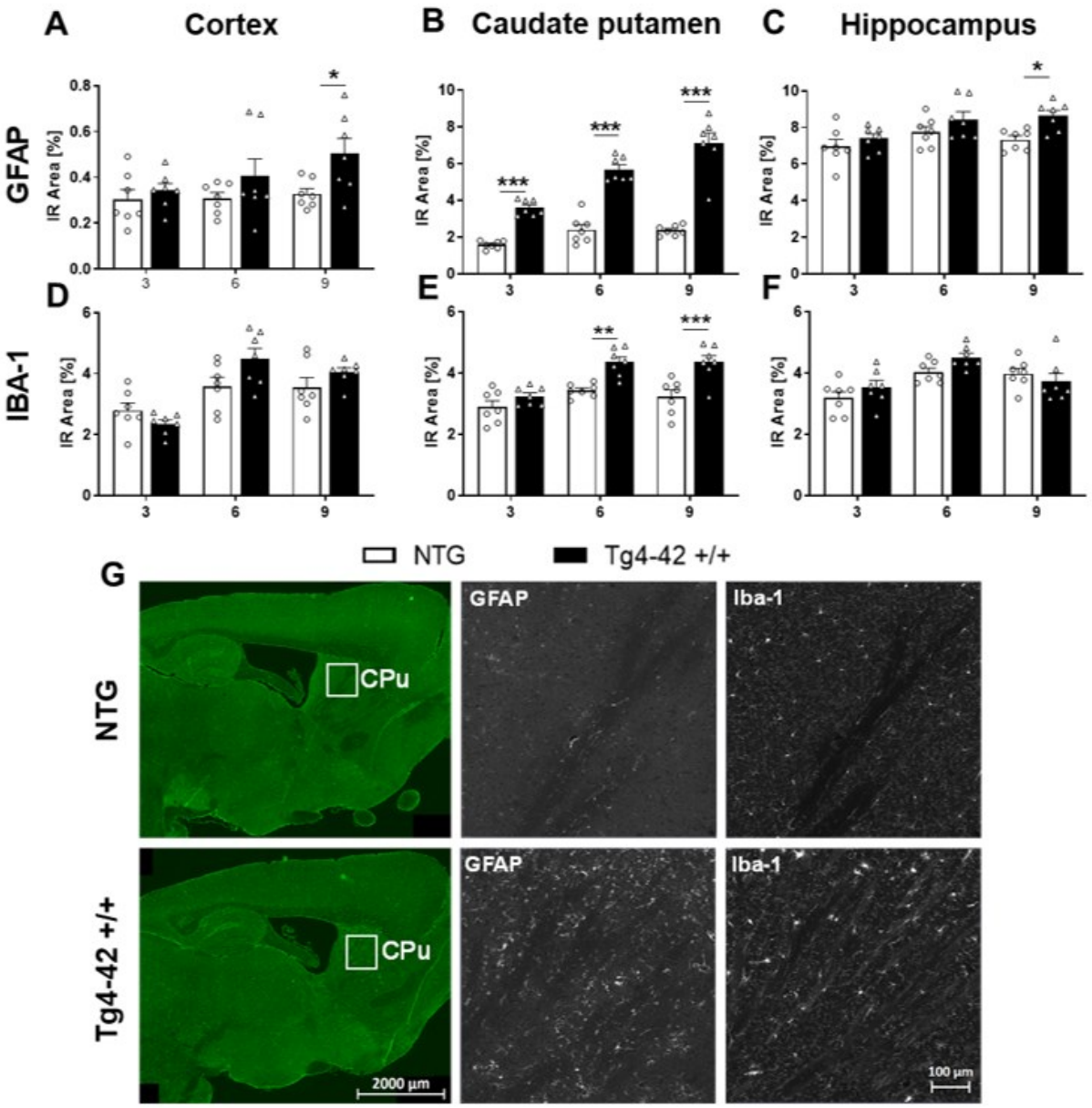

*Figure 17: Progressive neuroinflammation of Tg4-42 +/+ mice. Immunoreactive area in percent of GFAP expression levels labeling reactive astrocytes in the cortex (A), caudate putamen (B), hippocampus (C) and Iba-1 expression levels labeling activated microglia in the cortex (D), caudate putamen (E) and hippocampus (F). (A-F) Statistics: Two-way ANOVA followed by Bonferroni`s post hoc test. n = 7 per group. Data are represented as mean ± SEM. *p<0.05, **p<0.01, ***p<0.001. (G) Representative images of GFAP and Iba-1 labeling of caudate putamen samples in 9-month-old Tg4-42 +/+ and non-transgenic mice (NTG).*

4.1.9 Neuronal loss & neurodegeneration

As a well-established biomarker for neurodegeneration (102), concentration of neurofilament light chain protein was determined in the cerebrospinal fluid of Tg4-42 +/+ mice. Results revealed significantly increased NF-L levels in 9 month old Tg4-42 +/+ mice compared to NTG animals (Figure *16* A). Furthermore, histological analysis and quantification of neuronal nuclei (NeuN) in the proximal CA1 region of the hippocampus revealed a significant decrease of neurons in this region (Figure 16 B). Representative images of NeuN labeling in hippocampus samples are shown in Figure 16 C, D.

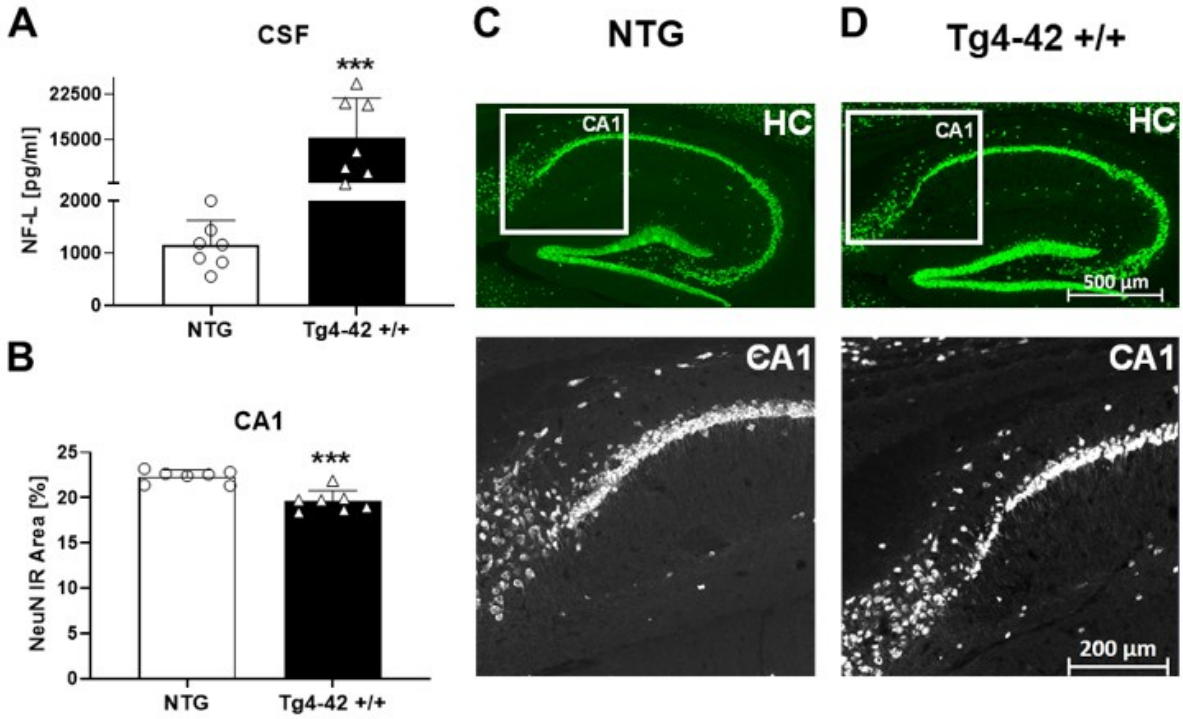

*Figure 18: Evaluation of Neurodegeneration in the hippocampus of 9-month-old Tg4-42 +/+ mice. (A) Murine neurofilament light chain levels (NF-L) in CSF samples as pg/ml. (B) NeuN expression levels labeling neurons in the CA1 region of the hippocampus as immunoreactive area in percent. (A-B) Statistics: Unpaired t-test. n = 7 per group. Data are represented as mean ± SEM. **p<0.01, ***p<0.001. (C, D) Representative images of NeuN labeling in hippocampus samples of 9-month-old Tg4-42 +/+ and non-transgenic mice (NTG).*

While cognitive deficits, amyloid deposits or neurofibrillary tangles and inflammation are observable in many AD mouse models, neurodegenerative pathology as characterized by e.g. hippocampal neuron loss is only observed in a few models (103-108). For this reason, a further evaluation of the genetic features in the Tg4-42 mouse model was performed using molecular

methods. Due to the observation that Tg4-42 mice develop neuronal loss these mice represent a promising model for the development of new drugs or drug efficacy studies (109).

The following data has already been published in Scientific Reports (100):

4.1.10 Retinoic acid receptor beta knockdown

To further evaluate the genetic features of Tg4-42 mice, whole genome sequencing was performed to determine the integration site(s) of the transgene and estimate the transgene copy number as well as assess the presence of structural variants surrounding the transgene integration site and the transgene sequence itself (100).

Targeted Locus Amplification of the Tg4-42 +/+ mouse model showed that the Aβ4-42 transgene is inserted in more than 20 copies of head to tail orientation at position 17,431,476 - 17,651,381 (mouse genome assembly mm9) on chromosome 14 (see complete gene sequencing report in the appendix). Only the last transgene copy is in reverse orientation. Furthermore, exon 2 of the retinoic acid receptor beta (RARB) gene was deleted in Tg4-42 +/+ mice (Figure 19 A).

To analyze how this genetic deletion influences RARB RNA expression levels and if expression of whole mRNA is affected, primer pair 1 which binds between exon 5 and 6 was designed. Quantitative PCR using primer pair 1 showed expression levels that were almost reduced to 50 % in hemizygous Tg4-42 +/- and almost immeasurable in homozygous Tg4-42 +/+ animals (Figure 19 C). To validate that the same amount of cDNA was used in all samples, HPRT was used as housekeeping gene (100).

To confirm these results, two further primer pairs were used, binding from exon 2 to 3 and from exon 7 to 8 and thus outside of the deleted gene region of RARB (Figure 19 B). qPCR was further performed using cDNA of three different homozygous Tg4-42 +/+ and three wild type (WT) striatal samples. Results show that all three primer pairs showed a significant knockdown of RARB RNA levels in all Tg4-42 +/+ animals (Figure 19 D; 100).

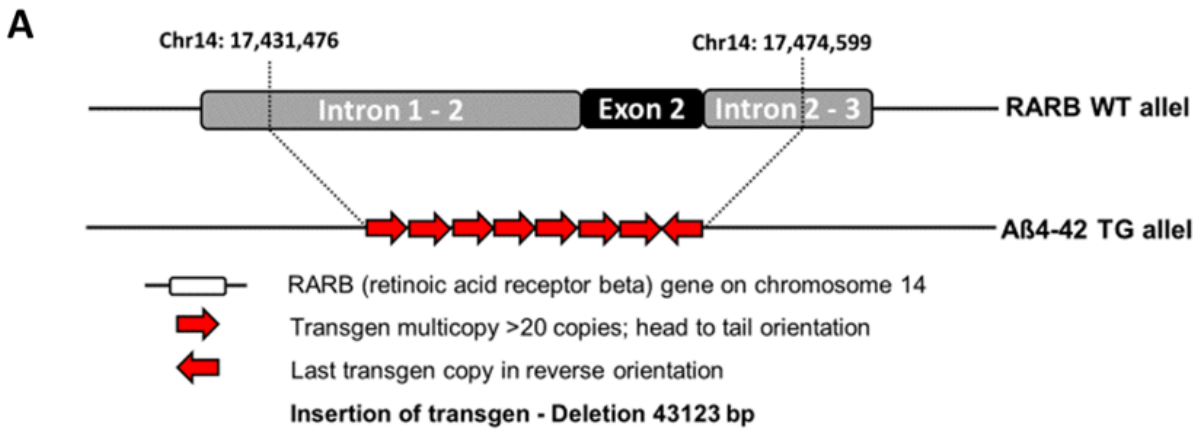

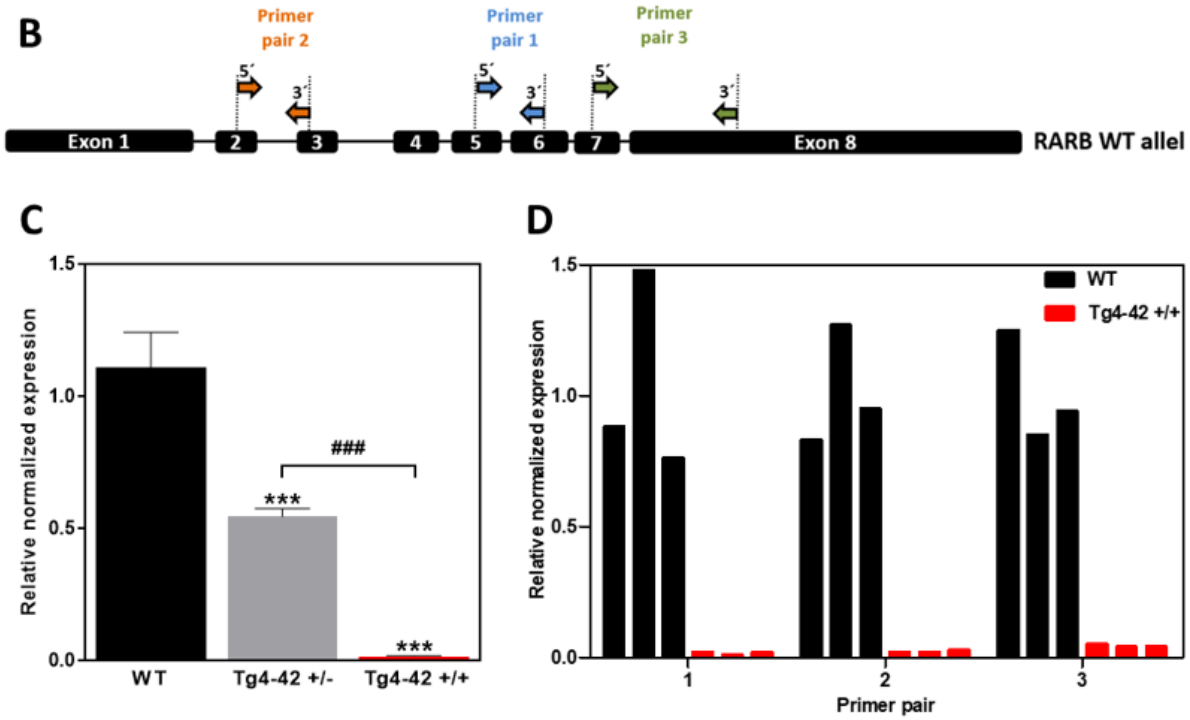

*Figure 19: Gene expression analyses of Tg4-42 +/+ mice. (A) Whole genome sequencing showing the transgene integration site and the deletion of RARB exon 2 on the mouse genome. (B) Binding sites of three different primer pairs used to detect the expression levels of the retinoic acid receptor beta. (C) Gene expression levels measured with conventional qPCR by primer pair 1 in three wild type (WT), three hemizygous (Tg4-42 +/-) and three homozygous (Tg4-42 +/+) striatal samples after cDNA synthesis. HPRT was used as a housekeeping gene to normalize expression levels of the RARB gene. Statistics: One-way ANOVA followed by Tukey`s multiple comparisons test. n = 3 per group. Data are represented as mean ± SEM. ***p<0.001 against WT and ### as indicated. (D) qPCR results of three wild type (WT) and three Tg4-42 +/+ striatal samples using primer pair 1, 2 and 3. Mean Cq values of RARB were normalized with mean Cq values of HPRT (100).*

To confirm the gene expression results on protein level Western blot analysis was performed. Many different approaches like two different protein extraction methods, different protein concentrations, three different primary antibodies (ab53161, Abcam; orb11327, Biorbyt; sc-514585, Santa Cruz Biotechnology; dilution 1:500), different incubation settings and different gel detection methods were used but did not show satisfactory results because of the non-specificity or low sensitivity of used antibodies (data not shown; 100).

Moreover, protein analysis with Mass spectrometry was performed in an untargeted as well as targeted approach but unfortunately the concentration of RARB protein in WT animals was under the limit of detection.

As the traditional Western blot as well as the mass spectrometry analysis did not show any valid results on protein level, Simple Western blot analysis was performed. Therefore, a monoclonal retinoic acid receptor beta 2 antibody (sc-514585, Santa Cruz Biotechnology), already unsuccessfully used for classical Western blotting, was tested in different concentrations. The antibody showed a specific signal at 48 kDa in WT animals which decreased at higher antibody dilutions. Moreover, the specificity control (SP-CTRL) without a biological sample, to evaluate if the primary antibody sticks to capillary wall material and a negative control (N-CTRL) without the primary antibody to check for cross-reactivity, showed no unspecific signal (Figure 20 A, B). For further experiments the lowest tested antibody dilution (1:10) was used. In this study we focused on the analysis of homozygous Tg4-42 +/+ mice compared to wild type animals to clearly visualize differences in retinoic acid receptor beta protein levels caused by RARB gene knockout. Nevertheless, to confirm the qPCR data total protein was extracted from three homozygous Tg4-42 +/+, three hemizygous Tg4-42 +/- and three wild type striatal samples and measured by the Simple Western blot system. The analysis revealed a significant knockdown of retinoic acid receptor beta protein in Tg4-42 +/+ mice and therefore confirmed the qPCR results while protein levels in Tg4-42 +/- were not significantly reduced compared to wild type animals. GAPDH was used as loading control (Figure 20 C-E; 100).

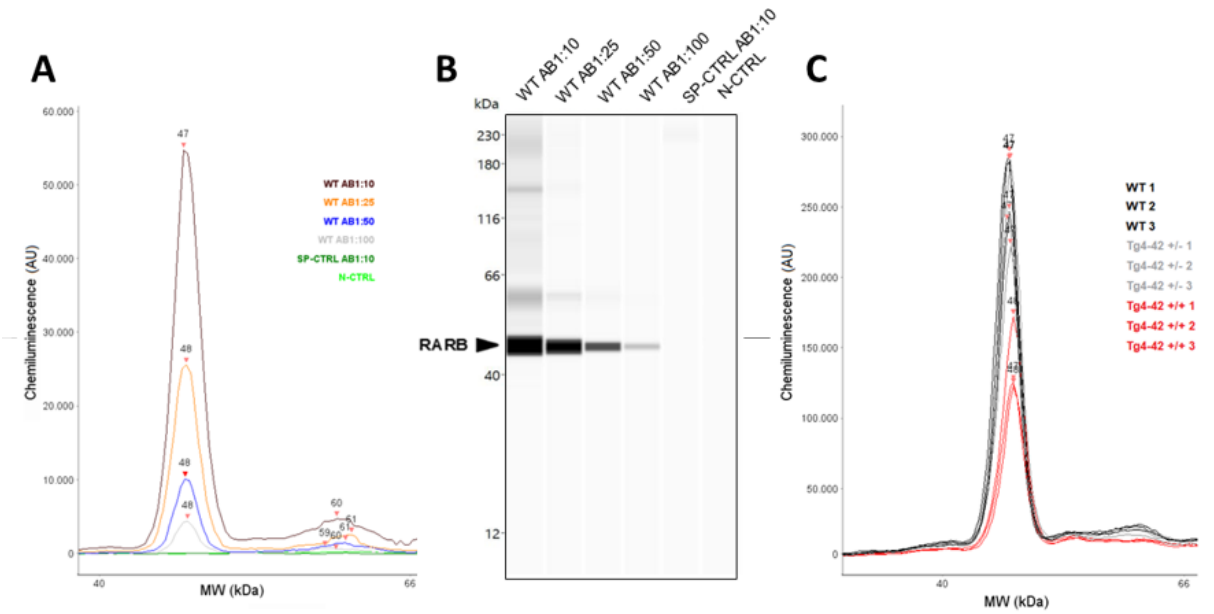

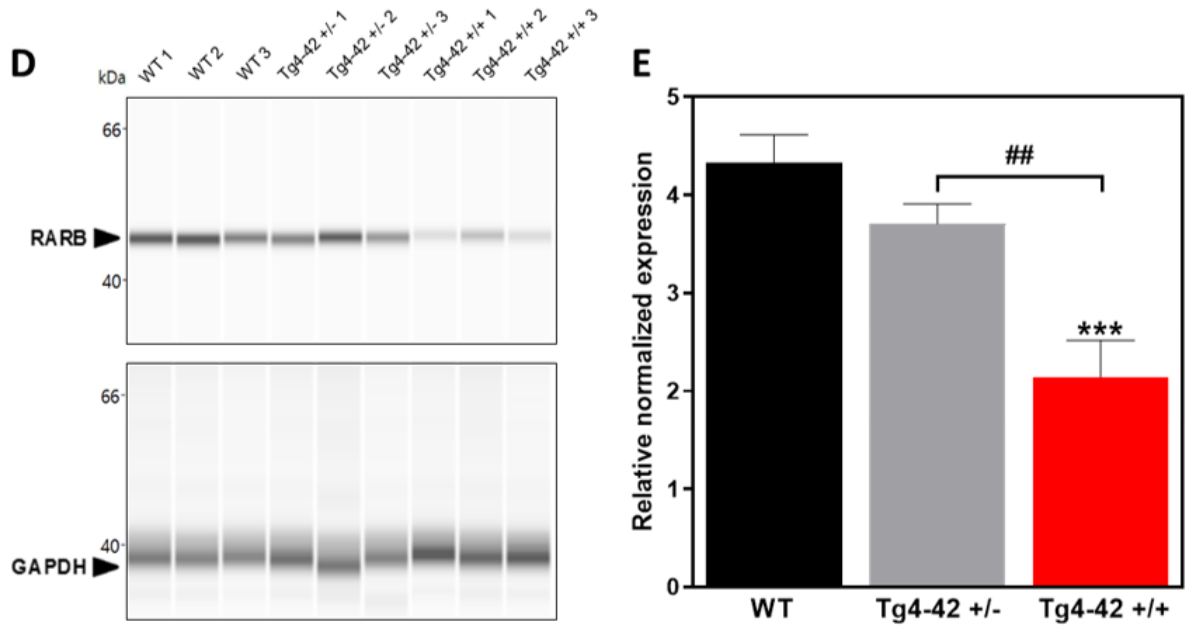

*Figure 20: Simple Western protein analysis of the retinoic acid receptor beta in wild type (WT), Tg4-42 +/- and Tg4-42 +/+ mice. a, b) Different antibody dilutions of a monoclonal retinoic acid receptor beta 2 antibody were tested with the Simple Western blot system to determine its binding capacity and optimal antibody concentration. A specificity control (SP-CTRL) and a negative control (N-CTRL) were used to detect unspecific binding of the column and cross reactions, respectively (A, B). After protein extraction, striatal protein samples of three different WT, Tg4-42 +/- and Tg4-42 +/+ mice were measured by the Simple Western system. GAPDH was used as loading control (C, D). (E) Quantification of RARB protein of three wild type (WT), three hemizygous (Tg4-42 +/-) and three homozygous (Tg4-42 +/+) striatal samples as shown in (C, D) normalized to GAPDH. (E) Statistics: One-way ANOVA followed by Tukey`s multiple comparisons test. n = 3 per group. Data are represented as mean ± SEM. ***p<0.001 against WT and ## p<0.01 as indicated (100).*

4.2 Treatment of APP_{SL} mice

The first part of this thesis dealt with a basic characterization of Tg4-42 +/+ and NTG control mice over age. Due to the retinoic acid receptor beta knockdown and the very likely influence on the phenotype of these mice a well-established APP model, the APP_{SL} mouse, was used for the treatment study.

In this treatment study 7 months old APP_{SL} transgenic mice received either the test item (AD-9308) or vehicle (APP_{SL}) orally by drinking water for 2 or 4 months. Non transgenic wild type littermates (NTG) which also received the vehicle were used as controls. After 2 months of treatment behavior tests like the Open Field, Y-maze and Irwin test were performed to evaluate the anxiety and activity levels, spontaneous alternation behavior and the general health conditions of these mice. 7 of these tested mice of each group were sacrificed after the behavioral tests. After 4 months of treatment 15 mice of each group were tested again performing the Elevated Plus Maze, Y-maze, Irwin and Morris Water Maze test to evaluate activity and anxiety levels, spontaneous alternation, general health conditions as well as cognitive deficits in spatial reference memory. After that all animals were sacrificed and tissue of all groups was collected for biochemical and histological analyses.

4.2.1 General health and body weight

Treatment with AD-9308 was very well tolerated and only 2 mice from the APP_{SL} + AD-9308 group died within the treatment period. These mice did not show any noticeable symptoms and were lying dead in cage one day. After necropsy one mouse showed a large, filled bladder which could indicate a closure of the urethra. Furthermore, one mouse of the APP_{SL} group died within the study because of unknown reasons. General health conditions were checked using the Irwin test after 2 and 4 months of treatment. All animals were in a good health condition and animals were weighed once weekly. APP_{SL} and APP_{SL} + AD-9308 mice showed a significant lower body weight compared to NTG animals but no significant differences between the APP_{SL} + AD-9308 and the APP_{SL} group were detected (Figure 21).

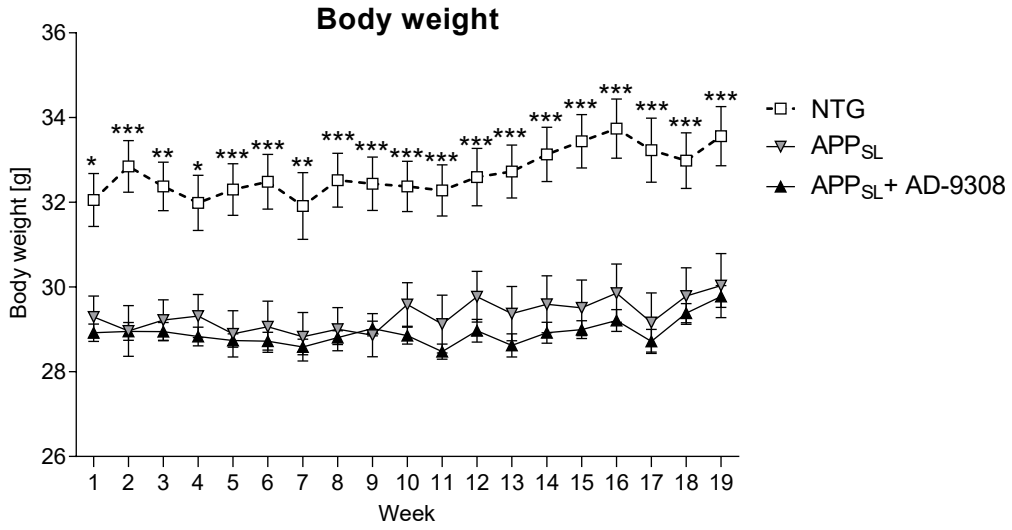

*Figure 21: Analysis of body weight. Graph represents the progression of body weights [g] per group measured once a week over the treatment period of 4 months. Each point represents the mean + SEM of all animals per group and day. No significantly differences between the treatment group APP_{SL} + AD-9308 and the APP_{SL} group were detected. Statistics: Two-way ANOVA followed by Bonferroni's post hoc test. NTG: n = 15, APP_{SL}: n = 14, APP_{SL} + AD-9308: n = 13. Data are represented as mean ± SEM. * p<0.05, ** p<0.01, *** p<0.00).*

4.2.2 Analysis of general activity levels (Open Field test)

After 2 months of treatment the Open Field test was performed. Several parameters like the total activity, total hyperactivity, total distance, total rearing duration, total rearing numbers, total thigmotaxis and defecation were evaluated in this test. No significant differences between the APP_{SL}+AD-9308 and APP_{SL} animals were evaluated (Figure 22 A-G). Only the total rearing duration and the total rearing numbers were significantly decreased in APP_{SL} and APP_{SL}+AD-9308 mice compared to NTG animals but no treatment effect could be detected (Figure 22 D, E).

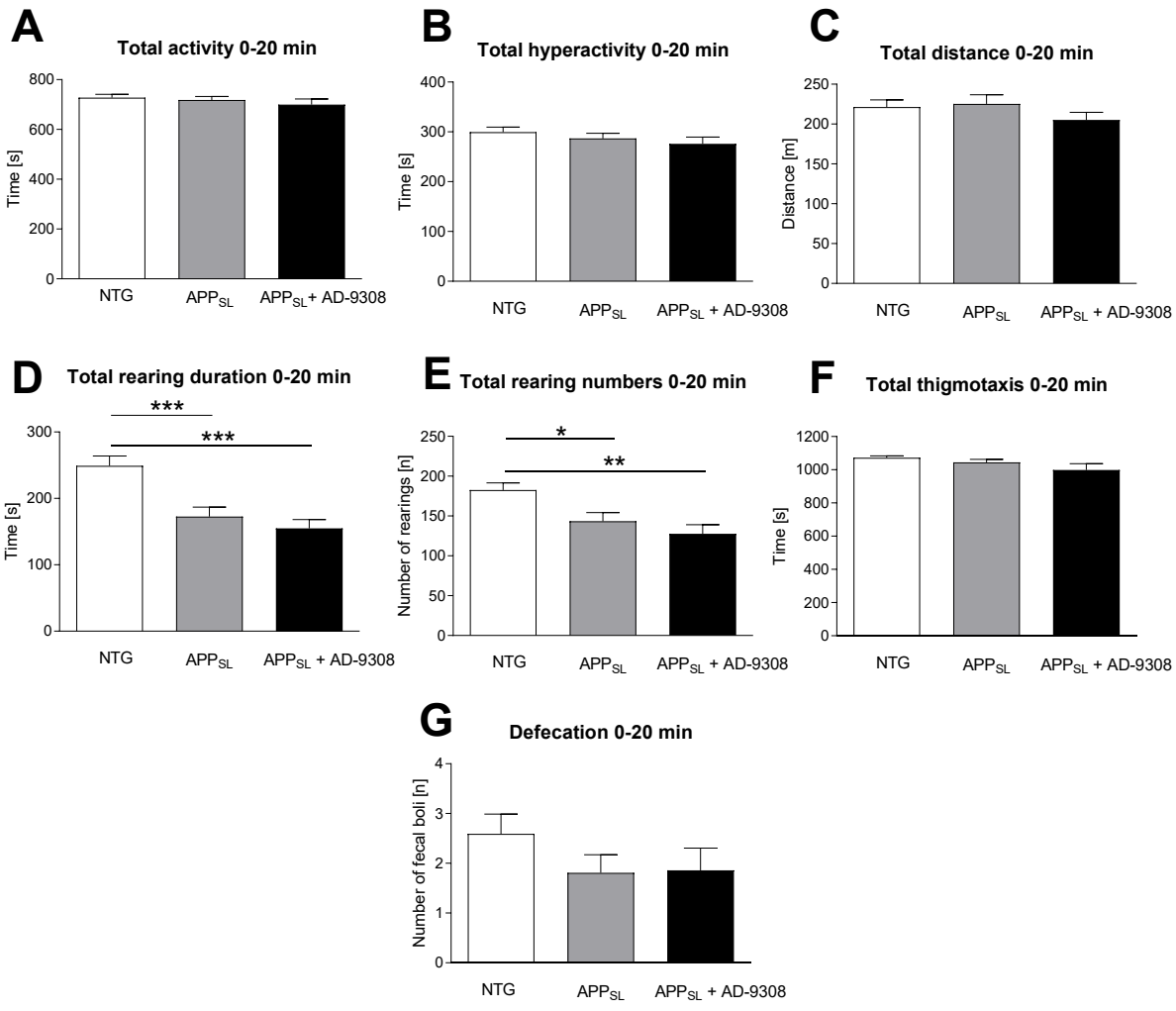

*Figure 22: Open Field test after 2 months of treatment: Graphs represents total activity (A), total hyperactivity (B), total distance (C), total rearing duration (D), total rearing numbers (E), total thigmotaxis (F) and defecation (G) after 2 months of treatment. Significant differences in total rearing duration and rearing numbers between APP_{SL} + AD-9308 vs. NTG and APP_{SL} vs. NTG were detected. Statistics: One-way ANOVA followed by Bonferroni's post hoc test. n = 22 per group. Data are represented as mean ± SEM. * p<0.05, ** p<0.01, *** p<0.001.*

4.2.3 Analysis of anxious behavior (Elevated Plus Maze test)

The Elevated Plus Maze test was performed after 4 months of treatment. The duration mice spent in open arms, closed arms, the neutral zone, the number of entries in open arms, closed arms and the neutral zone, the distance, speed and the first entry in open and closed arms were measured in this test but no significant differences were observed between all groups (Figure 23 A-J).

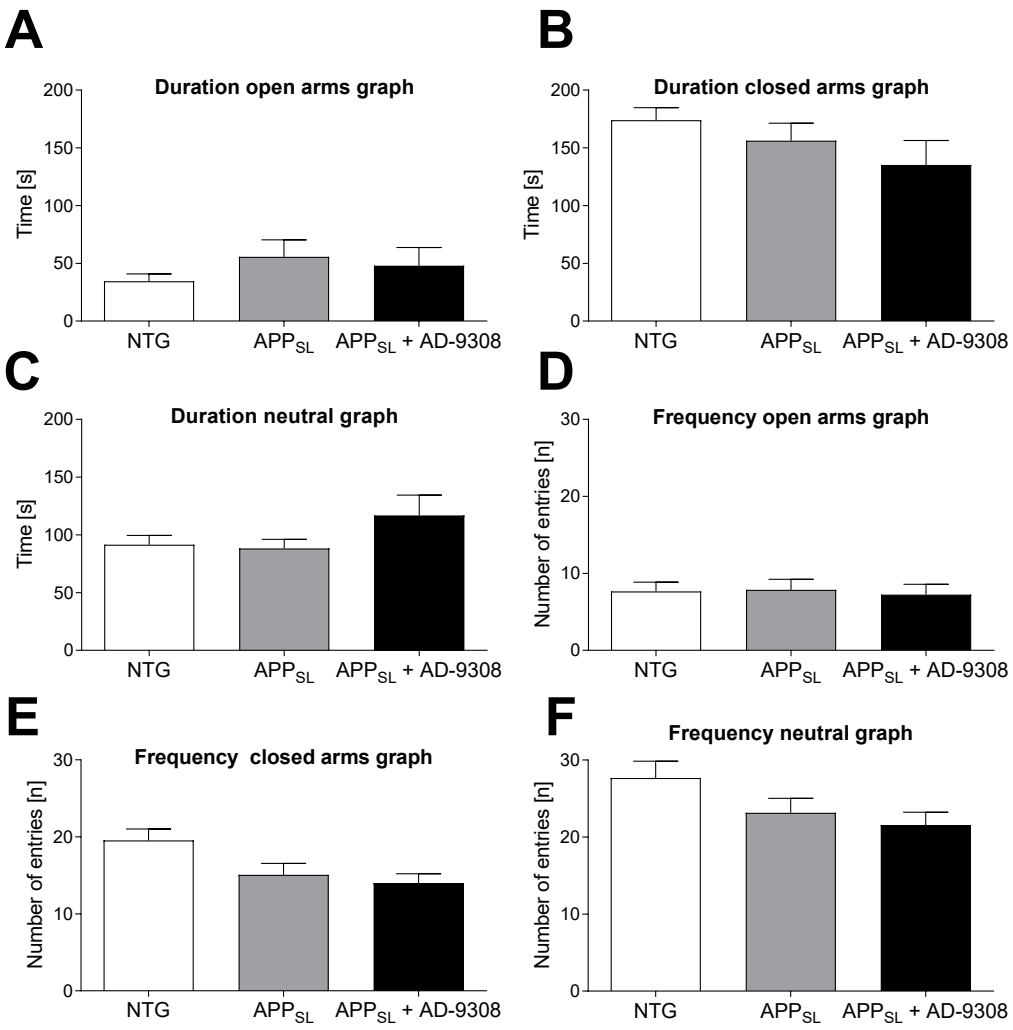

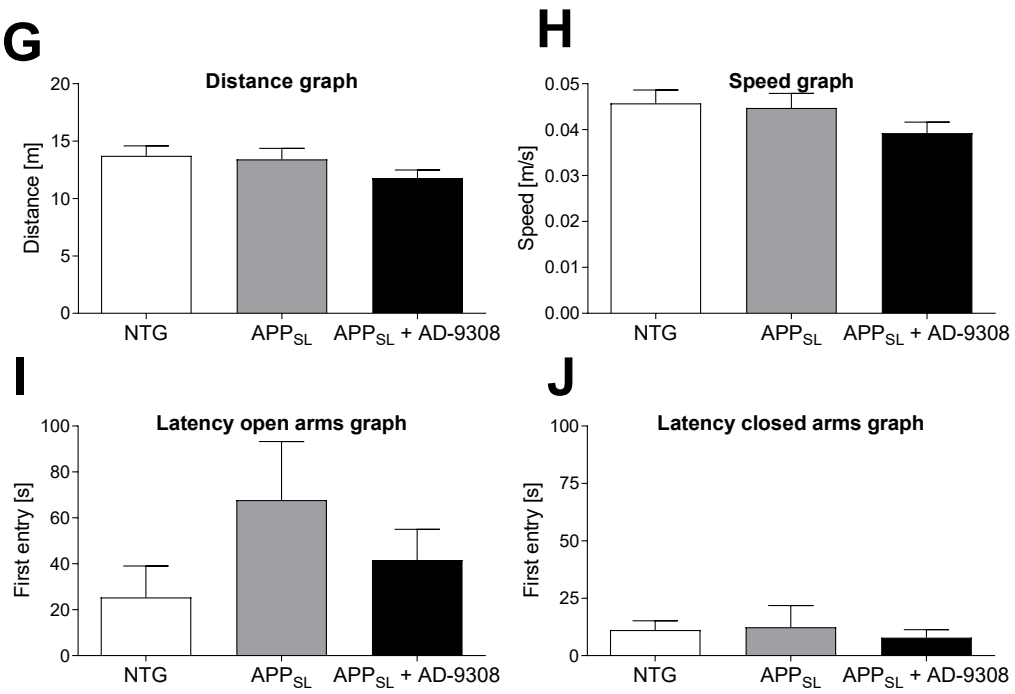

Figure 23: Elevated plus maze test after 4 months of treatment. Duration in open arms (A), duration in closed arms (B), duration in the neutral zone (C), number of entries in open arms (D), number of entries in closed arms (E), number of entries in the neutral zone (F), distance (G), speed (H), first entry in open arms (I) and first entry in closed arms (J) were measured in APP_{SL} + AD-9308, APP_{SL} and NTG mice. No significant differences were detected in this test. Statistics: One-way ANOVA followed by Bonferroni's post hoc test. NTG: n = 15, APP_{SL}: n = 14, APP_{SL} + AD-9308: n = 13. Data are represented as mean ± SEM.

4.2.4 Analysis of spontaneous alternation (Modified Y-maze)

The Modified Y-maze test was performed after 2 and 4 months of treatment. After 2 months of treatment no significant changes were evaluated in spontaneous alternating behavior between the different groups (Figure 24 A-G). Interestingly the non performer rate which includes animals who did not move the whole minute from the place were they were entered into the maze increased stronger in APP_{SL} + AD-9308 and APP_{SL} than in NTG mice (Figure 24 H).

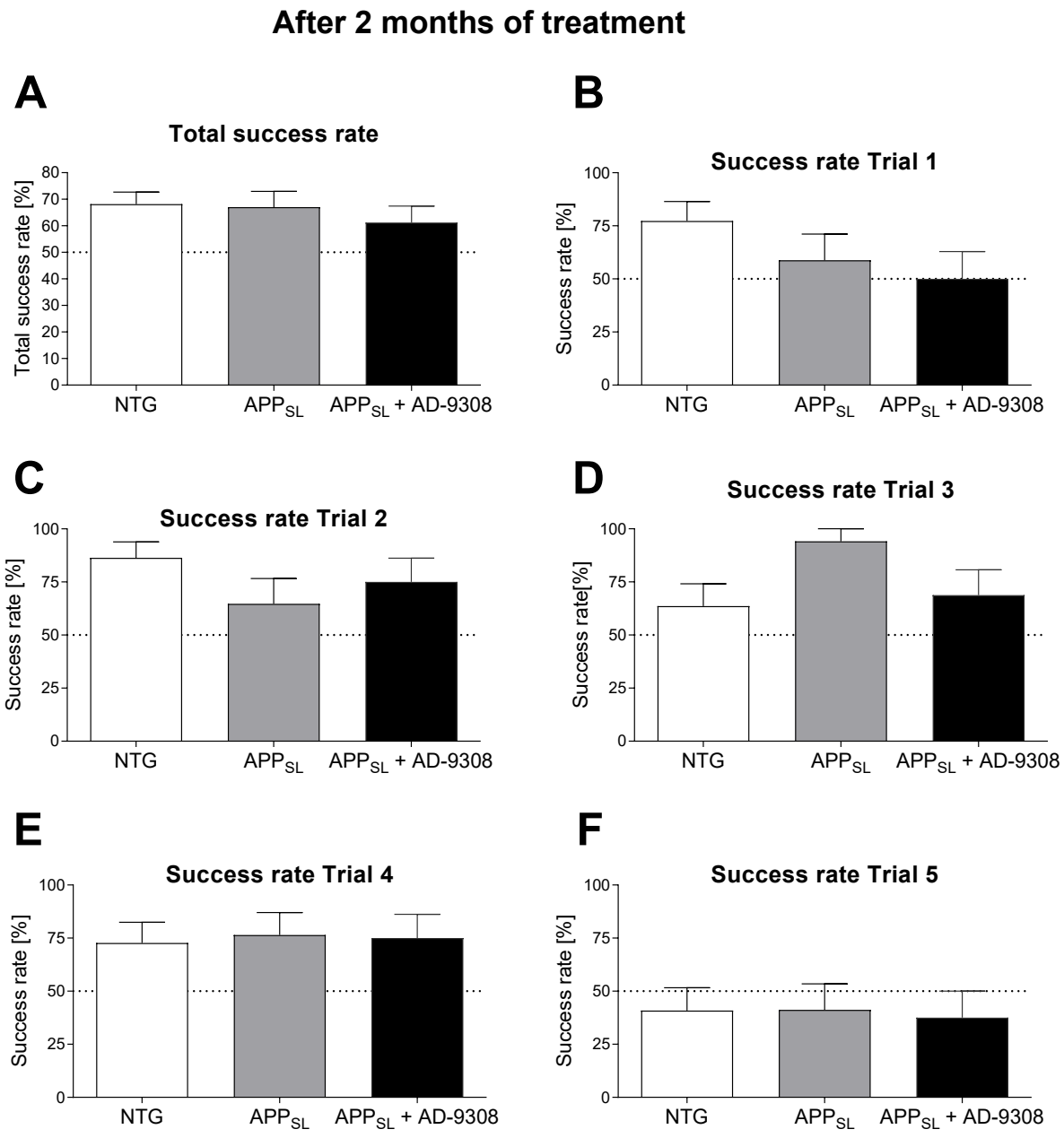

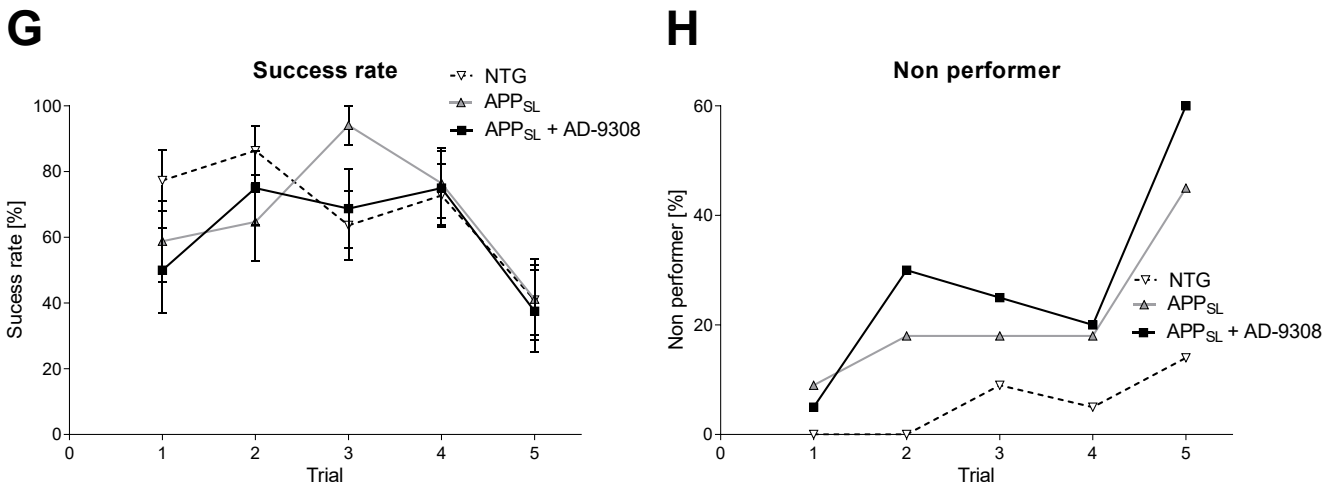

Figure 24: Modified Y - maze test after 2 months of treatment. Graphs represent the total success rate of all 5 trials (A), success rate of trial 1 (B), success rate of trial 2 (C), success rate of trial 3 (D), success rate of trial 4 (E), success rate of trial 5 (F), success rate of each trial (G) and non performer rate (H). Mice which did not move the whole minute and did not chose any arm were assigned to the non performer group for that trial. Statistics: One-way (A-F) or Two-way (G, H) ANOVA followed by Bonferroni's post hoc test. n = 22 per group. Data are represented as mean ± SEM.

After 4 months of treatment animals were tested in the Y-maze test again to evaluate their spontaneous alteration behavior. Mice did only perform the first trial and then the non-performer rate increased dramatically in all groups. For that reason, only the success rate of trial 1 and the non performer rate were evaluated in this test. No significant differences were detected in the success rate of trial 1 in any of the groups (Figure 25 A). The non-performer rate was significantly increased in trial 4 in APP_{SL}+ AD-9308 mice compared to the NTG group (Figure 25 B).

After 4 months of treatment

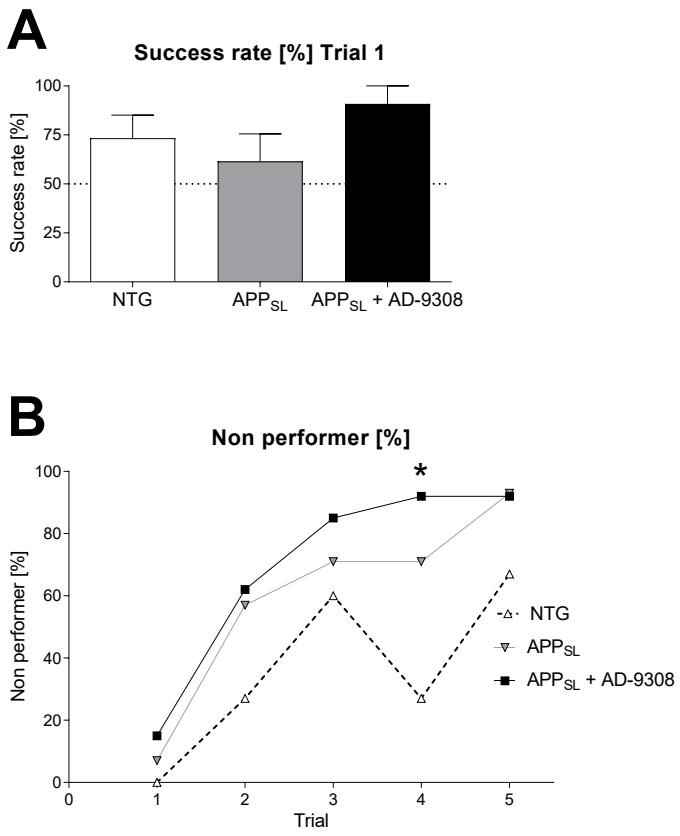

*Figure 25: Modified Y - maze test after 4 months of treatment. Success rate of trial 1 (A) and non performer rate were evaluated in APP_{SL} + AD-9308, APP_{SL} and NTG mice after 4 month of treatment. Mice which did not move the whole minute and did not choose any arm were assigned to the non performer group for that trial. Statistics: One-way (A) or Two-way (B) ANOVA followed by Bonferroni's post hoc test. NTG: n = 15, APP_{SL}: n = 14, APP_{SL} + AD-9308: n = 13. Data are represented as mean ± SEM. * p<0.05.*

4.2.5 Investigation of spatial learning and memory (Morris Water Maze test)

After 4 months of treatment the Morris Water Maze test was performed. In all three different groups an improvement during the testing period for time and swim length to reach the platform was observed. Treatment with AD-9308 improved spatial learning in the MWM task and was significant starting on day 2 compared to APP_{SL} animals (Figure 26 A, B).

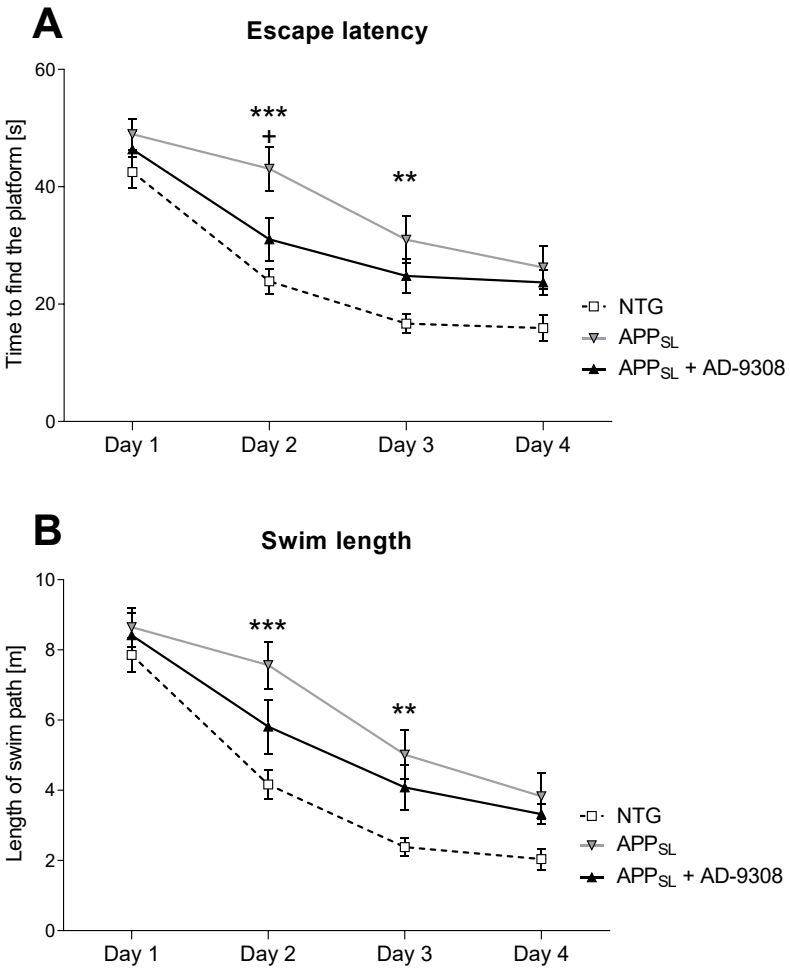

*Figure 26: MWM learning curves after 4 months of treatment: Graphs represent escape latency (A) and the swim length (B) recorded in the MWM. On day 2 and 3 of training, significant differences were detected between animals of groups APP_{SL} vs. NTG (*) and APP_{SL} + AD-9308 vs. APP_{SL} (+). Statistics: Two-way ANOVA followed by Bonferroni's post hoc test. NTG: n = 15, APP_{SL}: n = 14, APP_{SL} + AD-9308: n = 13. Data are represented as mean ± SEM. **p<0.01; ***p<0.001.*

Floating behavior was significantly decreased but thigmotaxis behavior was significantly increased between APP_{SL} and NTG animals (Figure 27 A, B).

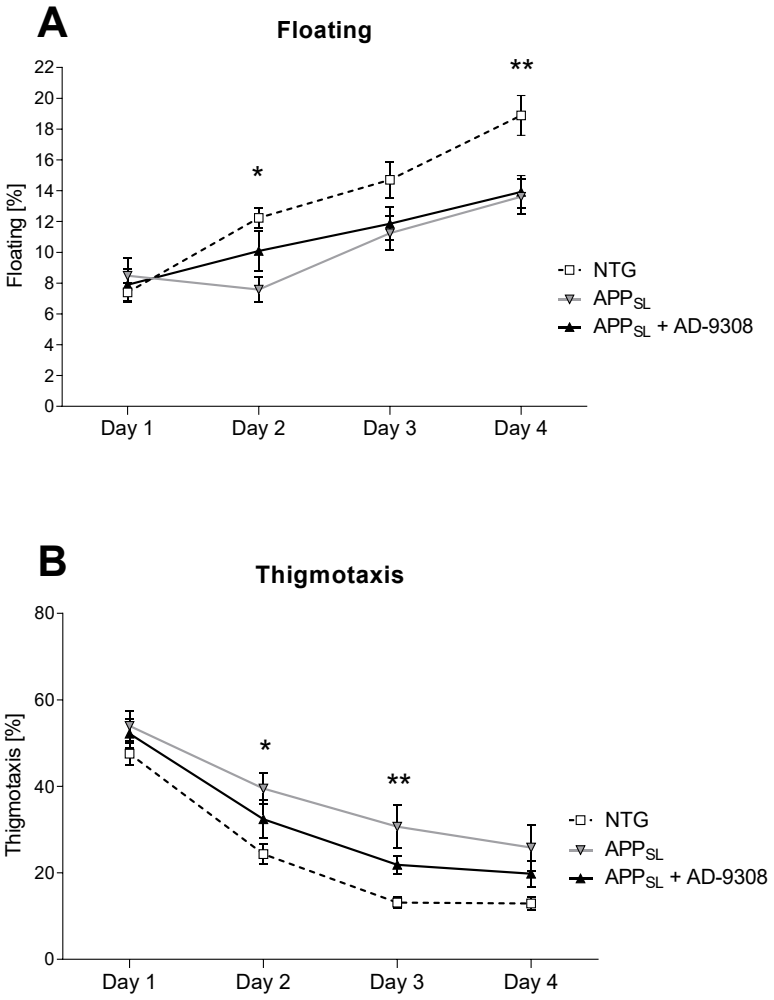

*Figure 27: Measuring of floating and thigmotaxis in the MWM test after 4 months of treatment: Graphs represent floating (A) and thigmotaxis (B) recorded in the MWM. On day 2, 3 or 4 of training, significant differences were detected between APP_{SL} and NTG animals. Statistics: Two-way ANOVA followed by Bonferroni's post hoc test. NTG: n = 15, APP_{SL}: n = 14, APP_{SL} + AD-9308: n = 13. Data are represented as mean ± SEM. *p<0.05, **p<0.01.*

Results of the MWM probe trial showed no differences between the three groups regarding target zone crossings (Figure 28 A). When investigating the abidance in the target quadrant (NE quadrant) APP_{SL} animals showed a significantly reduced length of stay compared to the 25 % by chance length of stay of NTG animals. Furthermore, the time NTG and APP_{SL}+ AD-9308 animals spent in the NE quadrant was significantly increased compared to the three other quadrants (Figure 28 B, C).

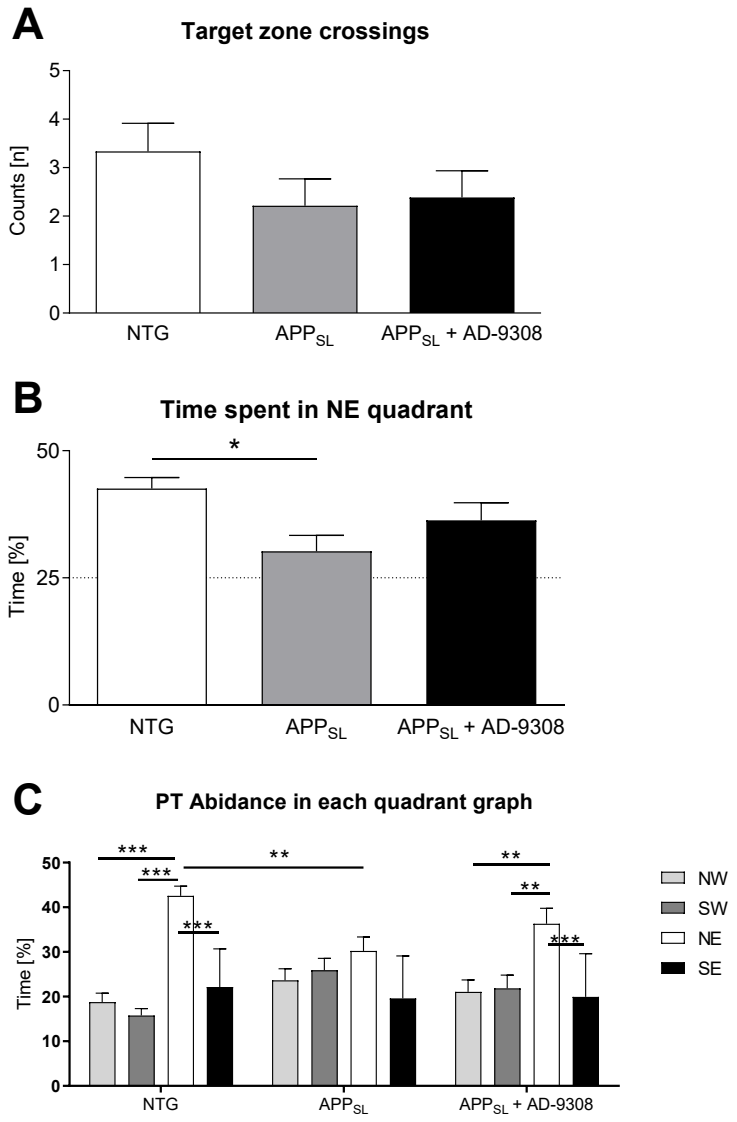

*Figure 28: MWM probe trial after 4 months of treatment: Graphs represent target zone crossings (A), time spent in NE quadrant (B) and time spent in each quadrant (C) recorded in the MWM probe trial. Statistics: Two-way ANOVA followed by Bonferroni's post hoc test (A) and one sample t -Test (B, C). NTG: n = 15, APP_{SL}: n = 14, APP_{SL} + AD-9308: n = 13. Data are represented as mean ± SEM. *p<0.05, **p<0.01, *** p<0.001.*

4.2.6 NMR-based metabolic phenotyping

In order to assess metabolic differences in APP_{SL} + AD-9308 compared to APP_{SL} and APP_{SL} compared to NTG mice, NMR metabolic profiling was performed after 2 and 4 months of treatment in serum, different brain regions (cortex, hippocampus, cerebellum, rest of the left hemisphere) and different organs (heart, kidneys, liver, lung, spleen). By comparing metabolic fingerprints between APP_{SL} + AD-9308 and APP_{SL} mice as well as APP_{SL} and NTG mice no clustering in the PCA and O-PLS-DA was observed after 2 months of treatment in all measured samples. Moreover, reduced NMR spectra showed no altered metabolite levels between APP_{SL} + AD-9308 and APP_{SL} mice as well as APP_{SL} and NTG mice in all measured samples after 2 months of treatment (data not shown).

Interestingly, acetate was increased in serum in APP_{SL} + AD-9308 compared to APP_{SL} mice after 4 months of treatment (Figure 29). Nevertheless, no further altered metabolites were observed in APP_{SL} + AD-9308 and APP_{SL} mice as well as APP_{SL} and NTG mice after 4 months of treatment in all measured samples.

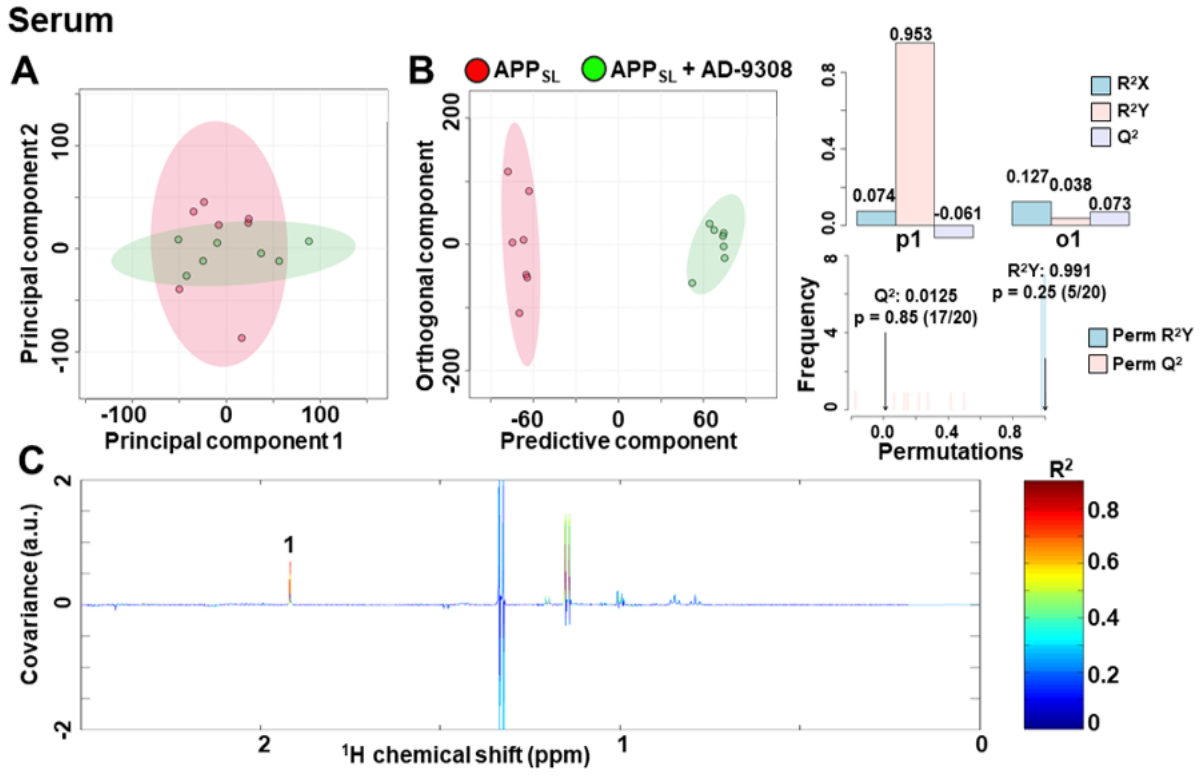

Figure 29: NMR metabolic profiling after 4 months of treatment. (A) PCA and (B) O-PLS-DA plot of serum samples. (C) Reduced NMR spectra reveal altered metabolites in normalized serum samples. 1: acetate. Positive covariance corresponds to increased metabolite levels in

APP_{SL} + AD-9308 compared to APP_{SL} mice after 4 months of treatment. Predictivity is represented by R^2 and Q^2.

Subsequently the amount of acetate in serum was analyzed using the integrated signals in the normalized spectra. In line with the multivariate statistical analysis, acetate was significantly increased in APP_{SL} + AD-9308 animals compared to APP_{SL} mice (Figure 30).

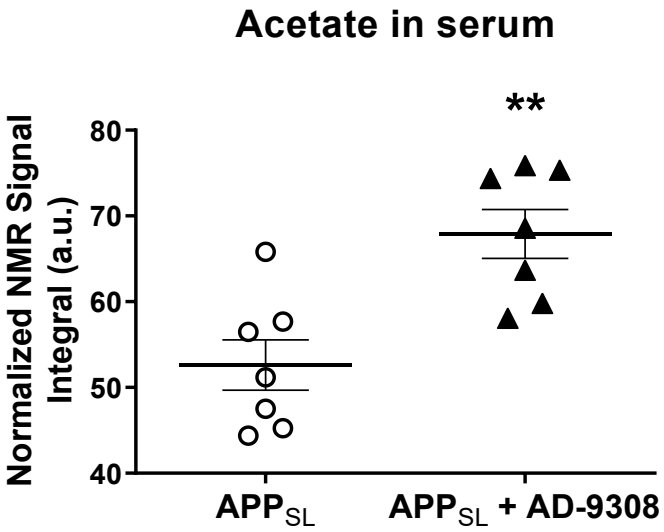

*Figure 30: Quantification of acetate levels in APP_{SL} + AD-9308 mice compared to APP_{SL} mice. Quantification of acetate in serum samples (n = 7): Unpaired t-test. Data are represented as mean ± SEM. **p< 0.01.*

4.2.7 Qualitative histological assessment of human amyloid-β levels, inflammation marker and neuronal loss

Mouse brains of all groups were processed and no major problems occurred during histological analysis. Measurements in repeated sections led to comparable background throughout all sections from mice of all groups. No differences in tissue quality were detected during histological procedures and the tissue quality was generally good for all samples.

Examples of immunofluorescence labeling on sagittal sections of APP_{SL} + AD-9308, APP_{SL} and NTG mice are provided in Figure 31, Figure 32 and Figure 33. Single channel magnifications show labeling of the cortex; images were taken at the position indicated by the white rectangle in the overview image on the left. Slides were stained with NeuN (to detect neuronal changes), GFAP (to detect astrogliosis), Iba-1 (to detect microgliosis) and a human specific Aβ antibody to detect total human Aβ levels of APP_{SL} mice. Already in 7-month-old APP_{SL} mice a slight increase in human Aβ levels were investigated which further increased with a higher age in APP_{SL} and APP_{SL} + AD-9308 compared to NTG mice. Also a significant increase in astro- and microgliosis were evaluated in APP_{SL} and APP_{SL} + AD-9308 compared to NTG mice increasing with a higher age of the animals.

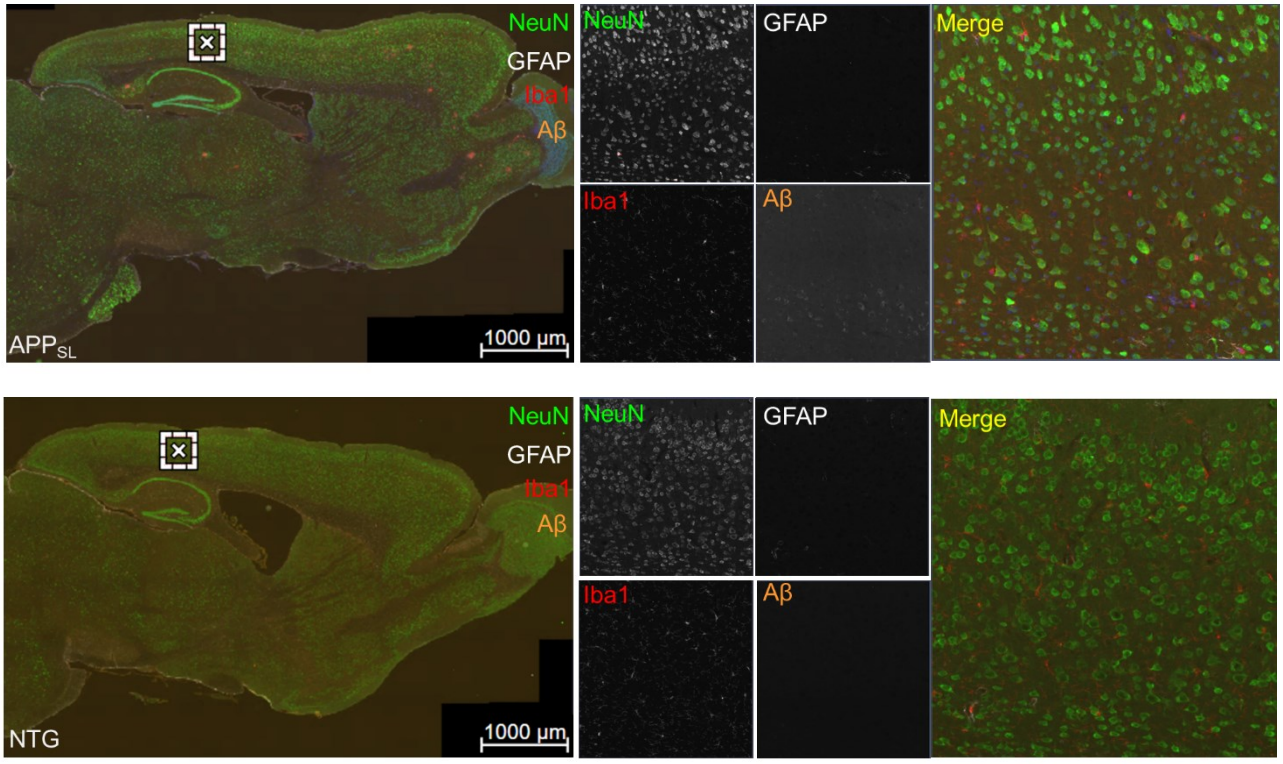

Figure 31: Immunofluorescent signal of NeuN, GFAP, Iba-1 and amyloid-β in 7-month-old APP_{SL} and NTG mice. Images show examples of immunofluorescent labeling on sagittal sections of APP_{SL} and NTG mice at study start (baseline). Single channel magnifications show

labeling of the cortex; images were taken at the position indicated by the white rectangle in the overview image on the left.

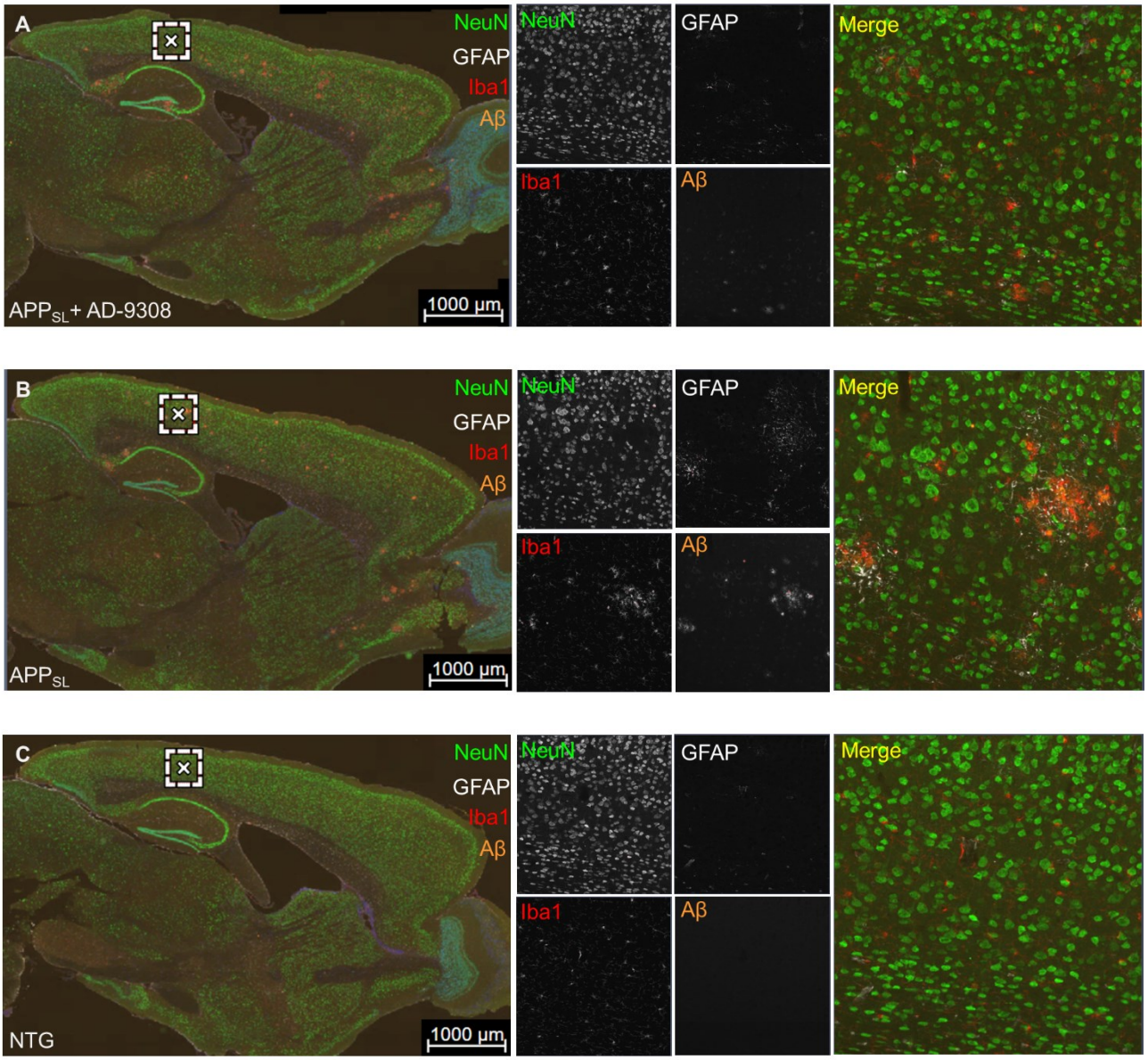

Figure 32: Immunofluorescent signal of NeuN, GFAP, Iba-1 and amyloid-β in 9-month-old APP$_{SL}$ + AD-9308, APP$_{SL}$ and NTG mice. Images show examples of immunofluorescent labeling on sagittal sections of all groups. Single channel magnifications show labeling of the cortex; images were taken at the position indicated by the white rectangle in the overview image.

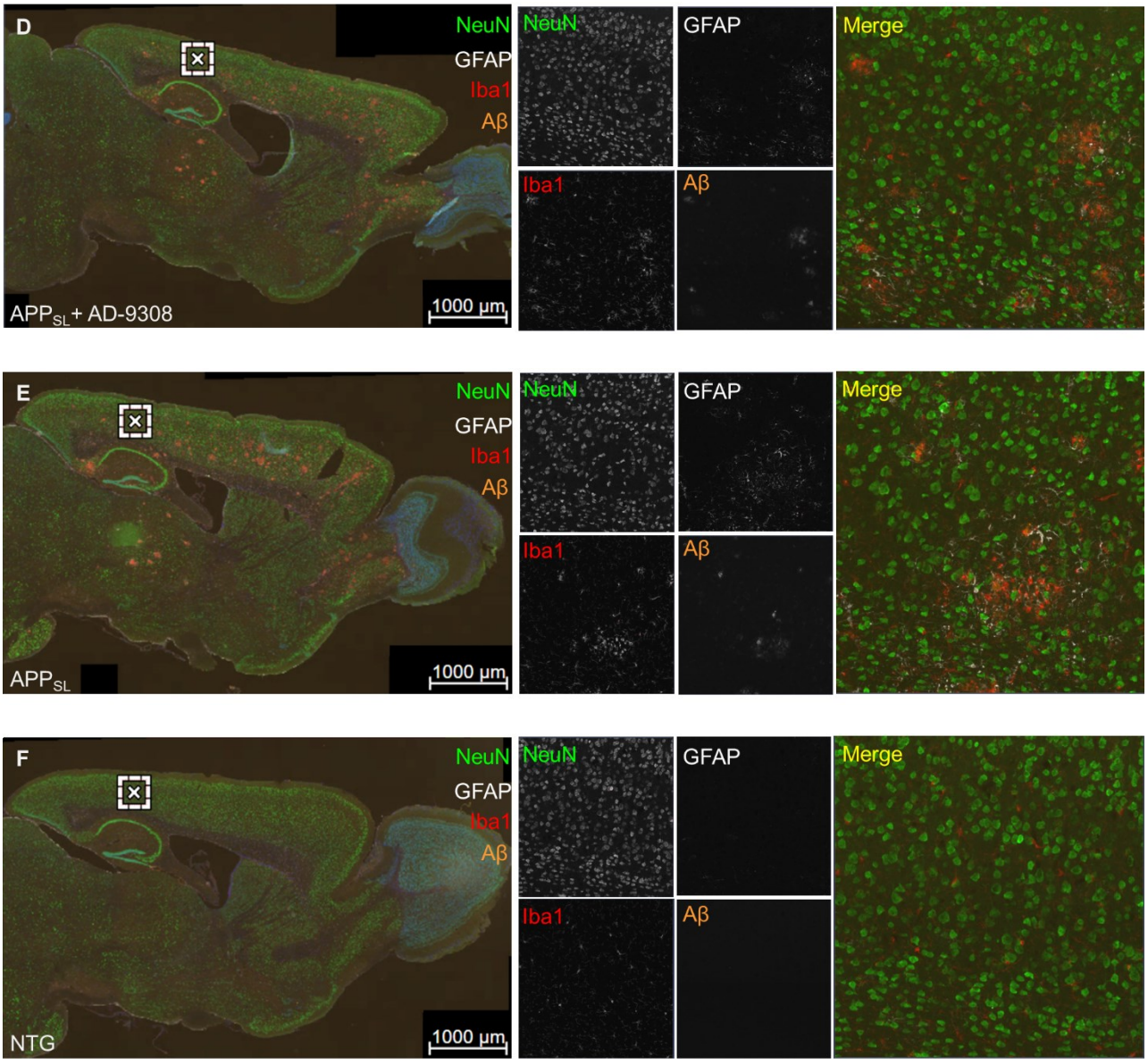

Figure 33: Immunofluorescent signal of NeuN, GFAP, Iba-1 and amyloid-β in 11-month-old APP_{SL} + AD-9308, APP_{SL} and NTG mice. Images show examples of immunofluorescent labeling on sagittal sections of all groups. Single channel magnifications show labeling of the cortex; images were taken at the position indicated by the white rectangle in the overview image.

4.2.8 Measurement of amyloid-β levels

Frozen samples of 6 APP_{SL} + AD-9308 and APP_{SL} animals were analyzed for human Aβ1-38, Aβ1-40 and Aβ1-42 in the DEA (soluble) and FA (total) fraction of the left cortex by an immunosorbent assay (Aβ Peptide Panel 1 (6E10); K15200E-2; Meso Scale Discovery). Because human Aβ levels are not detectable in NTG animals, this assay was only performed in APP_{SL} + AD-9308 and APP_{SL} mice

While Aβ1-38, was very low and close to the detection limit, the other two species of interest, Aβ1-40 and Aβ1-42 were well within the detection range. Values of one animal of the APP_{SL} + AD-9308 group were under the limit of detection, identified as an outlier by the Grubb`s test and excluded from analysis. Significantly decreased total Aβ1-40 levels were detected in APP_{SL} + AD-9308 compared to APP_{SL} mice (Figure 34 D). No significant differences were observed in soluble and total Aβ1-38, in soluble Aβ1-40 and soluble and total Aβ1-42 levels (Figure 34 A-C & E, F) of all groups.

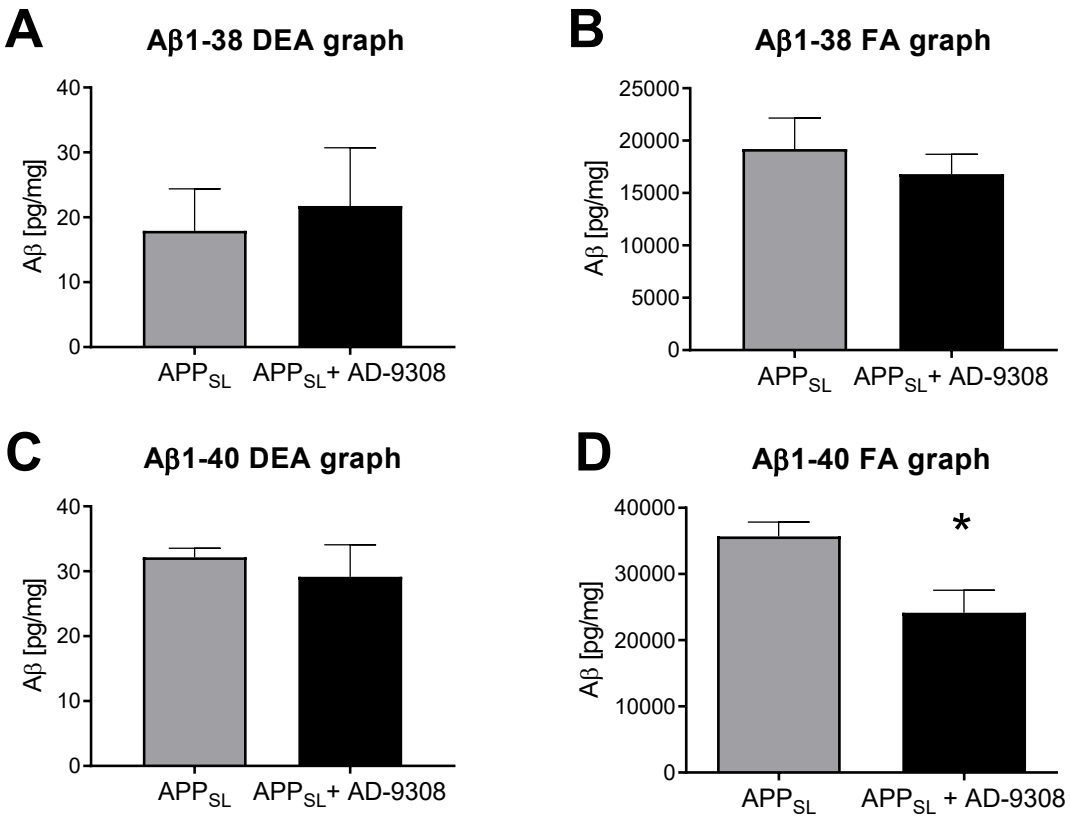

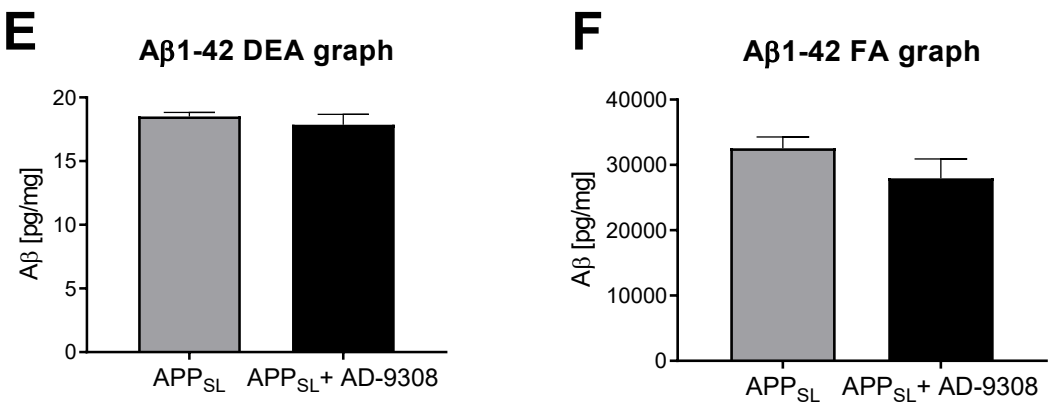

*Figure 34: Quantification of human amyloid-β levels in 11-month-old APP_{SL} + AD-9308, APP_{SL} and NTG mice. Aβ1-38 (A, B), Aβ1-40 (C, D) and Aβ1-42 (E, F) in the DEA (soluble, A,C,E) and FA (total, B,D,F) fractions from the left cortex using an immunosorbent assay. Significantly decreased levels in total Aβ1-40 were detected in APP_{SL} + AD-9308 compared to APP_{SL} mice. Statistics: Unpaired t-test. NTG: n = 15, APP_{SL}: n = 14, APP_{SL} + AD-9308: n = 13. Data are represented as mean ± SEM. *p<0.05.*

Furthermore, immunofluorescence of human amyloid-β was evaluated with the 6E10 mouse monoclonal antibody, and the signal was quantified in the cerebral cortex (Figure 35 A, B), and hippocampal formation (Figure 36 A, B). Statistical analyses show highly significant increased total human Aβ levels of APP_{SL} + AD-9308 and APP_{SL} mice compared to NTG animals but no treatment effects were determined. The readouts of immunoreactive area (Figure 28 A, Figure 36 A) and object density (Figure 28 B, Figure 36 B) show that the amyloid signal is significantly higher in APP_{SL} mice but absent from NTG mice, indicating a high specificity of the 6E10 monoclonal antibody. Treatment with AD-9308 had no significant effect in APP_{SL} mice.

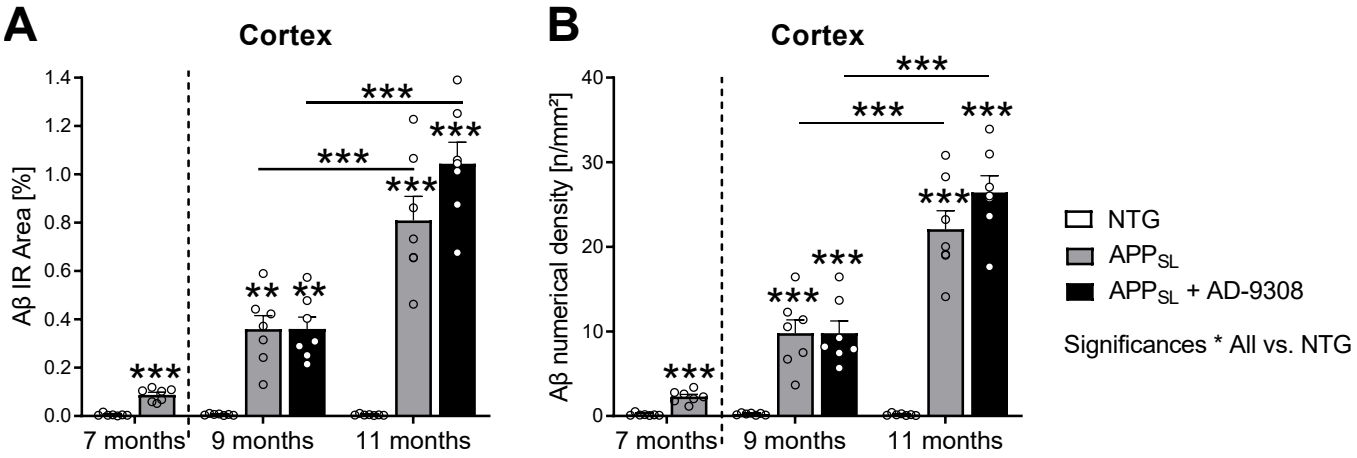

*Figure 35: Quantification of amyloid-β immunofluorescence in the cerebral cortex. Immunoreactive area (A) and numerical density (B) were measured within the AOI on 5 brain sections per mouse (n = 7 per group). Note the strong increase in Aβ levels in APP_{SL} and APP_{SL} + AD-9308 compared to NTG mice, whereas the APP_{SL} + AD-9308 mice show no significant differences compared to APP_{SL} mice. Statistics: Data at 7 months were analyzed by Unpaired t-test and data from 9 and 11 months were evaluated using two-way ANOVA followed by Bonferroni's post hoc test. Data are represented as mean ± SEM. **p<0.01, ***p<0.001.*

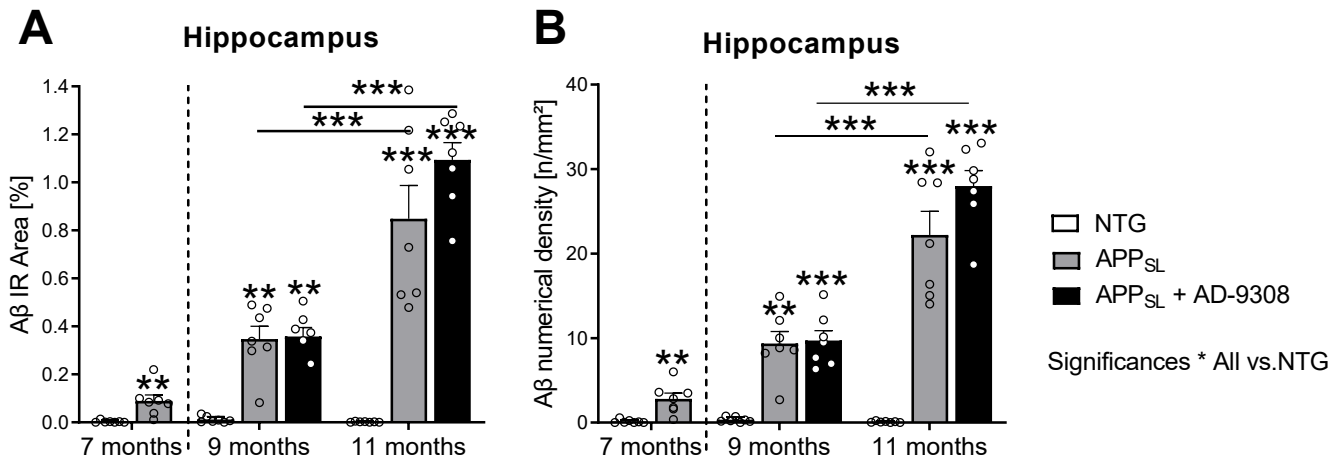

*Figure 36: Quantification of amyloid-β immunofluorescence in the hippocampus. Immunoreactive area (A) and numerical density (B) were measured within the AOI on 5 brain sections per mouse (n = 7 per group). Note the strong increase in Aβ levels in APP_{SL} and APP_{SL} + AD-9308 compared to NTG mice, whereas the APP_{SL} + AD-9308 mice show no significant differences compared to APP_{SL} mice. Statistics: Data at 7 months were analyzed by Unpaired t-test and data from 9 and 11 months were evaluated using two-way ANOVA followed by Bonferroni's post hoc test. Data are represented as mean ± SEM. **p<0.01, ***p<0.001.*

4.2.9 Evaluation of Neurodegeneration

No significant differences in murine neurofilament light chain levels were detected in the cerebrospinal fluid of 11-month-old APP_{SL} + AD-9308, APP_{SL} and NTG mice. (n = 12, data not shown).

Immunofluorescence of NeuN was detected with guinea pig polyclonal antibody in APP_{SL} + AD-9308, APP_{SL} and NTG mice and the signal was quantified in the cerebral cortex (Figure 37 A, B), and hippocampal formation (Figure 38 A, B). Statistical analyses show no neuronal changes in APP_{SL} + AD-9308 and APP_{SL} mice compared to NTG animals and no treatment effects were determined but significantly increased NeuN levels were detected in the cortex and hippocampus of 7-month-old APP_{SL} compared to NTG mice.

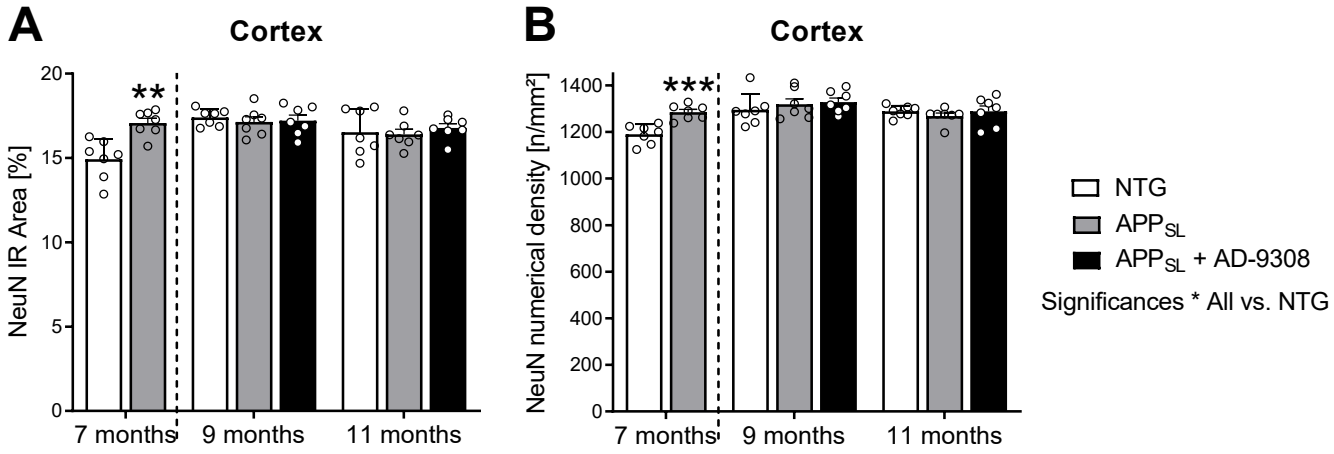

*Figure 37: Quantification of NeuN immunofluorescence in the cerebral cortex. Immunoreactive area (A) and numerical density (B) were measured within the AOI on 5 brain sections per mouse (n = 7 per group). There were significantly increased NeuN levels in APP_{SL} compared to NTG mice at 7 months. Statistics: Data at 7 months were analyzed by Unpaired t-test and data from 9 and 11 months were evaluated using two-way ANOVA followed by Bonferroni's post hoc test. Data are represented as mean ± SEM. **p<0.01, ***p<0.001.*

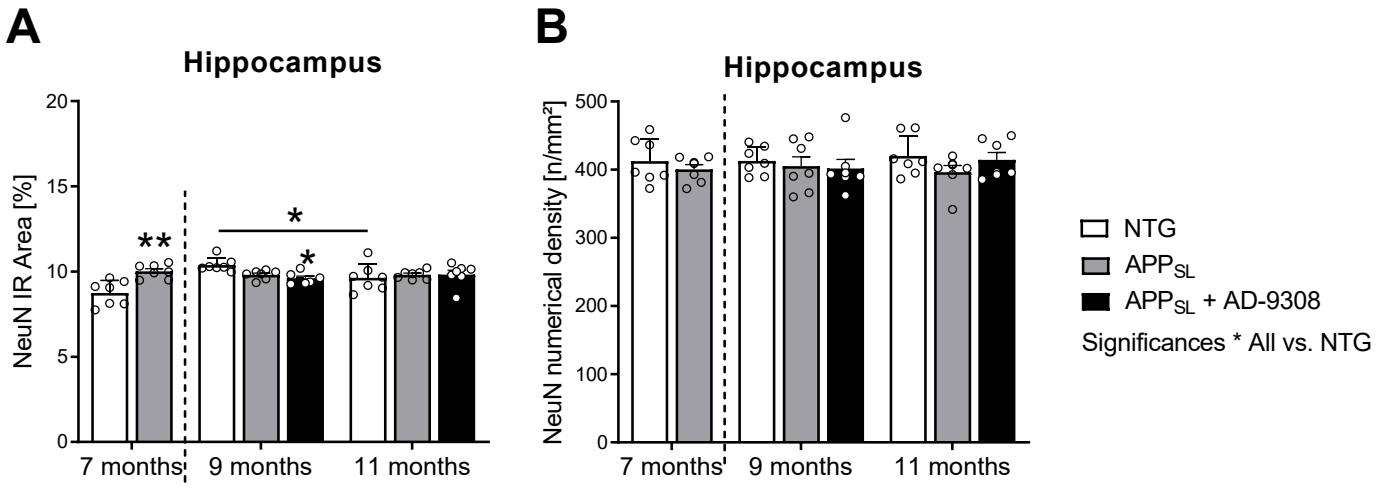

*Figure 38: Quantification of NeuN immunofluorescence in the hippocampus. Immunoreactive area (A) and numerical density (B) were measured within the AOI on 5 brain sections per mouse (n = 7 per group). APP_{SL} + AD-9308 mice show no significant differences compared to APP_{SL} mice. Statistics: Data at 7 months were analyzed by Unpaired t-test and data from 9 and 11 months were evaluated using two-way ANOVA followed by Bonferroni's post hoc test. Data are represented as mean ± SEM. **p<0.01, ***p<0.001.*

4.2.10 Measurement of Neuroinflammation

Immunofluorescence of GFAP to detect astrogliosis, was analyzed with a goat polyclonal antibody. The signal was quantified in the cerebral cortex (Figure 39 A, B) and hippocampal formation (Figure 40 A, B). Statistical analyses show a highly significant increase in astrogliosis in the cortex of APP_{SL} + AD-9308 and APP_{SL} mice compared to NTG animals starting at 7 months of age (Figure 39 A, B) but no treatment effects were determined. Moreover, highly significant increased astrogliosis was measured in the hippocampus of APP_{SL} + AD-9308 and APP_{SL} mice compared to NTG animals at 11 months of age (Figure 40 A, B).

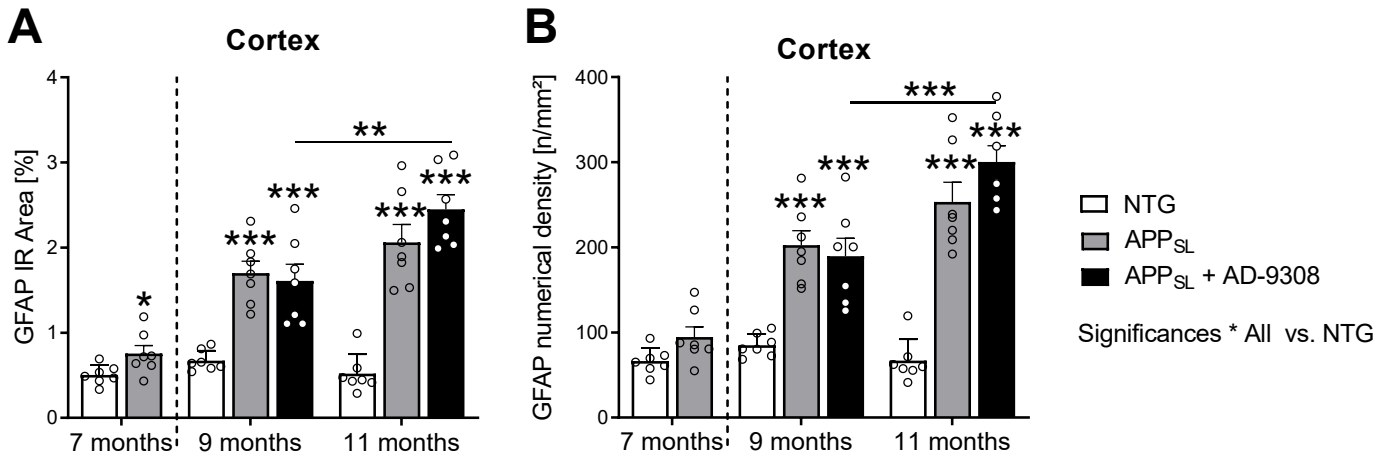

*Figure 39: Quantification of GFAP immunofluorescence in the cerebral cortex. Immunoreactive area (A) and numerical density (B) were measured within the AOI on 5 brain sections per mouse (n = 7 per group). Note the strong increase in GFAP levels in APP_{SL} + AD-9308 and APP_{SL} compared to NTG mice, whereas APP_{SL} + AD-9308 mice show no significant differences compared to APP_{SL} mice. Statistics: Data at 7 months were analyzed by Unpaired t-test and data from 9 and 11 months were evaluated using two-way ANOVA followed by Bonferroni's post hoc test. Data are represented as mean ± SEM. *p<0.05, **p<0.01, ***p<0.001.*

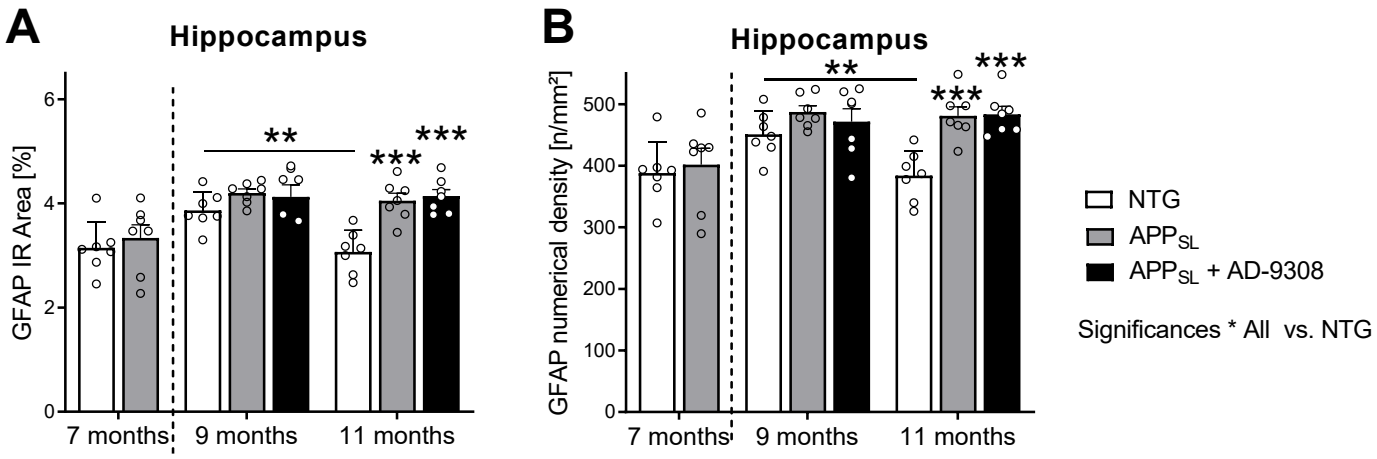

*Figure 40: Quantification of GFAP immunofluorescence in the hippocampus. Immunoreactive area (A) and numerical density (B) were measured within the AOI on 5 brain sections per mouse (n = 7 per group). Significantly increased astrogliosis was detected in APP_{SL} + AD-9308 and APP_{SL} compared to NTG mice at 11 months of age. APP_{SL} + AD-9308 mice showed no significant differences compared to APP_{SL} mice. Statistics: Data at 7 months were analyzed by Unpaired t-test and data from 9 and 11 months were evaluated using two-way ANOVA followed by Bonferroni's post hoc test. Data are represented as mean ± SEM. **p<0.01, ***p<0.001.*

Immunofluorescence of Iba-1 to detect microgliosis was performed with rabbit polyclonal antibody. The signal was quantified in the cerebral *cortex (Figure 41 A, B),* and hippocampal formation (Figure 42 A, B). The immunoreactive area and the numerical density showed a highly significant increase in microgliosis in APP_{SL} + AD-9308 and APP_{SL} mice compared to NTG animals already at the age of 7 months in the cortex and hippocampus. Iba-1 signal further increased in both areas at 9 and 11 months. However, treatment with AD-9308 had no significant effect on any of the readouts in all APP_{SL} transgenic mice.

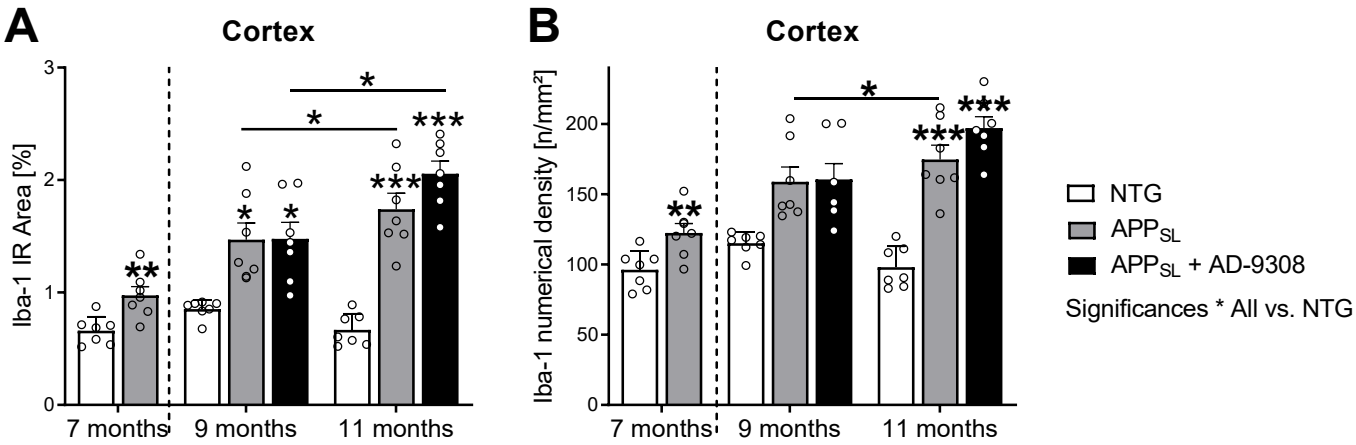

Figure 41: Quantification of Iba-1 immunofluorescence in the cerebral cortex. Immunoreactive area (A) and numerical density (B) were measured within the AOI on 5 brain sections per mouse (n = 7 per group). Significantly increased microgliosis was detected in APP_{SL} + AD-9308 and APP_{SL} compared to NTG mice starting at 7 months of age. APP_{SL} + AD-9308 mice showed no significant difference compared to APP_{SL} mice. Statistics: Data at 7 months were analyzed by Unpaired t-test and data from 9 and 11 months were evaluated using two-way ANOVA followed by Bonferroni's post hoc test. Data are represented as mean ± SEM. **p<0.05, **p<0.01, ***p<0.001.*

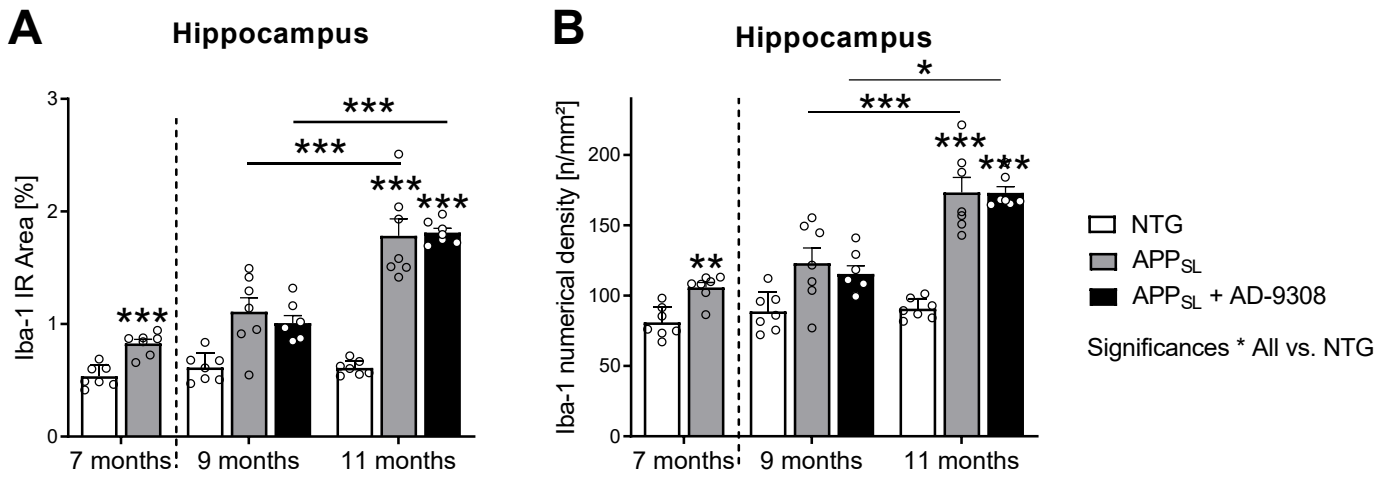

Figure 42: Quantification of Iba-1 immunofluorescence in the hippocampus. Immunoreactive area (A) and numerical density (B) were measured within the AOI on 5 brain sections per mouse (n = 7 per group). Significantly increased microgliosis was detected in APP_{SL} + AD-9308 and APP_{SL} compared to NTG mice starting at 7 months of age. APP_{SL} + AD-9308 mice showed no significant difference compared to APP_{SL} mice. Statistics: Data at 7 months were analyzed by Unpaired t-test and data from 9 and 11 months were evaluated using two-way ANOVA followed by Bonferroni's post hoc test. Data are represented as mean ± SEM. **p<0.05, **p<0.01, ***p<0.001.*

4.2.11 Evaluation of mitochondrial function

Assessment of Thiobarbituric acid reactive substances (TBARS) as marker for oxidative stress in serum revealed significantly decreased levels in APP_{SL} + AD-9308 compared to APP_{SL} animals (Figure 43). All data points from the TBARS measurement were well within the detection range.

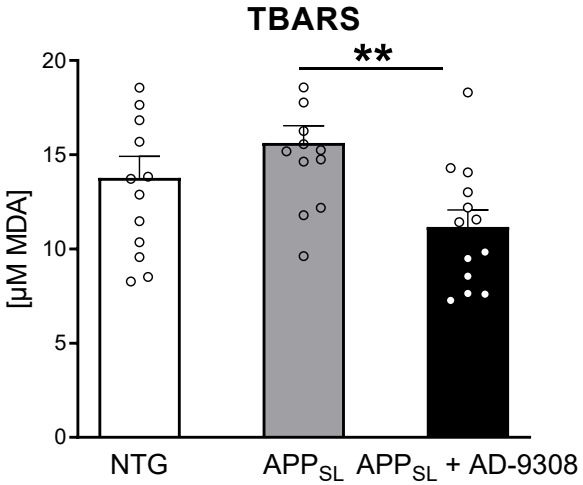

*Figure 43: Measurement of mitochondrial function. Assessment of TBARS; values are presented in µM malondialdehyde (MDA) equivalents. Statistics: One-way ANOVA followed by Tukey``s post hoc test. n = 13 per group. Data are represented as mean ± SEM. **p<0.01.*

Assessment of 4-hydroxy-2-nonenal (4-HNE) as marker for oxidative stress in serum, cortex and hippocampus did not reveal any significant changes between APP_{SL} + AD-9308, APP_{SL} and NTG animals although all data points of the 4-HNE measurement were well within the detection range (data not shown).

In addition, ROS levels as well as complex I activity determination revealed no changes between all investigated groups (data not shown).

5 DISCUSSION

The central aims of this thesis were to perform a comprehensive characterization of the novel Tg4-42 mouse model by integrating metabolomic phenotyping and already established approaches as well as the evaluation of the effects of an ALDH2 agonist on AD disease progression in APP_{SL} mice.

5.1 Tg4-42 characterization

In the first part of this study, *in vivo* results demonstrated impaired learning behavior and memory deficits in Tg4-42 mice. Untargeted NMR-based metabolic profiling showed significantly decreased glutamine and 4-aminobutyrate levels in different brain areas compared to NTG mice. To verify these results, enzymes within this pathway were analyzed histologically showing that glutaminase as well as GAD67 were significantly increased in Tg4-42 +/+ mice. Based on these results, downstream effects were analyzed showing increased Aβ42 levels, increased neuroinflammation, loss of neurons as well as a knockdown of the retinoic acid receptor beta in Tg4-42 +/+ transgenic mice, the latter questioning the cause of the evaluated phenotype of these mice to be solely dependent on Aß4-42 expression.

Changes in body weight can severely influence the outcome of behavior studies. It has been shown that for example an increased body weight can influence motor performance in some mouse strains (110). A reduced body weight of APP overexpressing mouse models has been described in several studies (111-113). Analysis of the general health status of Tg4-42 +/+ mice demonstrated a significant decrease in body weight, which did further not increase over age compared to NTG controls. Similar but not significant results that 3 and 7 month old homozygous Tg4-42 mice have a lower body weight than age-matched wild type mice are also shown in the literature (110). For that reason, it is important to be aware that different body weights can influence behavioral results and therefore to pay attention to a similar weight distribution between all groups at study start.

The open field test is a powerful tool to measure spontaneous activity and can be beneficial for assessing disease progression in animals (114, 115). It is reported that locomotive activity can be influenced by different factors for example environmental conditions or experimenter handling leading to variations in activity (116). In the here presented study general activity levels were significantly decreased over age in Tg4-42 +/+ animals compared to NTG controls. Furthermore, the total distance Tg4-42 +/+ mice travelled in the open field were similar to NTG mice but the total distance decreased in Tg4-42 +/+ mice with a higher age. In line with these results no impaired locomotor activity during the open field test were shown in 3 and 7 months

old Tg4-42 +/+ mice by Wagner et al. In their study these transgenic homozygous mice travelled the same distance as wild type control mice but the travelled distance decreased in 7 months old compared to 3 month old Tg4-42 +/+ mice (110). These results indicate that the activity level decreases in Tg4-42 +/+ mice at a higher age which is also described in other transgenic mouse lines for example in 5xFAD mice (110). Therefore, it is important to determine relevant time points to assess activity measurements, which can vary by animal model, age and sex.

Likewise, anxious behavior was assessed with a widely used behavioral assay called the elevated plus maze test. In the here presented study Tg4-42 +/+ mice spent more time in the closed arms compared to NTG controls which suggests increased anxiety levels in these transgenic animals. Furthermore, the number of entries in open and closed arms, distance traversed and speed decreased over age in Tg4-42 +/+ mice which is in line with the lower activity levels measured in the open field test. In contrast, no significant changes in anxiety levels of 3 and 6 months old Tg4-42 mice were observed by Lopez-Noguerola et al (117). These differing results could be caused be many various factors. It is known that the time of testing can be influenced by circadian rhythm, light cycle and any inconsistencies in the phase of the light cycle where mice are tested. Furthermore, handling of the mice prior to testing can differ between research groups or experimenters and any stress animals are exposed to immediately before testing could influence the outcome and alter rodent`s behavior (118). Another important point to consider is that behavioral testing protocols, experiment settings or also previous behavioral tests the animals had to perform usually differs between studies which can further lead to various responses in the same mouse model.

The results of the Morris water maze behavioral test confirm and expand previous basic results showing that Tg4-42 +/+ mice develop severe learning and spatial reference memory deficits (53, 63, 64, 109) starting already at 3 month of age. The relationship between spatial memory and hippocampal lesion size was investigated in rats by Broadbent et al. After bilateral dorsal hippocampal lesions of approximately 100 % of total hippocampal volume, the spatial memory performance of these rats was severely impaired (119). Other investigations by Moser et al. in Lister rats indicate that only 20-40 % of the total hippocampus is essential for unimpaired spatial learning and that spatial learning in these rats requires the dorsal but not the ventral hippocampus (120). While Hartmann et al. associated spatial learning deficits in rats in the absence of other behavioral impairments with neurodegeneration in the dorsal hippocampal CA1 region (121), Volpe et al. showed that the volume of hippocampal damage did not predict the rats performance but that the extent of CA1 pyramidal neuron loss correlated significantly with delayed spatial performance (122). Additionally, Olsen et al. demonstrated in male wistar

rats a significant impairment of spatial memory performance as the number of viable CA1 neurons declined. These results indicate that the severe hippocampal dysfunctions in Tg4-42 +/+ mice already at an early age as also reported by Bouter et al. are very likely related to the observed severe neuron loss in the CA1 region of the hippocampus.

Additionally, floating behavior increased significantly in Tg4-42 +/+ mice compared to NTG controls which reveals a progressive loss of motivation over the 4 days of consecutive training in the MWM. These results are in line with the significantly decreased activity levels evaluated in the open field test. The loss of motivation and similar symptoms like apathy are often described in AD patients and are the most common behavioral changes associated with cortical pathology (123, 124). Besides problems to learn the task and motivational issues, Tg4-42 +/+ mice did not show a preference for the target quadrant in the probe trial of the MWM test which indicates severe memory dysfunctions already at 3 month of age. These memory deficits are in agreement with previous results in this mouse model and are also shown in other APP transgenic mouse lines. Moreover, memory impairments are common features in AD patients which occur in early stages of disease development (53, 125, 126). Thus, the impairment in memory function observed in Tg4-42 +/+ mice may likely correspond to early clinical stages of AD.

In order to find new biomarkers and to gain deeper insight into the pathways underlying disease progression, NMR spectroscopy was used to determine alterations in the metabolite profile of Tg4-42 +/+ mice and NTG controls. In the present study for the first time two different brain regions of 9-month-old Tg4-42 +/+ mice were analyzed with NMR spectroscopy. The two significantly decreased metabolites glutamine and 4-aminobutyrate (GABA) are known to play a key role in the glutamate/GABA-glutamine cycle which is necessary for neurotransmission and a normal brain function. Glutamate is synthesized and converted to glutamine in astrocytes, transported to neurons where it is converted to glutamate and released into the extracellular space (127). This action of glutamate is terminated by its removal from receptor sites by active transport mechanisms. Malfunctions in this pathway result in excitotoxicity which is a fundamental mechanism leading to neurodegeneration (128). Interestingly, a study by Doert et al. using ^{1}H- and ^{13}C-NMR spectroscopy in an APP_{SL} mouse model of AD showed decreased glutamine and glutamate concentrations while GABA levels were elevated (129). Besides that, reduced glucose metabolism was detected via ^{18}F-FDG-PET in the cerebellum of aged Tg4-42 mice (110). In line with the findings reported here for animals, several publications describe metabolic changes and alterations in glutamine and GABA as well as lactate levels in the brain of AD patients (17, 130-132). Seidl et al. determined a number of different amino acids like glutamate, aspartate, GABA, glycine, taurine, glutamine, serine,

arginine in *post mortem* tissue samples of AD patients resulting in increased levels of GABA, glutamate and aspartate concentrations in some of the investigated brain areas (133). Additionally, further studies assessed metabolic changes by decreased glutamate and glutamine levels in AD patients, which may thus be potential biomarkers in the early clinical diagnosis of AD (134, 135).

To investigate this further glutamate and GABA metabolizing enzymes like glutamate-decarboxylase and glutaminase were analyzed by immunofluorescent labelling. GAD67 as well as glutaminase were significantly increased in the brain of Tg4-42 +/+ mice. These results fit to a study by Boissiere and colleagues who analyzed GAD67 expression in the caudate nucleus and putamen in AD patients with the result that the expression of GAD67 mRNA was higher in AD patients than in control subjects (136). Another study investigated glutamate metabolizing enzymes like glutamine synthetase, glutamate dehydrogenase and phosphate-activated glutaminase in the prefrontal cortex of AD patients. Again, concentrations of these enzymes were found to be significantly increased in AD patients which may suggest pathological changes of regulatory enzymes of glutamate metabolism in AD brains like in the here presented study (137). All these findings in AD patients are very similar to the ones found for 9-month-old Tg4-42 +/+ mice, strongly indicating impairments of the glutamate/GABA-glutamine cycle in human and mouse AD brains. Due to these similarities to AD patients, the here presented Tg4-42 mouse model seems to be a promising model for translational research.

Astroglial glutamate uptake can be inhibited by Aβ peptides and this in turn can result in neuronal cell death mediated by neurotoxic glutamate (138, 139). For that reason, total and soluble Aβ42 levels were further investigated in the here presented study by using two different methods and antibodies. Aβ42 accumulations in specific brain regions and also differences between concentrations of total and soluble Aβ42 levels were observed in Tg4-42 +/+ mice. As the levels of GAD67 as well as Aβ42 levels were increased in Tg4-42 +/+ mice compared to NTG animals, this would confirm a connection between regulatory enzymes of the glutamate pathway and Aβ. Previous Tg4-42 mouse studies showed strong Aβ accumulation in the CA1 cell layer of the hippocampus using a pan-Aβ antibody to perform immunohistochemical analyses (65, 117). Moreover Wang et al. described a significant decrease of amyloid-β production in 5xFAD mice due to a reduction of GAD67 (140) which further indicates a connection between these proteins.

Furthermore, it has previously been described that Aβ42 toxicity can initiate downstream pathological processes that represent key effectors of cellular dysfunction and cell death (141). Beyond that, Aβ oligomers and Aβ deposition is also associated with impaired spatial memory

in APP transgenic mice (142). The toxicity of amyloid-β oligomers is well-described in human and mouse AD brains and can lead to an alteration in the balance between pro- and anti-oxidative processes which can result in an increased activation of surrounding astrocytes and microglia (143).

For this reason, inflammatory markers like GFAP and Iba-1 were analyzed in the brains of Tg4-42 +/+ mice. Results revealed increased astrocytosis in the cortex as well as in the hippocampus of 9-months-old mice and in the caudate putamen region starting already at 3 months and increasing over age. Increased microgliosis was only observed in the caudate putamen of Tg4-42 +/+ mice starting at 6 month of age. These findings show for the first time the progressive increase of neuroinflammation over age in Tg4-42 +/+ mice. Some of these results are in line with previous characterization studies showing increased astrogliosis and microgliosis in different brain regions of 2 months old hemizygous and 7-8 month old homozygous Tg4-42 mice (53, 63).

It has been described that activation of microglia and the subsequent release of pro-inflammatory factors induces the loss of brain homeostasis, causing neuronal injury and eventually neuronal death (7, 144). In the Tg4-42 +/+ mouse model increased murine neurofilament light chain (NF-L) levels in CSF samples were measured which indicates severe cerebral axonal degeneration. NF-L is a promising biomarker in blood and CSF to detect neurodegeneration in brain disorders like AD (145). In Aβ-positive AD patients, levels of NF-L were associated with hypometabolism in AD-vulnerable brain regions (146). Further studies described significantly increased NF-L levels in plasma and CSF of AD patients and high NF-L levels correlated with poor cognition and AD-related brain atrophy (147, 148). Neuronal dysfunction and neuron loss are the most severe hallmarks of AD but most AD mouse models lack this key feature (57). Neuronal loss was therefore investigated in 9-month-old Tg4-42 +/+ animals which revealed a significantly decreased number of neurons in the CA1 region of the hippocampus. These findings are comparable with two different studies by Bouter et al., where massive age-dependent neuron loss was described in 7-8 and 12 month old Tg4-42 +/+ animals (53, 63).

Using quantitative PCR, the transcriptional impact of transgene integration in Tg4-42 +/+ mice was demonstrated. Whole genome sequencing located the integration site of the transgene on chromosome 14, which caused a deletion of exon 2 of the retinoic acid receptor beta. TLA combined with next generation sequencing is best suited for a robust detection of integration sites or transgene sequence variants (99, 149). For further validation of the genomic integration site, it is possible to perform Sanger sequencing, although Baudhuin and colleagues question the necessity of this confirmation (150). To clarify the impact of transgene

insertion on protein level, the Simple Western blot system was used. This novel capillary electrophoresis-based Western blot technology requires much smaller amounts of tissue than traditional Western blotting which is important if limited sample amounts are available. Moreover, big advantages are the higher sensitivity as well as reproducibility and excellent quantification options by analysis of the *Area Under the Curve* which led to the decision to use the capillary Western approach in this study (151, 152). The Simple Western blot system analyses showed highly decreased RARB protein levels in Tg4-42 +/+ mice. Thus, the integration of the Aβ4-42 transgene appears to substantially disrupt RARB gene regulation, resulting in a knockdown of this gene and in turn downregulation of RARB protein. The described behavioral phenotype of the Tg4-42 +/+ mouse model could therefore be caused by the Aβ4-42 transgene or by RARB knockout (100, 153).

As a common effect of gene knockout or knockdown in mice, reduced body weight is often reported (154). Interestingly, a generated RARB null mutant mouse model described in the literature with a disruption of all isoforms of RARB shows a very similar phenotype compared to Tg4-42 +/+ mice. This described RARB knockout mouse model has an unaltered body weight at birth but after 2 month of age a weight decrease of ~25 % was measured in male RARB knockout mice compared to wild type littermates (155). These results indicate a very likely genetic influence on the significant lower body weight of Tg4-42 +/+ mice that we evaluated in the present study.

Furthermore, retinoic acid receptor beta deficiency eliminates hippocampal CA1 long-term potentiation and causes severely impaired spatial learning in the Morris water maze behavioral test, like it was the case in our study in Tg4-42 +/+ animals. Since these severe impairments in spatial learning were already pronounced in 3-month-old Tg4-42 +/+ mice, this would rather hint towards an effect of the RARB knockdown. It was expected that concentrations of the inserted transgene increase with age and therefore show a progressive deterioration in spatial learning behavior over age as observed in other APP models.

In contrast, hemizygous Tg4-42 animals did not show any memory deficits, probably due to the unaltered, physiological RARB protein levels in these mice (64, 156). The described RARB knockout mice are viable, fertile and are described to have no grossly apparent phenotype (53, 156). Nevertheless, it is described that a loss of both wild type alleles of the RARB gene leads to a cell deficit on the ganglion cell population, which of course can influence the phenotype (157). Furthermore, no other observed pathologies like neuroinflammation or changes in amyloid-beta levels are described in RARB knockout mice which indicates that the phenotype in Tg4-42 +/+ mice is presumably based on a synergetic effect of RARB knockdown and Aβ4-42 overexpression.

On the other hand, therapeutic intervention studies with a monoclonal antibody or with enriched housing conditions were able to reduce hippocampal neuron loss and showed a rescue of spatial reference memory deficits in homozygous Tg4-42 mice. These data would rather indicate that the observed phenotype of Tg4-42 +/+ mice is not influenced by the RARB knockdown and solely caused by the Aβ4-42 transgene (106, 109). Further analyses are needed to elucidate the exact mechanism of interaction between RARB knockdown and Aβ4-42 overexpression. Since for the recent project usage of the Tg4-42 +/+ mouse model would have been a risk and interpretation of data eventually not possible, we decided to switch to a different, however, well described animal model of AD research, the APP_{SL} mice.

5.2 Treatment of APP_{SL} mice

In the second part of this study *in vivo* results demonstrated a significant improvement of spatial learning in APP_{SL} treated with the ALDH2 activator AD-9308 when compared to their controls. Besides that, untargeted metabolic phenotyping revealed increased serum acetate levels in AD-9308 treated APP_{SL} mice. Additionally, further measurements were performed to analyze the effects of the ALDH2 activator on biomarker levels of APP_{SL} mice and revealed decreased Aβ-40 and MDA levels caused by AD-9308 treatment.

In terms of behavioral changes in these mice with and without treatment with the ALDH2 activator AD-9308 a whole series of experiments was performed.

The open field test is widely used and best suited to evaluate possible changes in locomotion and exploration (114). The total rearing time and number of rearings were significantly decreased in APP_{SL} mice compared to NTG controls whereas no significant differences were observed in all of the tested groups in activity, thigmotaxis and distance. Similar findings were shown by Havas et al. were APP_{SL} mice did not display any significant differences at 3, 6 or 9 months in spontaneous activity or thigmotaxis compared to NTG littermates (158). In contrast Faizi et al. demonstrated in a very similar mouse model, named the Thy1-$hAPP^{Lond/Swe+}$ mice, which also contained the London and Swedish mutations, that these mice moved a longer distance and showed a significantly increased velocity in the open field at an age of 5 to 6-month. These animals did not show a genotype effect in the time spent in the periphery versus the center zones of the arena which suggests that the increased locomotion is primarily caused by hyperactivity rather than anxiety-like behavior (159). This assumption is in line with the results of the here presented study, were no significant changes in anxious behavior were evaluated which demonstrate that APP_{SL} mice do not exhibit anxious behavior with increasing age.

Deficits in spontaneous alternation behavior have been previously reported in a similar model, the $hAPP^{Lond/Swe+}$ mice, by Faizi et al. In that study 5 to 6-month-old APP_{SL} mice showed significantly less spontaneous alternation both in the T-maze and the Y-maze compared to NTG mice (159). Several studies reported age-dependent deficits of rewarded alternation on a T-maze in transgenic mice that overexpress only the Swedish mutation of human APP. In these studies, natural alternation behavior was observed at 3 month of age whereas animals showed impairments at 9 to 10 month of age (160, 161). In the here presented study spontaneous alternation behavior which detects hippocampal dysfunctions as well as the motivation of the animal to explore the environment, showed no differences between all tested groups. These results suggest no severe hippocampal dysfunctions in 9 and 11-month-old APP_{SL} mice. Interestingly in trial 5, the non-performer rate, which includes mice that did not

move from the position where they were entered into the maze, was much higher in APP_{SL} mice than in NTG mice. Furthermore, it was observed that approximately 60 % of 11-month-old APP_{SL} mice belonged to the non-performer group after the second trial. This rapid increase in non-performing mice could be explained by repeated testing where animals are getting used to the task and remember that they will be taken out of the maze after a certain time. It has been reported in the literature that training history as well as previous handling and testing can have an effect on the behavior of mice which can for example result in reduced exploratory activity (162). Moreover, decreases in activity are sometimes explained with a lack of motivation to explore the environment and to perform the tasks. Most likely a combination of both, re-testing in the same behavioral test as well as a lack of motivation to explore the environment at a higher age was decisive in 11-month-old APP_{SL} mice. Lack of motivation, also called apathy is described to be a common neuropsychiatric symptom in AD patients (163, 164). As 11-month-old APP_{SL} mice developed apathy-like behavior, this model seems to be suitable to study further AD linked behavior in future translational studies.

Besides behavioral changes AD is characterized by a series of biomarker changes involving also the two main peptide player Aβ and tau and especially Aβ oligomerization is known to be a key pathological event in AD (165, 166). Thus, total human Aβ levels were measured in 7, 9 and 11-month-old APP_{SL} mice resulting in significantly increased total human Aβ levels over age. A similar age dependent increase in human Aβ levels and plaque load in the brain of 3, 6 and 9-month-old APP_{SL} mice was previously analyzed by Havas et al (158). Moreover, studies report that oligomerization of Aβ in AD brains contributes to neurodegeneration (166). However, in the here presented study no significant differences in NeuN levels of APP_{SL} could be found, indicating that these animals show no significant neurodegeneration up to 11 months of age. Similar results were previously described which suggests that APP_{SL} mice do not develop neuronal loss in any of the investigated brain regions.

Aβ species are also the main constituent in plaque formation which is commonly accompanied by inflammatory processes like astro- and microgliosis of the affected brain regions and are described as characteristic features of AD progression (167). For that reason, activated microglia as well as the total amount of astrocytes were evaluated by immunohistochemistry which resulted in increased levels of activated microglia and astroglia starting in 7-month-old APP_{SL} mice and significantly increasing over age. These results are consistent with previous published studies were increased total astroglia levels as well as increased activated microglia levels in APP_{SL} mice were observed (158, 168, 169). APP_{SL} mice exhibit age dependent neuroinflammation which is described to contribute to AD disease progression and severity (170). In summary it can be stated that the observed phenotype in the here presented study

of the APP_{SL} mice corresponds to the already published phenotype of these mice. From this it can be deduced that the robust APP_{SL} phenotype provides stable, reproducible results which make this model very suitable for treatment studies.

Whether or not an oral treatment with the ALDH2 activator AD-9308 over a longer time period is able to counteract the above-mentioned AD phenotype was a main question of the present work. First of all, AD-9308 treatment was well-tolerated in APP_{SL} transgenic mice when administered via the drinking water for up to 4 months. Although transgenic APP_{SL} mice showed a reduced body weight already at study start, the compound did not cause significant body weight changes. Interestingly Chen et al. reported that treated male C57BL/6J mice which received another ALDH2 agonist were significantly lighter compared to non-treated mice (171). A further study reported a decreased heart weight / body weight ratio in ALDH2 treated rats indicating a possible influence of the compound on the body weight. This however, was not observed in APP_{SL} mice in the here presented study (172), suggesting, that the ALDH2 agonist AD-9308 causes less side effects compared to already published ALDH2 modulators. Since memory loss is the most common symptom in AD patients and knowing that the hippocampus is a brain region that is strongly involved in memory, the influence of the ALDH2 activator on spatial memory was further investigated. In the present study a significant improvement in spatial memory in AD-9308 treated APP_{SL} mice compared to controls was observed. In the here presented study an ALDH2 activator was used to increase the detoxification activity of ALDH2. In contrast many other studies investigated the effects of the ALDH2 enzyme using ALDH2 knockout ($ALDH2^{-/-}$) mice.

Interestingly Souza et al. reported that 6-month-old $ALDH2^{-/-}$ mice exhibited decreased performance in the Morris Water Maze task. During the probe trial these $ALDH2^{-/-}$ mice spent less time in the target quadrant and had fewer platform crossings compared to wild type mice (173). Moreover, accumulation of formaldehyde was discovered in brains of these $ALDH2^{-/-}$ mice which leads to an impairment in spatial memory behavior. These findings are consistent with observations in AD patients where low activity variants or loss-of function mutations in the ALDH2 gene lead to formaldehyde overload and dementia in AD patients (174). These results indicate that increasing the catalytic activity of ALDH2 and consequently removal of toxic intermediates can have a positive effect on spatial memory in APP_{SL} mice and eventually in AD patients.

To investigate these further, untargeted metabolic phenotyping was performed which revealed elevated serum acetate levels in AD-9308 treated compared to vehicle treated APP_{SL} mice. As ALDH2 is the key enzyme in converting acetaldehyde to acetate these elevated acetate levels in APP_{SL} + AD-9308 mice could be explained through the enhanced activity of ALDH2 as an

effect of AD-9308. Acetaldehyde is known as a toxic, cancerogenic intermediate mainly produced by the metabolism of alcohol but it is described that it can be generated *in situ* from the metabolism of pyruvate, threonine, alanine, as an intermediate in sugar`s metabolism and possibly also from other substrates (175, 176). Kiyoshi et al. evaluated slightly lower blood acetate levels in ALDH2 knockout compared to wild type mice which is due to the deficient effect of ALDH2 enzyme activity (177). Thus, enhancing ALDH2 activity seems to have positive effects on the detoxification of reactive aldehydes from endogenous metabolism.

Besides the above mentioned toxic intermediates also amyloid-β peptides are known to be present in neuronal mitochondria, decreasing energy and enhancing ROS production (96). The effect of ALDH2 on brain amyloid-β levels in this study was weak and only total Aβ1-40 levels were significantly reduced by AD-9308. No significant treatment effects on total Aβ levels were observed in the cortex and hippocampus but amyloid-β levels similarly increased with age in AD-9308-treated and vehicle-treated APP_{SL} mice. Solito et al. examined the role of ALDH2 on the development of endothelial dysfunction caused by Aβ1-40 which is known to be involved in AD-associated cerebral amyloid angiopathy. In their study the ALDH2 activator was able to abolish Aβ-induced 4-HNE accumulation, apoptosis and vascular leakiness and fully restore the pro-angiogenic endothelial phenotype (178). These findings emphasize the importance of targeting lipid peroxidation products by enhancing the catalytic activity of ALDH2 which could be able to rescue blood vessels from toxic damage.

Amyloid pathology is always accompanied by inflammatory processes such as chronic inflammation and reactive gliosis, which are well-described and prominent features in AD (169). Here, no treatment benefits on neuroinflammation could be detected in AD-9308-treated APP_{SL} mice. Nevertheless, Joshi et al. recently reported that intraperitoneal injection of ethanol induced increased Aβ42 and neuroinflammation in form of cytokine levels in the brains of 5-month-old ALDH2 deficient mice. After treatment with an ALDH2 activator by subcutaneous minipumps over the time period of 3 months, most ethanol-induced changes like Aβ42, 4-HNE, MDA and mitochondrial H_2O_2 levels as well as selected cytokine levels were significantly reduced. This means that increasing the catalytic activity of ALDH2 and therefore boosting the clearance of toxic aldehydes can have a beneficial effect on AD-related pathological changes (179).

Several studies reported that oxidative stress plays a major role in the pathogenesis of AD (180, 181) and like in humans age-dependent increase of oxidative stress has been reported for APP_{SL} mice, previously (167). The measurement of lipid peroxides, which are unstable indicators of oxidative stress in decomposing cells to form more complex and reactive compounds such as malondialdehyde (MDA) and 4-hydroxynonenal (4-HNE), was also

performed in the here presented study. Thiobarbituric acid reactive substances (TBARS), as marker for oxidative stress were significantly reduced in the APP_{SL} + AD-9308 group compared to transgenic controls whereas no significant changes could be detected in 4-HNE levels. In contrast to that Grath et al. reported significantly higher levels of 4-HNE in the plasma of AD patients and the concentration of 4-HNE was related to the degree of cognitive impairment but MDA levels were not elevated in these AD patients. A possible explanation for these discrepancies could be the used type of assay because TBARS assays also measures unspecific breakdown products (95). Moreover, Ohsawa et al. showed enhanced accumulation of ROS and end products in ALDH2 deficient mice (182). In the current study ROS levels and complex 1 activity determination revealed no changes. Because ROS are known as highly reactive, low concentrated and extremely unstable molecules the detection of these substances is very difficult and could be influenced by many different factors, for example tissue sampling, sample preparation or storage conditions. Therefore, these species are hard to be measure directly, even the indirect assessments of their abundance and reactivity is tricky. The detection of hydrogen peroxide (H_2O_2), which is the most interesting candidate regarding intracellular signaling, using colorimetric substrates (e.g. DCFDA) is discussed to be less sensitive and to interact with other oxidants. For this reason, the biggest challenge of measuring certain reactive oxygen species products is to find specific, discrete molecules which do not react by nature with several different molecules in the cells (183, 184).

Based on results of the current study with AD-9308, it is not yet possible to specify which pathways are influenced by this ALDH2 activator. For that reason, further analyses are necessary in order to better understand the effect of AD-9308. Mitochondrial dysfunction and oxidative stress which induce lipid peroxidation are described to occur as central features in neurodegenerative diseases like AD. To measure lipid peroxidation mostly thiobarbituric acid reacting substances (TBARS) are observed by a spectrophotometric assay named TBARS. This assay measures malondialdehyde (MDA) as well as other aldehydes generated from lipid hydroperoxides by the hydrolytic conditions of the reaction. In recent years the specificity of TBARS over other compounds as MDA has been controversial. Moreover, it was described that most thiobarbituric acid reactive material in human body fluids is not related to lipid peroxidation (185). Therefore, it would be advisable to confirm the results of the TBARS assay with other more specific assays such as ELISA kits to detect MDA or high-performance liquid chromatography–mass spectrometry (HPLC/MS). Since antibody-based assays are typically validated and demonstrate good performance with improved specificity (186-190).

It was demonstrated by Solito et al. that increasing the activity of ALDH2 can restore mitochondrial functions in the endothelium and prevents Aβ induced dysfunction. For that

reason, a very interesting approach would be to analyze the influence of ALDH2 activator on vascular effects of amyloid, including loss of endothelial barrier function and angiogenesis (178, 191).

Under physiological conditions, the brain is protected from damage by a careful balance between prooxidant and antioxidant mechanisms which include antioxidant enzymes and free-radical-scavenging chemicals such as ascorbate or vitamin E (192).

To prevent or repair the damage caused by ROS and to regulate redox-sensitive signalling pathways, cells contain a large number of antioxidants which convert toxic metabolites to harmless products. For example, the superoxide-dismutases convert superoxide radical into hydrogen peroxide and molecular oxygen, while catalases or peroxidases convert hydrogen peroxide into water. These are two examples where toxic species like superoxide radical as well as hydrogen peroxide are converted into water. For this reason, another interesting approach would be the measurement of antioxidant enzymes with the capacity to scavenge free radicals like superoxide dismutase (SOD), catalase or glutathione peroxidase.

Western blots and activity assays are various methods used to determine protein concentrations and enzymatic activity in cells depending on the amount of protein needed for each assay. Other techniques including immunohistochemistry can further evaluate the levels and location of the various antioxidant enzymes in tissues (193).

It is reported that mitochondrial malfunctions play a distinct role in AD pathogenesis. Mitochondrial functions decline in AD and impaired mitochondria are morphologically different (194, 195). Therefore, a variety of mitochondrial markers to prove the integrity of mitochondria are discussed in the literature. Mitochondrial serine/threonine-protein kinases (PINK1) are thought to protect cells from stress-induced mitochondrial dysfunction and are closely involved in mitochondrial quality control by identifying damaged mitochondria and induce autophagy of those mitochondria. Moreover, cytochrome C is a promising marker to show that the outer mitochondria membrane is intact. Cytochrome C is widely suggested to be localized solely in the mitochondrial intermembrane space under physiological conditions (196). The release of cytochrome C from mitochondria to the cytosol where then the caspase family of proteases get activated, is considered to be a primary trigger leading to the onset of apoptosis. Measuring the amount of cytochrome C leaking from mitochondria to the cytosol and out of the cell, is a sensitive method to monitor the degree of apoptosis. Additional mitochondrial markers are proinhibitin-2, porin (VDAC), HSP60, TOMM20, JC1 or TMRM. Because mitochondria are closely involved in apoptosis and cell death, the measurement of apoptotic markers (e.g. caspase-3) could be an interesting approach (197, 198).

In summary, further investigations have to be performed to better understand the effects of the ALDH2 activator AD-9308 and the underlying biochemical pathways.

6 CONCLUSION

In summary, the first study part evaluated key pathological features in Tg4-42 +/+ mice including significantly altered metabolites in two different brain regions as well as metabolic changes of the glutamate/GABA-glutamine cycle. Moreover, increased NF-L levels which indicates neuronal degeneration, were observed. Neuronal dysfunction as well as changes in the underlying pathways occur long before neuronal loss and can therefore function as early markers of AD. Moreover, increased Aβ42 and neuroinflammation levels over age as well as neuronal loss in homozygous Tg4-42 mice were measured. Furthermore *in vivo* experiments showed severe memory deficits in Tg4-42 +/+ mice which are in line with previous results obtained by Bouter et al. (53). Additionally, this study showed decreased expression and reduced protein levels of the retinoic acid receptor beta in brain tissue of Tg4-42 +/+ mice which question the cause of the previously described phenotype of these mice to be solely dependent on Aß4-42 expression. This first part of the study provides a comprehensive characterization of the Tg4-42 +/+ mouse model and offers researchers the opportunity to gain a deeper understanding of pathological features of AD.

In the second part of this study significantly increased serum acetate levels in ALDH2 treated compared to vehicle treated APP_{SL} mice were measured by NMR. As ALDH2 is the key enzyme in converting toxic acetaldehyde to acetate these elevated acetate levels in APP_{SL} treated mice could be explained through the enhanced activity of ALDH2 through the compound, which seems to have positive effects on the detoxification of reactive aldehydes from endogenous metabolism. Furthermore, a variety of behavioral tests with several measured parameters were performed in APP_{SL} mice after 2 and 4 months of treatment with the ALDH2 activator AD-9308. A significant improvement of spatial learning in AD-9308-treated animals compared to vehicle treated animals could be observed. Additionally, treatment with AD-9308 significantly decreased Aβ-40 and MDA levels in APP_{SL} mice. Further analyses have to be performed to better understand the pharmacological effects of this compound. Our results demonstrate that increasing the detoxification activity of ALDH2 seems to be a promising approach to target Alzheimer´s disease pathology.

7 REFERENCES

1. Karlawish J, Jack CR, Jr., Rocca WA, Snyder HM, Carrillo MC. Alzheimer's disease: The next frontier-Special Report 2017. Alzheimer's & dementia : the journal of the Alzheimer's Association. 2017;13(4):374-80.
2. Small DH, Cappai R. Alois Alzheimer and Alzheimer's disease: a centennial perspective. Journal of neurochemistry. 2006;99(3):708-10.
3. Sery O, Povova J, Misek I, Pesak L, Janout V. Molecular mechanisms of neuropathological changes in Alzheimer's disease: a review. Folia Neuropathol. 2013;51(1):1-9.
4. Brannon WL. Alois Alzheimer (1864-1915). I. Contributions to neurology and psychiatry. J S C Med Assoc. 1994;90(9):399-401.
5. Maurer K, Volk S, Gerbaldo H. Auguste D and Alzheimer's disease. Lancet. 1997;349(9064):1546-9.
6. 2016 Alzheimer's disease facts and figures. Alzheimer's & dementia : the journal of the Alzheimer's Association. 2016;12(4):459-509.
7. Cai Z, Hussain MD, Yan LJ. Microglia, neuroinflammation, and beta-amyloid protein in Alzheimer's disease. Int J Neurosci. 2014;124(5):307-21.
8. Arshavsky YI. Why Alzheimer's disease starts with a memory impairment: neurophysiological insight. Journal of Alzheimer's disease : JAD. 2010;20(1):5-16.
9. Caselli RJ, Beach TG, Yaari R, Reiman EM. Alzheimer's disease a century later. J Clin Psychiatry. 2006;67(11):1784-800.
10. Tan CC, Yu JT, Tan L. Biomarkers for preclinical Alzheimer's disease. J Alzheimers Dis. 2014;42(4):1051-69.
11. Esquerda-Canals G, Montoliu-Gaya L, Guell-Bosch J, Villegas S. Mouse Models of Alzheimer's Disease. J Alzheimers Dis. 2017;57(4):1171-83.
12. International AsD. World Alzheimer Report 2019 - Attitudes to dementia [Commissioned report]. London: Alzheimer's Disease International; 2019 [Available from: https://www.alz.co.uk/research/WorldAlzheimerReport2019.pdf.
13. Auer SR, Span E, Reisberg B. Dementia service centres in Austria: A comprehensive support and early detection model for persons with dementia and their caregivers - theoretical foundations and model description. Dementia (London). 2015;14(4):513-27.
14. Dorszewska J, Prendecki M, Oczkowska A, Dezor M, Kozubski W. Molecular Basis of Familial and Sporadic Alzheimer's Disease. Curr Alzheimer Res. 2016;13(9):952-63.
15. Mayeux R, Stern Y. Epidemiology of Alzheimer disease. Cold Spring Harbor perspectives in medicine. 2012;2(8):a006239.
16. Lane CA, Hardy J, Schott JM. Alzheimer's disease. Eur J Neurol. 2018;25(1):59-70.
17. Liu P, Fleete MS, Jing Y, Collie ND, Curtis MA, Waldvogel HJ, et al. Altered arginine metabolism in Alzheimer's disease brains. Neurobiology of aging. 2014;35(9):1992-2003.
18. Suzuki K, Terry RD. Fine structural localization of acid phosphatase in senile plaques in Alzheimer's presenile dementia. Acta neuropathologica. 1967;8(3):276-84.
19. Wiśniewski HM, Ghetti B, Terry RD. Neuritic (senile) plaques and filamentous changes in aged rhesus monkeys. Journal of neuropathology and experimental neurology. 1973;32(4):566-84.
20. Serrano-Pozo A, Frosch MP, Masliah E, Hyman BT. Neuropathological alterations in Alzheimer disease. Cold Spring Harbor perspectives in medicine. 2011;1(1):a006189-a.
21. Nelson PT, Alafuzoff I, Bigio EH, Bouras C, Braak H, Cairns NJ, et al. Correlation of Alzheimer disease neuropathologic changes with cognitive status: a review of the literature. Journal of neuropathology and experimental neurology. 2012;71(5):362-81.
22. Montine TJ, Phelps CH, Beach TG, Bigio EH, Cairns NJ, Dickson DW, et al. National Institute on Aging-Alzheimer's Association guidelines for the neuropathologic assessment of Alzheimer's disease: a practical approach. Acta neuropathologica. 2012;123(1):1-11.

23. Bouras C, Hof PR, Giannakopoulos P, Michel JP, Morrison JH. Regional distribution of neurofibrillary tangles and senile plaques in the cerebral cortex of elderly patients: a quantitative evaluation of a one-year autopsy population from a geriatric hospital. Cereb Cortex. 1994;4(2):138-50.
24. Braak H, Thal DR, Ghebremedhin E, Del Tredici K. Stages of the pathologic process in Alzheimer disease: age categories from 1 to 100 years. Journal of neuropathology and experimental neurology. 2011;70(11):960-9.
25. Davies L, Wolska B, Hilbich C, Multhaup G, Martins R, Simms G, et al. A4 amyloid protein deposition and the diagnosis of Alzheimer's disease: prevalence in aged brains determined by immunocytochemistry compared with conventional neuropathologic techniques. Neurology. 1988;38(11):1688-93.
26. Mirra SS. The CERAD neuropathology protocol and consensus recommendations for the postmortem diagnosis of Alzheimer's disease: a commentary. Neurobiology of aging. 1997;18(4 Suppl):S91-S4.
27. Wisniewski HM, Vorbrodt AW, Moretz RC, Lossinsky AS, Grundke-Iqbal I. Pathogenesis of neuritic (senile) and amyloid plaque formation. Exp Brain Res. 1982;Suppl 5:3-9.
28. Braak H, Braak E. Neuropathological stageing of Alzheimer-related changes. Acta neuropathologica. 1991;82(4):239-59.
29. Ohm TG, Müller H, Braak H, Bohl J. Close-meshed prevalence rates of different stages as a tool to uncover the rate of Alzheimer's disease-related neurofibrillary changes. Neuroscience. 1995;64(1):209-17.
30. Blennow K, Zetterberg H. Biomarkers for Alzheimer's disease: current status and prospects for the future. J Intern Med. 2018;284(6):643-63.
31. James BD, Wilson RS, Boyle PA, Trojanowski JQ, Bennett DA, Schneider JA. TDP-43 stage, mixed pathologies, and clinical Alzheimer's-type dementia. Brain : a journal of neurology. 2016;139(11):2983-93.
32. Kovacs GG, Milenkovic I, Wöhrer A, Höftberger R, Gelpi E, Haberler C, et al. Non-Alzheimer neurodegenerative pathologies and their combinations are more frequent than commonly believed in the elderly brain: a community-based autopsy series. Acta neuropathologica. 2013;126(3):365-84.
33. Gomez-Isla T, Spires T, De Calignon A, Hyman BT. Neuropathology of Alzheimer's disease. Handb Clin Neurol. 2008;89:233-43.
34. Matsui T, Ingelsson M, Fukumoto H, Ramasamy K, Kowa H, Frosch MP, et al. Expression of APP pathway mRNAs and proteins in Alzheimer's disease. Brain research. 2007;1161:116-23.
35. Weidemann A, König G, Bunke D, Fischer P, Salbaum JM, Masters CL, et al. Identification, biogenesis, and localization of precursors of Alzheimer's disease A4 amyloid protein. Cell. 1989;57(1):115-26.
36. Haass C, Kaether C, Thinakaran G, Sisodia S. Trafficking and proteolytic processing of APP. Cold Spring Harbor perspectives in medicine. 2012;2(5):a006270-a.
37. Haass C, Schlossmacher MG, Hung AY, Vigo-Pelfrey C, Mellon A, Ostaszewski BL, et al. Amyloid beta-peptide is produced by cultured cells during normal metabolism. Nature. 1992;359(6393):322-5.
38. Lai A, Sisodia SS, Trowbridge IS. Characterization of sorting signals in the beta-amyloid precursor protein cytoplasmic domain. The Journal of biological chemistry. 1995;270(8):3565-73.
39. Wilkins HM, Swerdlow RH. Amyloid precursor protein processing and bioenergetics. Brain research bulletin. 2017;133:71-9.
40. King GD, Perez RG, Steinhilb ML, Gaut JR, Turner RS. X11α modulates secretory and endocytic trafficking and metabolism of amyloid precursor protein: mutational analysis of the yenpty sequence. Neuroscience. 2003;120(1):143-54.

41. Zhang Y-w, Thompson R, Zhang H, Xu H. APP processing in Alzheimer's disease. Molecular brain. 2011;4:3-.
42. Haass C. Take five--BACE and the gamma-secretase quartet conduct Alzheimer's amyloid beta-peptide generation. The EMBO journal. 2004;23(3):483-8.
43. Kummer MP, Heneka MT. Truncated and modified amyloid-beta species. Alzheimer's Research & Therapy. 2014;6(3):28.
44. Olsson F, Schmidt S, Althoff V, Munter LM, Jin S, Rosqvist S, et al. Characterization of intermediate steps in amyloid beta (Aβ) production under near-native conditions. The Journal of biological chemistry. 2014;289(3):1540-50.
45. Takami M, Nagashima Y, Sano Y, Ishihara S, Morishima-Kawashima M, Funamoto S, et al. gamma-Secretase: successive tripeptide and tetrapeptide release from the transmembrane domain of beta-carboxyl terminal fragment. The Journal of neuroscience : the official journal of the Society for Neuroscience. 2009;29(41):13042-52.
46. Bibl M, Gallus M, Welge V, Lehmann S, Sparbier K, Esselmann H, et al. Characterization of cerebrospinal fluid aminoterminally truncated and oxidized amyloid-β peptides. Proteomics Clin Appl. 2012;6(3-4):163-9.
47. Haass C, Selkoe DJ. Soluble protein oligomers in neurodegeneration: lessons from the Alzheimer's amyloid beta-peptide. Nat Rev Mol Cell Biol. 2007;8(2):101-12.
48. Dawkins E, Small DH. Insights into the physiological function of the beta-amyloid precursor protein: beyond Alzheimer's disease. Journal of neurochemistry. 2014;129(5):756-69.
49. Pike CJ, Overman MJ, Cotman CW. Amino-terminal deletions enhance aggregation of beta-amyloid peptides in vitro. The Journal of biological chemistry. 1995;270(41):23895-8.
50. Ancolio K, Dumanchin C, Barelli H, Warter JM, Brice A, Campion D, et al. Unusual phenotypic alteration of beta amyloid precursor protein (betaAPP) maturation by a new Val-715 --> Met betaAPP-770 mutation responsible for probable early-onset Alzheimer's disease. Proceedings of the National Academy of Sciences of the United States of America. 1999;96(7):4119-24.
51. Bayer TA, Wirths O. Focusing the amyloid cascade hypothesis on N-truncated Abeta peptides as drug targets against Alzheimer's disease. Acta neuropathologica. 2014;127(6):787-801.
52. Masters CL, Simms G, Weinman NA, Multhaup G, McDonald BL, Beyreuther K. Amyloid plaque core protein in Alzheimer disease and Down syndrome. Proceedings of the National Academy of Sciences of the United States of America. 1985;82(12):4245-9.
53. Bouter Y, Dietrich K, Wittnam JL, Rezaei-Ghaleh N, Pillot T, Papot-Couturier S, et al. N-truncated amyloid beta (Abeta) 4-42 forms stable aggregates and induces acute and long-lasting behavioral deficits. Acta neuropathologica. 2013;126(2):189-205.
54. Lemere CA. Developing novel immunogens for a safe and effective Alzheimer's disease vaccine. Prog Brain Res. 2009;175:83-93.
55. Kitazawa M, Medeiros R, Laferla FM. Transgenic mouse models of Alzheimer disease: developing a better model as a tool for therapeutic interventions. Curr Pharm Des. 2012;18(8):1131-47.
56. Vandamme TF. Use of rodents as models of human diseases. J Pharm Bioallied Sci. 2014;6(1):2-9.
57. Schaeffer EL, Figueiro M, Gattaz WF. Insights into Alzheimer disease pathogenesis from studies in transgenic animal models. Clinics (Sao Paulo). 2011;66 Suppl 1(Suppl 1):45-54.
58. Saito T, Saido TC. Neuroinflammation in mouse models of Alzheimer's disease. Clinical & experimental neuroimmunology. 2018;9(4):211-8.
59. Sasaguri H, Nilsson P, Hashimoto S, Nagata K, Saito T, De Strooper B, et al. APP mouse models for Alzheimer's disease preclinical studies. Embo j. 2017;36(17):2473-87.

60. Citron M, Oltersdorf T, Haass C, McConlogue L, Hung AY, Seubert P, et al. Mutation of the beta-amyloid precursor protein in familial Alzheimer's disease increases beta-protein production. Nature. 1992;360(6405):672-4.
61. Saito T, Matsuba Y, Mihira N, Takano J, Nilsson P, Itohara S, et al. Single App knock-in mouse models of Alzheimer's disease. Nat Neurosci. 2014;17(5):661-3.
62. Duyckaerts C, Potier MC, Delatour B. Alzheimer disease models and human neuropathology: similarities and differences. Acta neuropathologica. 2008;115(1):5-38.
63. Bouter C, Henniges P, Franke TN, Irwin C, Sahlmann CO, Sichler ME, et al. (18)F-FDG-PET Detects Drastic Changes in Brain Metabolism in the Tg4-42 Model of Alzheimer's Disease. Frontiers in aging neuroscience. 2019;10:425.
64. Bouter Y, Kacprowski T, Weissmann R, Dietrich K, Borgers H, Brauß A, et al. Deciphering the molecular profile of plaques, memory decline and neuron loss in two mouse models for Alzheimer's disease by deep sequencing. Frontiers in aging neuroscience. 2014;6:75.
65. Dietrich K, Bouter Y, Muller M, Bayer TA. Synaptic Alterations in Mouse Models for Alzheimer Disease-A Special Focus on N-Truncated Abeta 4-42. Molecules. 2018;23(4).
66. Hutter-Paier B, Huttunen HJ, Puglielli L, Eckman CB, Kim DY, Hofmeister A, et al. The ACAT inhibitor CP-113,818 markedly reduces amyloid pathology in a mouse model of Alzheimer's disease. Neuron. 2004;44(2):227-38.
67. Rockenstein E, Mallory M, Mante M, Sisk A, Masliaha E. Early formation of mature amyloid-beta protein deposits in a mutant APP transgenic model depends on levels of Abeta(1-42). Journal of neuroscience research. 2001;66(4):573-82.
68. Windisch M, Flunkert S, Havas D, Hutter-Paier B. Commentary to the recently published review "Drug pipeline in neurodegeneration based on transgenic mice models of Alzheimer's disease" by Li, Evrahimi and Schluesener. Ageing Res. Rev. 2013 Jan;12(1):116-40. Ageing Res Rev. 2013;12(4):852-4.
69. Biomarkers Definitions Working G. Biomarkers and surrogate endpoints: preferred definitions and conceptual framework. Clin Pharmacol Ther. 2001;69(3):89-95.
70. Strimbu K, Tavel JA. What are biomarkers? Curr Opin HIV AIDS. 2010;5(6):463-6.
71. Califf RM. Biomarker definitions and their applications. Exp Biol Med (Maywood). 2018;243(3):213-21.
72. Huss R. Chapter 19 - Biomarkers. In: Atala A, Allickson JG, editors. Translational Regenerative Medicine. Boston: Academic Press; 2015. p. 235-41.
73. Blennow K, Zetterberg H. Biomarkers for Alzheimer's disease: current status and prospects for the future. Journal of Internal Medicine. 2018;284(6):643-63.
74. Corella D, Ordovas JM. Biomarkers: background, classification and guidelines for applications in nutritional epidemiology. Nutr Hosp. 2015;31 Suppl 3:177-88.
75. Sancesario GM, Bernardini S. Alzheimer's disease in the omics era. Clin Biochem. 2018;59:9-16.
76. Wilkins JM, Trushina E. Application of Metabolomics in Alzheimer's Disease. Front Neurol. 2017;8:719.
77. Emwas AH. The strengths and weaknesses of NMR spectroscopy and mass spectrometry with particular focus on metabolomics research. Methods Mol Biol. 2015;1277:161-93.
78. Emwas AH, Roy R, McKay RT, Tenori L, Saccenti E, Gowda GAN, et al. NMR Spectroscopy for Metabolomics Research. Metabolites. 2019;9(7).
79. Larive CK, Barding GA, Jr., Dinges MM. NMR spectroscopy for metabolomics and metabolic profiling. Anal Chem. 2015;87(1):133-46.
80. Wang H, Tan L, Wang HF, Liu Y, Yin RH, Wang WY, et al. Magnetic Resonance Spectroscopy in Alzheimer's Disease: Systematic Review and Meta-Analysis. J Alzheimers Dis. 2015;46(4):1049-70.

81. Motsinger-Reif AA, Zhu H, Kling MA, Matson W, Sharma S, Fiehn O, et al. Comparing metabolomic and pathologic biomarkers alone and in combination for discriminating Alzheimer's disease from normal cognitive aging. Acta Neuropathol Commun. 2013;1:28.
82. Kaddurah-Daouk R, Rozen S, Matson W, Han X, Hulette CM, Burke JR, et al. Metabolomic changes in autopsy-confirmed Alzheimer's disease. Alzheimer's & dementia : the journal of the Alzheimer's Association. 2011;7(3):309-17.
83. Casanova R, Varma S, Simpson B, Kim M, An Y, Saldana S, et al. Blood metabolite markers of preclinical Alzheimer's disease in two longitudinally followed cohorts of older individuals. Alzheimer's & dementia : the journal of the Alzheimer's Association. 2016;12(7):815-22.
84. Chen C-H, Ferreira JCB, Gross ER, Mochly-Rosen D. Targeting aldehyde dehydrogenase 2: new therapeutic opportunities. Physiol Rev. 2014;94(1):1-34.
85. Szeto JYY, Lewis SJG. Current Treatment Options for Alzheimer's Disease and Parkinson's Disease Dementia. Curr Neuropharmacol. 2016;14(4):326-38.
86. Yiannopoulou KG, Papageorgiou SG. Current and future treatments for Alzheimer's disease. Ther Adv Neurol Disord. 2013;6(1):19-33.
87. Desler C, Lillenes MS, Tønjum T, Rasmussen LJ. The Role of Mitochondrial Dysfunction in the Progression of Alzheimer's Disease. Curr Med Chem. 2018;25(40):5578-87.
88. Huang MLH, Chiang S, Kalinowski DS, Bae D-H, Sahni S, Richardson DR. The Role of the Antioxidant Response in Mitochondrial Dysfunction in Degenerative Diseases: Cross-Talk between Antioxidant Defense, Autophagy, and Apoptosis. Oxid Med Cell Longev. 2019;2019:6392763-.
89. Praticò D, Delanty N. Oxidative injury in diseases of the central nervous system: focus on alzheimer’s disease. The American Journal of Medicine. 2000;109(7):577-85.
90. Ferrer MD, Sureda A, Mestre A, Tur JA, Pons A. The Double Edge of Reactive Oxygen Species as Damaging and Signaling Molecules in HL60 Cell Culture. Cellular Physiology and Biochemistry. 2010;25(2-3):241-52.
91. Collin F. Chemical Basis of Reactive Oxygen Species Reactivity and Involvement in Neurodegenerative Diseases. Int J Mol Sci. 2019;20(10):2407.
92. Darley-Usmar V, Wiseman H, Halliwell B. Nitric oxide and oxygen radicals: a question of balance. FEBS Lett. 1995;369(2-3):131-5.
93. Wang X, Wang W, Li L, Perry G, Lee HG, Zhu X. Oxidative stress and mitochondrial dysfunction in Alzheimer's disease. Biochim Biophys Acta. 2014;1842(8):1240-7.
94. Nunomura A, Perry G, Aliev G, Hirai K, Takeda A, Balraj EK, et al. Oxidative Damage Is the Earliest Event in Alzheimer Disease. Journal of Neuropathology & Experimental Neurology. 2001;60(8):759-67.
95. McGrath LT, McGleenon BM, Brennan S, McColl D, McILroy S, Passmore AP. Increased oxidative stress in Alzheimer's disease as assessed with 4-hydroxynonenal but not malondialdehyde. QJM: An International Journal of Medicine. 2001;94(9):485-90.
96. Ohta S, Ohsawa I. Dysfunction of mitochondria and oxidative stress in the pathogenesis of Alzheimer's disease: on defects in the cytochrome c oxidase complex and aldehyde detoxification. J Alzheimers Dis. 2006;9(2):155-66.
97. Kraeuter AK, Guest PC, Sarnyai Z. The Open Field Test for Measuring Locomotor Activity and Anxiety-Like Behavior. Methods Mol Biol. 2019;1916:99-103.
98. Jawhar S, Trawicka A, Jenneckens C, Bayer TA, Wirths O. Motor deficits, neuron loss, and reduced anxiety coinciding with axonal degeneration and intraneuronal Abeta aggregation in the 5XFAD mouse model of Alzheimer's disease. Neurobiology of aging. 2012;33(1):196.e29-40.
99. de Vree PJ, de Wit E, Yilmaz M, van de Heijning M, Klous P, Verstegen MJ, et al. Targeted sequencing by proximity ligation for comprehensive variant detection and local haplotyping. Nat Biotechnol. 2014;32(10):1019-25.

100. Hinteregger B, Loeffler T, Flunkert S, Neddens J, Birner-Gruenberger R, Bayer TA, et al. Transgene integration causes RARB downregulation in homozygous Tg4–42 mice. Scientific reports. 2020;10(1):6377.
101. Calsolaro V, Edison P. Neuroinflammation in Alzheimer's disease: Current evidence and future directions. Alzheimer's & dementia : the journal of the Alzheimer's Association. 2016;12(6):719-32.
102. Dhiman K, Blennow K, Zetterberg H, Martins RN, Gupta VB. Cerebrospinal fluid biomarkers for understanding multiple aspects of Alzheimer's disease pathogenesis. Cell Mol Life Sci. 2019;76(10):1833-63.
103. Hall AM, Roberson ED. Mouse models of Alzheimer's disease. Brain research bulletin. 2012;88(1):3-12.
104. LaFerla FM, Green KN. Animal models of Alzheimer disease. Cold Spring Harbor perspectives in medicine. 2012;2(11).
105. Wirths O, Bayer TA. Neuron loss in transgenic mouse models of Alzheimer's disease. Int J Alzheimers Dis. 2010;2010.
106. Huttenrauch M, Brauss A, Kurdakova A, Borgers H, Klinker F, Liebetanz D, et al. Physical activity delays hippocampal neurodegeneration and rescues memory deficits in an Alzheimer disease mouse model. Translational psychiatry. 2016;6:e800.
107. Elder GA, Gama Sosa MA, De Gasperi R. Transgenic mouse models of Alzheimer's disease. The Mount Sinai journal of medicine, New York. 2010;77(1):69-81.
108. Mariani MM, Malm T, Lamb R, Jay TR, Neilson L, Casali B, et al. Neuronally-directed effects of RXR activation in a mouse model of Alzheimer's disease. Scientific reports. 2017;7:42270.
109. Antonios G, Borgers H, Richard BC, Brauss A, Meissner J, Weggen S, et al. Alzheimer therapy with an antibody against N-terminal Abeta 4-X and pyroglutamate Abeta 3-X. Scientific reports. 2015;5:17338.
110. Wagner JM, Sichler ME, Schleicher EM, Franke TN, Irwin C, Low MJ, et al. Analysis of Motor Function in the Tg4-42 Mouse Model of Alzheimer's Disease. Front Behav Neurosci. 2019;13:107.
111. Alexandru A, Jagla W, Graubner S, Becker A, Bauscher C, Kohlmann S, et al. Selective hippocampal neurodegeneration in transgenic mice expressing small amounts of truncated Abeta is induced by pyroglutamate-Abeta formation. The Journal of neuroscience : the official journal of the Society for Neuroscience. 2011;31(36):12790-801.
112. Lalonde R, Dumont M, Staufenbiel M, Strazielle C. Neurobehavioral characterization of APP23 transgenic mice with the SHIRPA primary screen. Behav Brain Res. 2005;157(1):91-8.
113. Pugh PL, Richardson JC, Bate ST, Upton N, Sunter D. Non-cognitive behaviours in an APP/PS1 transgenic model of Alzheimer's disease. Behav Brain Res. 2007;178(1):18-28.
114. Seibenhener ML, Wooten MC. Use of the Open Field Maze to measure locomotor and anxiety-like behavior in mice. J Vis Exp. 2015(96):e52434-e.
115. Bryan KJ, Lee H, Perry G, Smith MA, Casadesus G. Frontiers in Neuroscience
Transgenic Mouse Models of Alzheimer's Disease: Behavioral Testing and Considerations. In: nd, Buccafusco JJ, editors. Methods of Behavior Analysis in Neuroscience. Boca Raton (FL): CRC Press/Taylor & Francis
Taylor & Francis Group, LLC.; 2009.
116. Tatem KS, Quinn JL, Phadke A, Yu Q, Gordish-Dressman H, Nagaraju K. Behavioral and locomotor measurements using an open field activity monitoring system for skeletal muscle diseases. J Vis Exp. 2014(91):51785-.
117. Lopez-Noguerola JS, Giessen NME, Ueberück M, Meißner JN, Pelgrim CE, Adams J, et al. Synergistic Effect on Neurodegeneration by N-Truncated Aβ and Pyroglutamate Aβ in a Mouse Model of Alzheimer's Disease. Frontiers in aging neuroscience. 2018;10:64.
118. Walf AA, Frye CA. The use of the elevated plus maze as an assay of anxiety-related behavior in rodents. Nature protocols. 2007;2(2):322-8.

119. Broadbent NJ, Squire LR, Clark RE. Spatial memory, recognition memory, and the hippocampus. Proceedings of the National Academy of Sciences of the United States of America. 2004;101(40):14515-20.
120. Moser MB, Moser EI, Forrest E, Andersen P, Morris RG. Spatial learning with a minislab in the dorsal hippocampus. Proceedings of the National Academy of Sciences of the United States of America. 1995;92(21):9697-701.
121. Hartman RE, Lee JM, Zipfel GJ, Wozniak DF. Characterizing learning deficits and hippocampal neuron loss following transient global cerebral ischemia in rats. Brain Research. 2005;1043(1):48-56.
122. Volpe BT, Davis HP, Towle A, Dunlap WP. Loss of hippocampal CA1 pyramidal neurons correlates with memory impairment in rats with ischemic or neurotoxin lesions. Behav Neurosci. 1992;106(3):457-64.
123. Landes AM, Sperry SD, Strauss ME, Geldmacher DS. Apathy in Alzheimer's disease. J Am Geriatr Soc. 2001;49(12):1700-7.
124. Thomas P, Clement JP, Hazif-Thomas C, Leger JM. Family, Alzheimer's disease and negative symptoms. Int J Geriatr Psychiatry. 2001;16(2):192-202.
125. Janus C. Search strategies used by APP transgenic mice during navigation in the Morris water maze. Learn Mem. 2004;11(3):337-46.
126. Backman L, Small BJ, Fratiglioni L. Stability of the preclinical episodic memory deficit in Alzheimer's disease. Brain. 2001;124(Pt 1):96-102.
127. McKenna MC. The glutamate-glutamine cycle is not stoichiometric: Fates of glutamate in brain. Journal of Neuroscience Research. 2007;85(15):3347-58.
128. Walton HS, Dodd PR. Glutamate–glutamine cycling in Alzheimer's disease. Neurochemistry International. 2007;50(7):1052-66.
129. Doert A, Pilatus U, Zanella F, Muller WE, Eckert GP. (1)H- and (1)(3)C-NMR spectroscopy of Thy-1-APPSL mice brain extracts indicates metabolic changes in Alzheimer's disease. J Neural Transm (Vienna). 2015;122(4):541-50.
130. Huang D, Liu D, Yin J, Qian T, Shrestha S, Ni H. Glutamate-glutamine and GABA in brain of normal aged and patients with cognitive impairment. Eur Radiol. 2017;27(7):2698-705.
131. Gueli MC, Taibi G. Alzheimer's disease: amino acid levels and brain metabolic status. Neurol Sci. 2013;34(9):1575-9.
132. Manyevitch R, Protas M, Scarpiello S, Deliso M, Bass B, Nanajian A, et al. Evaluation of Metabolic and Synaptic Dysfunction Hypotheses of Alzheimer's Disease (AD): A Meta-Analysis of CSF Markers. Curr Alzheimer Res. 2018;15(2):164-81.
133. Seidl R, Cairns N, Singewald N, Kaehler ST, Lubec G. Differences between GABA levels in Alzheimer's disease and Down syndrome with Alzheimer-like neuropathology. Naunyn Schmiedebergs Arch Pharmacol. 2001;363(2):139-45.
134. Hattori N, Abe K, Sakoda S, Sawada T. Proton MR spectroscopic study at 3 Tesla on glutamate/glutamine in Alzheimer's disease. Neuroreport. 2002;13(1):183-6.
135. Antuono PG, Jones JL, Wang Y, Li SJ. Decreased glutamate + glutamine in Alzheimer's disease detected in vivo with (1)H-MRS at 0.5 T. Neurology. 2001;56(6):737-42.
136. Boissiere F, Faucheux B, Duyckaerts C, Hauw JJ, Agid Y, Hirsch EC. Striatal expression of glutamic acid decarboxylase gene in Alzheimer's disease. Journal of neurochemistry. 1998;71(2):767-74.
137. Burbaeva G, Boksha IS, Tereshkina EB, Savushkina OK, Starodubtseva LI, Turishcheva MS. Glutamate metabolizing enzymes in prefrontal cortex of Alzheimer's disease patients. Neurochem Res. 2005;30(11):1443-51.
138. Matos M, Augusto E, Oliveira CR, Agostinho P. Amyloid-beta peptide decreases glutamate uptake in cultured astrocytes: Involvement of oxidative stress and mitogen-activated protein kinase cascades. Neuroscience. 2008;156(4):898-910.
139. Ong WY, Tanaka K, Dawe GS, Ittner LM, Farooqui AA. Slow excitotoxicity in Alzheimer's disease. J Alzheimers Dis. 2013;35(4):643-68.

140. Wang Y, Wu Z, Bai YT, Wu GY, Chen G. Gad67 haploinsufficiency reduces amyloid pathology and rescues olfactory memory deficits in a mouse model of Alzheimer's disease. Mol Neurodegener. 2017;12(1):73.
141. Glabe CG, Kayed R. Common structure and toxic function of amyloid oligomers implies a common mechanism of pathogenesis. Neurology. 2006;66(2 Suppl 1):S74-8.
142. Sadowski M, Pankiewicz J, Scholtzova H, Ji Y, Quartermain D, Jensen CH, et al. Amyloid-β Deposition Is Associated with Decreased Hippocampal Glucose Metabolism and Spatial Memory Impairment in APP/PS1 Mice. Journal of Neuropathology & Experimental Neurology. 2004;63(5):418-28.
143. Cieslik M, Czapski GA, Wojtowicz S, Wieczorek I, Wencel PL, Strosznajder RP, et al. Alterations of Transcription of Genes Coding Anti-oxidative and Mitochondria-Related Proteins in Amyloid beta Toxicity: Relevance to Alzheimer's Disease. Mol Neurobiol. 2019.
144. Saito T, Saido TC. Neuroinflammation in mouse models of Alzheimer's disease. Clin Exp Neuroimmunol. 2018;9(4):211-8.
145. Khalil M, Teunissen CE, Otto M, Piehl F, Sormani MP, Gattringer T, et al. Neurofilaments as biomarkers in neurological disorders. Nat Rev Neurol. 2018;14(10):577-89.
146. Benedet AL, Ashton NJ, Pascoal TA, Leuzy A, Mathotaarachchi S, Kang MS, et al. Plasma neurofilament light associates with Alzheimer's disease metabolic decline in amyloid-positive individuals. Alzheimers Dement (Amst). 2019;11:679-89.
147. Lin Y-S, Lee W-J, Wang S-J, Fuh J-L. Levels of plasma neurofilament light chain and cognitive function in patients with Alzheimer or Parkinson disease. Scientific reports. 2018;8(1):17368-.
148. Mattsson N, Andreasson U, Zetterberg H, Blennow K, Alzheimer's Disease Neuroimaging I. Association of Plasma Neurofilament Light With Neurodegeneration in Patients With Alzheimer Disease. JAMA neurology. 2017;74(5):557-66.
149. Tosh JL, Rickman M, Rhymes E, Norona FE, Clayton E, Mucke L, et al. The integration site of the APP transgene in the J20 mouse model of Alzheimer's disease. Wellcome Open Res. 2018;2:84-.
150. Baudhuin LM, Lagerstedt SA, Klee EW, Fadra N, Oglesbee D, Ferber MJ. Confirming Variants in Next-Generation Sequencing Panel Testing by Sanger Sequencing. J Mol Diagn. 2015;17(4):456-61.
151. Lu J, Allred CC, Jensen MD. Human adipose tissue protein analyses using capillary western blot technology. Nutr Diabetes. 2017;7(10):e287.
152. Nguyen U, Squaglia N, Boge A, Fung PA. The Simple Western™: a gel-free, blot-free, hands-free Western blotting reinvention. Nature Methods. 2011;8(11):v-vi.
153. Woychik RP, Alagramam K. Insertional mutagenesis in transgenic mice generated by the pronuclear microinjection procedure. The International journal of developmental biology. 1998;42(7):1009-17.
154. Reed DR, Lawler MP, Tordoff MG. Reduced body weight is a common effect of gene knockout in mice. BMC Genet. 2008;9:4.
155. Ghyselinck NB, Dupe V, Dierich A, Messaddeq N, Garnier JM, Rochette-Egly C, et al. Role of the retinoic acid receptor beta (RARbeta) during mouse development. The International journal of developmental biology. 1997;41(3):425-47.
156. Chiang MY, Misner D, Kempermann G, Schikorski T, Giguere V, Sucov HM, et al. An essential role for retinoid receptors RARbeta and RXRgamma in long-term potentiation and depression. Neuron. 1998;21(6):1353-61.
157. Zhou G, Strom RC, Giguere V, Williams RW. Modulation of retinal cell populations and eye size in retinoic acid receptor knockout mice. Mol Vis. 2001;7:253-60.
158. Havas D, Hutter-Paier B, Ubhi K, Rockenstein E, Crailsheim K, Masliah E, et al. A longitudinal study of behavioral deficits in an AbetaPP transgenic mouse model of Alzheimer's disease. J Alzheimers Dis. 2011;25(2):231-43.

159. Faizi M, Bader PL, Saw N, Nguyen TV, Beraki S, Wyss-Coray T, et al. Thy1-hAPP(Lond/Swe+) mouse model of Alzheimer's disease displays broad behavioral deficits in sensorimotor, cognitive and social function. Brain Behav. 2012;2(2):142-54.
160. Corcoran KA, Lu Y, Turner RS, Maren S. Overexpression of hAPPswe impairs rewarded alternation and contextual fear conditioning in a transgenic mouse model of Alzheimer's disease. Learn Mem. 2002;9(5):243-52.
161. Hsiao K, Chapman P, Nilsen S, Eckman C, Harigaya Y, Younkin S, et al. Correlative memory deficits, Abeta elevation, and amyloid plaques in transgenic mice. Science. 1996;274(5284):99-102.
162. Voikar V, Vasar E, Rauvala H. Behavioral alterations induced by repeated testing in C57BL/6J and 129S2/Sv mice: implications for phenotyping screens. Genes Brain Behav. 2004;3(1):27-38.
163. Nobis L, Husain M. Apathy in Alzheimer's disease. Curr Opin Behav Sci. 2018;22:7-13.
164. Robert PH, Darcourt G, Koulibaly MP, Clairet S, Benoit M, Garcia R, et al. Lack of initiative and interest in Alzheimer's disease: a single photon emission computed tomography study. Eur J Neurol. 2006;13(7):729-35.
165. Baranello RJ, Bharani KL, Padmaraju V, Chopra N, Lahiri DK, Greig NH, et al. Amyloid-beta protein clearance and degradation (ABCD) pathways and their role in Alzheimer's disease. Current Alzheimer research. 2015;12(1):32-46.
166. Gupta A, Goyal R. Amyloid beta plaque: a culprit for neurodegeneration. Acta Neurol Belg. 2016;116(4):445-50.
167. Löffler T, Flunkert S, Havas D, Schweinzer C, Uger M, Windisch M, et al. Neuroinflammation and related neuropathologies in APPSL mice: further value of this in vivo model of Alzheimer's disease. J Neuroinflammation. 2014;11:84-.
168. Imbimbo BP, Hutter-Paier B, Villetti G, Facchinetti F, Cenacchi V, Volta R, et al. CHF5074, a novel gamma-secretase modulator, attenuates brain beta-amyloid pathology and learning deficit in a mouse model of Alzheimer's disease. Br J Pharmacol. 2009;156(6):982-93.
169. Huttunen HJ, Havas D, Peach C, Barren C, Duller S, Xia W, et al. The acyl-coenzyme A: cholesterol acyltransferase inhibitor CI-1011 reverses diffuse brain amyloid pathology in aged amyloid precursor protein transgenic mice. J Neuropathol Exp Neurol. 2010;69(8):777-88.
170. Heneka MT, Carson MJ, El Khoury J, Landreth GE, Brosseron F, Feinstein DL, et al. Neuroinflammation in Alzheimer's disease. Lancet Neurol. 2015;14(4):388-405.
171. Chen L, Lang AL, Poff GD, Ding WX, Beier JI. Vinyl chloride-induced interaction of nonalcoholic and toxicant-associated steatohepatitis: Protection by the ALDH2 activator Alda-1. Redox biology. 2019;24:101205.
172. Hua Y, Chen H, Zhao X, Liu M, Jin W, Yan W, et al. Alda-1, an aldehyde dehydrogenase-2 agonist, improves long-term survival in rats with chronic heart failure following myocardial infarction. Mol Med Rep. 2018;18(3):3159-66.
173. D'Souza Y, Elharram A, Soon-Shiong R, Andrew RD, Bennett BM. Characterization of Aldh2 (-/-) mice as an age-related model of cognitive impairment and Alzheimer's disease. Molecular brain. 2015;8:27.
174. Ai L, Tan T, Tang Y, Yang J, Cui D, Wang R, et al. Endogenous formaldehyde is a memory-related molecule in mice and humans. Commun Biol. 2019;2:446-.
175. Ostrovsky YM. Endogenous ethanol—Its metabolic, behavioral and biomedical significance. Alcohol. 1986;3(4):239-47.
176. Li K, Guo W, Li Z, Wang Y, Sun B, Xu D, et al. ALDH2 Repression Promotes Lung Tumor Progression via Accumulated Acetaldehyde and DNA Damage. Neoplasia. 2019;21(6):602-14.
177. Kiyoshi A, Weihuan W, Mostofa J, Mitsuru K, Toyoshi I, Toshihiro K, et al. Ethanol metabolism in ALDH2 knockout mice – Blood acetate levels. Legal Medicine. 2009;11:S413-S5.

178. Solito R, Corti F, Chen C-H, Mochly-Rosen D, Giachetti A, Ziche M, et al. Mitochondrial aldehyde dehydrogenase-2 activation prevents β-amyloid-induced endothelial cell dysfunction and restores angiogenesis. Journal of Cell Science. 2013;126(9):1952-61.
179. Joshi AU, Van Wassenhove LD, Logas KR, Minhas PS, Andreasson KI, Weinberg KI, et al. Aldehyde dehydrogenase 2 activity and aldehydic load contribute to neuroinflammation and Alzheimer's disease related pathology. Acta Neuropathologica Communications. 2019;7(1):190.
180. Huang W-J, Zhang X, Chen W-W. Role of oxidative stress in Alzheimer's disease. Biomed Rep. 2016;4(5):519-22.
181. Chen Z, Zhong C. Oxidative stress in Alzheimer's disease. Neurosci Bull. 2014;30(2):271-81.
182. Ohsawa I, Nishimaki K, Murakami Y, Suzuki Y, Ishikawa M, Ohta S. Age-dependent neurodegeneration accompanying memory loss in transgenic mice defective in mitochondrial aldehyde dehydrogenase 2 activity. The Journal of neuroscience : the official journal of the Society for Neuroscience. 2008;28(24):6239-49.
183. Jambunathan N. Determination and detection of reactive oxygen species (ROS), lipid peroxidation, and electrolyte leakage in plants. Methods Mol Biol. 2010;639:292-8.
184. Griendling KK, Touyz RM, Zweier JL, Dikalov S, Chilian W, Chen Y-R, et al. Measurement of Reactive Oxygen Species, Reactive Nitrogen Species, and Redox-Dependent Signaling in the Cardiovascular System: A Scientific Statement From the American Heart Association. Circ Res. 2016;119(5):e39-e75.
185. Halliwell B, Whiteman M. Measuring reactive species and oxidative damage in vivo and in cell culture: how should you do it and what do the results mean? British journal of pharmacology. 2004;142(2):231-55.
186. Dasgupta A, Klein K. Chapter 2 - Methods for Measuring Oxidative Stress in the Laboratory. In: Dasgupta A, Klein K, editors. Antioxidants in Food, Vitamins and Supplements. San Diego: Elsevier; 2014. p. 19-40.
187. Abu Youssef HA, Elshazly MI, Rashed LA, Sabry IM, Ibrahim EK. Thiobarbituric acid reactive substance (TBARS) a marker of oxidative stress in obstructive sleep apnea. Egyptian Journal of Chest Diseases and Tuberculosis. 2014;63(1):119-24.
188. Sayre LM, Zelasko DA, Harris PL, Perry G, Salomon RG, Smith MA. 4-Hydroxynonenal-derived advanced lipid peroxidation end products are increased in Alzheimer's disease. Journal of neurochemistry. 1997;68(5):2092-7.
189. Zarkovic K. 4-hydroxynonenal and neurodegenerative diseases. Molecular aspects of medicine. 2003;24(4-5):293-303.
190. Kim C, Hwang S, Choi HJ, Lim TH, Kang J-s. The Effect of Aldehyde Dehydrogenase Activator, Alda-1®, on the Ethanol-induced Brain Damage in a Rat of Binge Ethanol Intoxication. bioRxiv. 2018:353854.
191. Siegel SJ, Bieschke J, Powers ET, Kelly JW. The oxidative stress metabolite 4-hydroxynonenal promotes Alzheimer protofibril formation. Biochemistry. 2007;46(6):1503-10.
192. Kurutas EB. The importance of antioxidants which play the role in cellular response against oxidative/nitrosative stress: current state. Nutrition journal. 2016;15(1):71.
193. Weydert CJ, Cullen JJ. Measurement of superoxide dismutase, catalase and glutathione peroxidase in cultured cells and tissue. Nature protocols. 2010;5(1):51-66.
194. Hawking ZL. Alzheimer's disease: the role of mitochondrial dysfunction and potential new therapies. Bioscience Horizons: The International Journal of Student Research. 2016;9.
195. Ridge PG, Kauwe JSK. Mitochondria and Alzheimer's Disease: the Role of Mitochondrial Genetic Variation. Curr Genet Med Rep. 2018;6(1):1-10.
196. Neupert W. Protein import into mitochondria. Annu Rev Biochem. 1997;66:863-917.
197. Truban D, Hou X, Caulfield TR, Fiesel FC, Springer W. PINK1, Parkin, and Mitochondrial Quality Control: What can we Learn about Parkinson's Disease Pathobiology? Journal of Parkinson's disease. 2017;7(1):13-29.

198. Brand MD, Nicholls DG. Assessing mitochondrial dysfunction in cells. The Biochemical journal. 2011;435(2):297-312.
199. George Paxinos KBJF. The Mouse Brain in Stereotaxic Coordinates (Englisch) Taschenbuch 2000. 296 p. 2nd edition, 2001.
200. Mathiasen JR, Moser VC. The Irwin Test and Functional Observational Battery (FOB) for Assessing the Effects of Compounds on Behavior, Physiology, and Safety Pharmacology in Rodents. Current Protocols in Pharmacology. 2018;83(1):e43.

8 APPENDIX

8.1 Reagents and chemicals

8.1.1 NMR-based metabolomics buffer:

0.08 M Na_2HPO_4 (AppliChem/A2943,1000)

0.04 % NaN_3 (Merck/1.06688.0100)

5 mM TSP (Eurisotop/D219PF)

Dissolved in ^2H_2O (SIAL/151882-1)

pH 7.3 adjusted with HCl (12.2 M) and NaOH (5 M)

8.1.2 Tissue homogenization buffer

250 mM Sucrose (Sigma-Aldrich/S0389)

1 mM EDTA (Sigma-Aldrich/E5134)

1 mM EGTA (Alfa Aesar/A16086)

20 mM Tris pH 7.4 (Roth/2449.2)

8.1.3 Formic Acid (FA) Neutralization Solution

1M Tris (Roth/2449.2)

0.5 M Na_2HPO_4 (Roth/4984)

0.05% NaN_3 (Sigma-Aldrich/S2002)

8.1.4 RIPA Buffer

50mM Tris-HCl pH 8.0 (Roth/2449.2; Merck/1.00317.1000)

150 mM NaCl (Merck/1.00317)

1mM EDTA (Sigma-Aldrich/ED2SC)

1% NP 40 (Sigma-Aldrich/74385)

0,1% SDS (VWR/33629.266)

0,5% Na-deoxycholat (Sigma-Aldrich/D6750)

1x Protease inhibitor cocktail (Millipore/539131-10VL)

1x Phosphatase inhibitor cocktail (Sigma-Aldrich/P0044-5ML)

Reagents/ chemicals	Manufacturer	Item number
1,1,3,3-Tetramethoxypropane (TMP)	Sigma-Aldrich	108383-100ML
A. bidest	Fresenius Kabi AG	B230673
Acetic acid	Merck	1.0000.631.0000
BSA	Sigma-Aldrich	A-7906
Butanol	VWR	20808.291
Buthyliertes Hydroxytoluol (BHT)	SAFC	W21,840-5-5K
Diethylamine	Sigma-Aldrich	D3131
D-Saccharose	Roth	4661.4
Formic acid	Sigma-Aldrich	F0507
Hydrochloric acid (HCl)	Merck	1.00317.1000
Paraformaldehyde	Merck	1.04003.1000
PBS	Pan Biotech	PO4-360000
Pyridine	Merck	8.22301.1000
Sodium borhydride	Sigma-Aldrich	213462
Sodium chloride	Merck	1.00317
Thiobarbituric acid	Sigma-Aldrich	T550-0
TriFast	VWR Life Science	031218-11
Triton X-100	AppliChem	A4975

8.2 Complete Gene Sequencing Report Cergentis (Utrecht, Netherlands)

Goal:

In this study a transgenic mouse Tg4-42 (TBA83) line was analyzed.

The aim of this experiment was to determine:

1. the integration site(s) of the transgene (TG)

2 assess the presence of structural variants surrounding the transgene integration site

3. assess the transgene sequence itself

4. estimate the TG copy number

Summary of the Results:

Name	Integration site(s)	Estimated Copy nr	SV
TBA83; Mouse spleen	mChr14:17431476-17474599	>20x	yes

Experiment:

TLA sample prep:

Isolated mouse spleen sample from the transgenic line was used for TLA sample prep.

TLA PCR:

Two primer pairs (set 6-7) were designed for the mouse TG.

Primers used in the analysis:

#	Name	position	Sequence
6	THR-Abeta4-42-F	TG:4350	CTGCCTTAGATTCCTGGATC
	THR-Abeta4-42-R	TG:4121	GACTTGGATTCTGTGGTGG
7	Thy-F	TG:5839	CAAATCAATGCGCATTCTCT
	Thy-R	TG:5578	TTTCTTTCCTCGGTGAGATG

The primer sets were used in individual TLA amplifications. PCR products were purified and library prepped using the Illumina NexteraXT protocol and sequenced on an Illumina Miseq sequencer. Reads were mapped using BWA-SW, which is a Smith-Waterman alignment tool. This allows partial mapping which is optimally suited for identifying break spanning reads. For mapping the mouse genome version mm9 was used.

Results - Integration site:

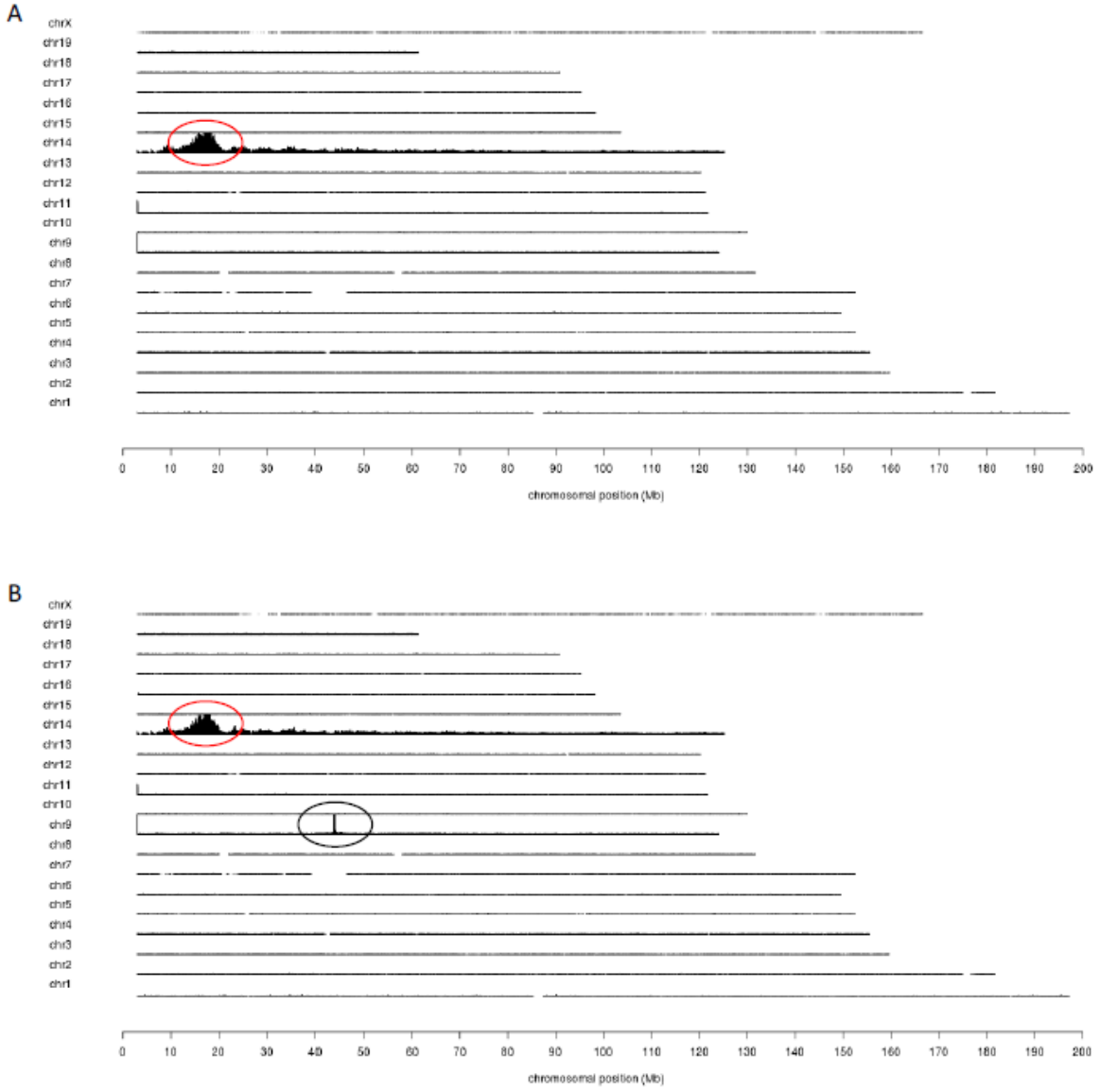

TLA sequence coverage across the mouse genome using primer set 6 (panel A) and set 7 (panel B). The different chromosomes are indicated on the y-axis, the chromosomal position on the x-axis. Similar results were obtained for both primer sets except using set 7 an additional coverage peak is found on the mouse Thy1 gene as expected (black circle). Encircled in red is the region containing the transgene integration site.

Using TLA highest coverage is observed on the sequences directly surrounding the location of the primer set. Here high coverage is observed on chr14 indicating this is the chromosome where the TG has integrated. Within chr14 highest coverage is observed in the region 15-25MB. Within this region the following fusion reads were identified marking the exact TG integration.

5’ fusion read: mChr14:17431476 (forw) fused to TG:4345 (forw)
..GTGCTCCTGCCTGCAGTCAGGATGAACCCCTTCTAAGATGATCTACAGCATTGCCCCC
ACTCACTGGTGCTGCCTTAGATTCCTGGATCACAAAACGCTTCCGACATGACTCAGGAT
ATGAAGTTCATCATCAAAAATTGGTGTTCTTTG..

3’ fusion read: TG:6724 (rev) fused to mChr14:17474599 (forw)
..GCCTCAGAGAGCACCCGCATCTCCCTAAGAACTGAGAGTGTGGTCACGGAGATGTCC
AGGGA
AGAGCACCTAGTGTGACAGAGACCACATCATATGACTCTGTAGGCAAGTCTGCTGCAGA
TCGCCTTTGGCACCCTTCAACTGCCGACAA..

As a result the TG was found to be integrated at mChr14:17431476-17474599 deleting all sequences in between.

Results - Transgene Sequence:

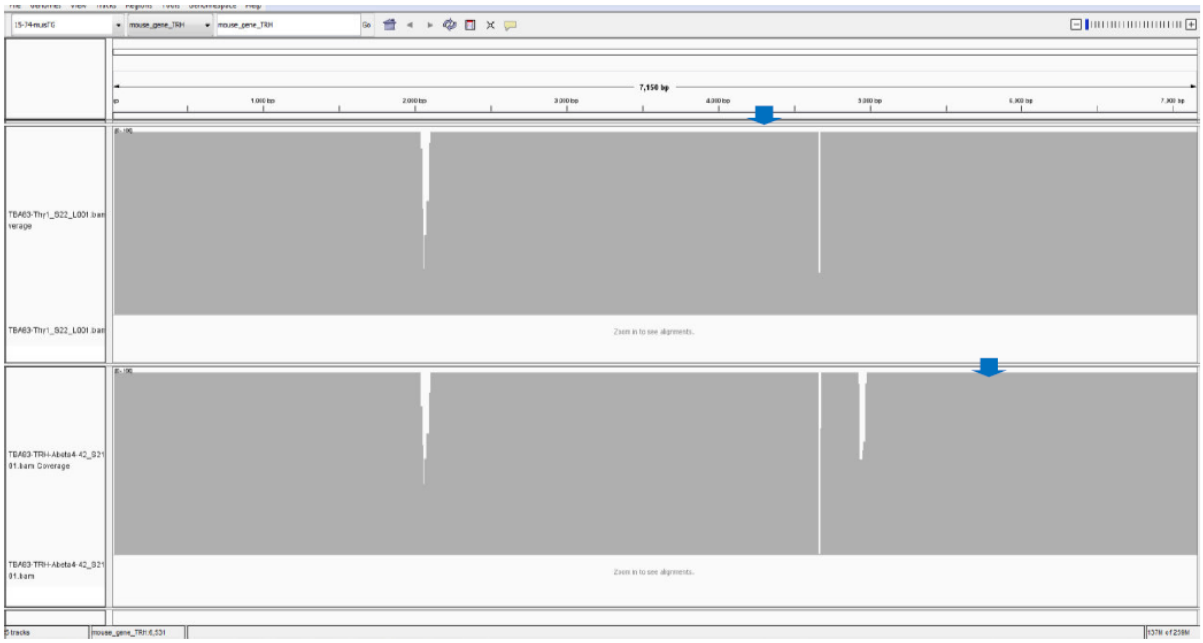

IGV screenshot of the TLA sequence coverage across the TG. Sequence coverage (in grey) generated with the different primer sets are depicted in the different panels as indicated. The positions of the primer sets on the TG sequence are indicated with the blue arrows. Y-axis is limited to 100x. Good coverage is observed across the TG except for TG:4642-4689 due to the high GC content of that region. From these data the following sequence variation was identified that was found with a frequency of minimal 10% using minimal 1 primer set. Complete tables are available from Cergentis upon request.

SNVs			TBA83-Thy1	TBA83-Thy1	TBA83-TRH-Abeta4-42	TBA83-TRH-Abeta4-42
pos	ref	alt	cov	SNP_%	cov	SNP_%
3692	C	T	996	17	44080	21
3744	C	T	753	95	37852	99
3761	G	T	835	94	42394	99
3762	C	T	837	93	42420	98
4961	T	G	12136	76	42	100
5136	G	A	47534	14	213	14
5298	C	T	71479	93	329	100
5996	A	G	50674	100	512	100
6645	G	A	3474	4	9773	21

INDELs			TBA83-Thy1	TBA83-Thy1	TBA83-TRH-Abeta4-42	TBA83-TRH-Abeta4-42
pos	ref	alt	cov	SNP_%	cov	SNP_%
4497	A	-6AGATGT	688	51	70302	64
4505	C	-7AAGTAAG	357	99	45594	99
4941	A	-2GG	9920	31	40	35
4941	A	-3GGG	9920	8	40	10
5925	A	-1G	60539	92	476	86
5927	A	+2CC	56287	99	417	97
5953	T	-1G	78485	98	615	98
5987	A	+1G	74918	67	656	77
5989	C	-1G	50752	99	512	99
5991	C	-2CT	50750	99	512	99
6003	A	-1G	50800	100	512	100

Results - Structural Variation:

The presence of fusion reads within the TG sequence allows for the detection of (potential) structural variation within the TG. Multiple fusion reads were identified in the TG sequence which are reported in the table below.

#seq1	pos1	ori1	seq2	pos2	ori2
mouse_gene_TRH	2350	+	mouse_gene_TRH	3286	+
mouse_gene_TRH	31	+	mouse_gene_TRH	2749	-
mouse_gene_TRH	2390	-	mouse_gene_TRH	3286	+

In addition the following read was found indicative of TG concatemers:

TG:7157 (forw) fused to ‘Unknown’ fused to TG:26 (forw)
GTCCTTATTCTCTCTCTACCTTCAGCCACTTAGTTTCCTACCTTAAGTCCTAGAATTGATC
CTGGCGTAATAGCGAAGAGGCCCGCACCGGGGCTGCAGGAATTCAGAGACCGGGAAC
CAAACTAGCCTTTAAAAAACATAAGTACAGGAG

Results - Copy number estimation:

An exact copy number cannot be determined using TLA. However, an estimation can be made based on the number of integration sites, number of fusion reads and the ratio of coverage on the TG and genome integration site. Here the TG/genome coverage ratio can be determined best, being between 1250 and 3000x on the TG and ~10x and 75x at the integration site on chromosome 14. From this the TG copy number is estimated to be >20x.

9 LICENSE